Winter 12-1-2019

INFLUENCE OF METABOLIC CAPACITY ON THE CONSEQUENCES OF SPREADING DEPOLARIZATION

Katelyn M. Reinhart
University of New Mexico

Katelyn M. Reinhart
Candidate

Neurosciences
Department

This dissertation is approved, and it is acceptable in quality and form for publication:

Approved by the Dissertation Committee:

C. William Shuttleworth, Ph.D., Chairperson

Lee Anna A. Cunningham, Ph.D.

Jennifer M. Gillette, Ph.D.

Russell A. Morton, Ph.D.

INFLUENCE OF METABOLIC CAPACITY ON THE CONSEQUENCES OF SPREADING DEPOLARIZATION

by

KATELYN M. REINHART

B.S., Biology & Biochemistry, University of Denver, 2011

DISSERTATION

Submitted in Partial Fulfillment of the
Requirements for the Degree of

Doctor of Philosophy
Biomedical Sciences

The University of New Mexico
Albuquerque, New Mexico

December 2019

DEDICATION

This dissertation work is dedicated to Donald Partridge, Ph.D. who is dearly missed by the UNM Neurosciences department— and whose puns will never be forgotten.

Influence of metabolic capacity on the consequences of spreading depolarization

By

Katelyn M. Reinhart
B.S., Biology & Biochemistry, University of Denver, 2011
Ph.D., University of New Mexico, 2019

ABSTRACT

In the United States, stroke is the fifth leading cause of death and stroke survivors often face long-term disability. After ischemic stroke, the ischemic territory can expand and recruit previously viable tissues into the lesioned area. During this critical period, there is an unsettling lack of interventions that prevent or treat secondary neuronal loss and cognitive decline. Clinical subdural recordings have revealed a close link between infarct progression and waves of *spreading depolarization*s (SD) in the acutely injured brain. SD is a slowly progressing wave of near-complete neuroglia depolarization that is extremely energetically demanding and this additional metabolic 'hit' of SD in vulnerable tissues (i.e. penumbra) could underlie secondary lesion progression. While deleterious to metabolically impaired neurons, SD may theoretically promote recovery and repair processes in otherwise healthy cortex, distant from the initial injury site. This dissertation work characterized the impact of tissue metabolic status on deleterious consequences of SD in order to test interventions that reduce neuronal injury without preventing SD outright. From this work, we now know that SD consequences can be targeted to limit deterioration of vulnerable tissues without preventing any theoretical benefits in remote brain regions that may play a role in cortical reorganization and recovery after focal ischemia.

Table of Contents

List of Figures

1. INTRODUCTION

1.1 Acute ischemic stroke

In the United States, approximately 795,000 strokes occur each year accounting for ~1 out of every 20 deaths. In 2013, stroke was the second-leading cause of death worldwide, behind ischemic heart disease (Benjamin et al., 2017) while stroke survivors often face serious long-term physical and/or mental disability. The vast majority (~87%) of individuals suffer ischemic strokes that occur when blood flow to the brain is reduced or blocked by an intravascular blood clot.

1.1.2 Current therapies are limited for stroke treatment

In 1996 the U.S. Food and Drug Administration (FDA) approved clinical use of tissue plasminogen activator (tPA), a pharmaceutical "clot-busting" agent, for the management of acute ischemic stroke patients. Infusion of tPA results in the conversion of the proteolytic enzyme, plasminogen, to its active form which solubilizes the clot to eventually restore blood flow. Since the original randomized controlled trial of tPA in patients ("Tissue Plasminogen Activator for Acute Ischemic Stroke," 1995), subsequent trials have revealed that, while ground-breaking in the treatment of stroke, benefits of tPA are limited to a narrow window of time up to 4.5 hours from initial symptom onset (Powers et al., 2018). This limited therapeutic window, along with various tPA contraindications, prevent the most ischemic stroke patients from receiving treatment. As such, studies reveal that only 3-5% of ischemic stroke patients receive tPA during this narrow window, further highlighting major limitations of intravenous thrombolytic efficacy (Albers and Olivot, 2007; Benjamin et al., 2017).

In addition to tPA, other reperfusion therapies (e.g. mechanical thrombectomy) have recently been incorporated into the 2018 healthcare professional guidelines for the early management of acute ischemic stroke patients (Powers et al., 2018). Mechanical thrombectomy is a minimally invasive surgical procedure for blood clot removal in order to improve cerebral perfusion after stroke. Recently, five randomized controlled trials have shown that mechanical thrombectomy can 1) improve global disability outcomes (Jovin et al., 2015) 2) be used as a stand-alone treatment or in conjunction with intravenous tPA (Bracard et al., 2016; Campbell et al., 2015; Goyal et al., 2015; Saver et al., 2015) and 3) be performed up to 24 hours after symptom onset in select ischemic stroke patients (Nogueira et al., 2018). While the 24h window increases the proportion of patients eligible for treatment (to 5-10% of acute ischemic stroke patients) (Bhaskar et al., 2018; Meurer et al., 2017), the procedure requires advanced imaging (not routinely preformed at time of presentation), a highly trained stroke specialist team, and is less effective for certain types of occlusions (i.e. small vessel occlusions, posterior circulation strokes, more distal clots) (Bhaskar et al., 2018). These challenges must be overcome in order to implement mechanical thrombectomy more widely for stroke management. Ultimately, while systemic thrombolysis and endovascular mechanical thrombectomy reperfusion therapies have revolutionized clinical standard of care guidelines, it is estimated that approximately 85% of all acute ischemic stroke patients still do not meet criteria for treatment (Bhaskar et al., 2018).

1.1.3 Progression of stroke injury when there are no available interventions

In addition to the rapid injury that occurs in brain regions directly supplied by the blocked vessel(s), tissue surrounding the infarct (i.e. the ischemic penumbra) remains susceptible to

further damage. This observation suggests that other mechanisms, secondary to initial ischemia, are contributing to lesion development and poor neurological outcomes. This is highlighted by clinical observations that the first 48 hours after ischemic stroke are characterized by patient instability, and up to 40% of patients are at risk of developing further neurological deficits and/or tissue deterioration during this time (DeGraba et al., 1999; Helleberg et al., 2016). This group of patients are prone to lengthy hospital stays and worse outcomes, including death, compared to stable patients without infarct progression (Helleberg et al., 2016). It is thus striking that no strategies are available beyond 24 hours (Powers et al., 2018) to limit the expansion of brain injury after ischemia. In order to improve therapeutic interventions that target delayed stroke injury, it is central to understand the fundamental mechanisms that contribute to initial as well as secondary brain injury following a sudden drop in cerebral blood supply.

1.2 Cellular mechanisms of injury

1.2.1. Rapid neuronal consequences of oxygen and/or glucose deprivation

Observations regarding the importance of cerebral circulation have been noted throughout history. Ancient civilizations of Mesopotamia utilized carotid artery compression to reduce the pain of circumcision, and magicians in the Middle Ages employed discrete occlusion techniques to cause rapid loss of consciousness in goats, thus puzzling their audiences (HOFF et al., 1945). The earliest documented experiments of ischemia were conducted in the spinal cord of animals in the 1600's, but it was not until 1836 that Astley Cooper developed a consistent method of artery occlusion in dogs for evaluating cerebrum pathology ("Astley Cooper," 1836; HOFF et al., 1945). Over the course of the next century, functional and

structural changes following cerebral anemia were examined and highlighted the importance of oxygen and glucose delivery, as well as metabolite clearance, for proper brain function.

When cerebral perfusion is occluded, brain tissue is deprived of important metabolic substrates, namely oxygen and glucose, that are primarily utilized for proper neuronal function. Although the brain represents only ~2% of the total body weight in humans, it consumes more energy compared to all other organs. It is estimated that brain utilizes ~20% of the body's total glucose-derived energy (Magistretti and Allaman, 2015; Mergenthaler et al., 2013) and is thus estimated to receive ~1/3 of the left ventricle's cardiac output in humans (Rossen et al., 1943). Evolutionary studies suggest that the preferential delivery of blood flow to the brain emerged during the development of higher cognitive centers that are characterized by increased glucose utilization and upregulation of genes involved in metabolism (Magistretti and Allaman, 2015). The tight relationship between neuronal firing and vascular supply is exploited by imaging modalities that monitor cerebral blood flow (CBF) as a proxy for determining relative levels of neuronal activity in certain brain regions. This coupling of CBF to neuronal activity (i.e. neurovascular coupling) provides the basis of techniques used for clinical studies or patient diagnoses including functional magnetic resonance imaging (fMRI) and near infrared spectroscopy (NIRS). After injury or ischemia, reduced blood flow is an immediate obstacle in matching vascular supply with neuronal energy demands.

Research into brain metabolic requirements became more widespread around the time of World War II. At this time, advances in aircraft technology enabled pilots to preform maneuvers at faster speeds and higher altitudes thus revealing "pilot fatigue," a phenomenon

characterized by rapid loss of consciousness (HOFF et al., 1945). In hopes of aiding the war effort, experiments by the neurophysiologist Herman Kabat and colleagues, found that complete arrest of cerebral circulation in dogs resulted in loss of consciousness within ~10 seconds, followed by loss of respiratory movements (~20-30s) (Kabat et al., 1941). Translating these findings into humans in 1941 Kabat, together with Lieutenant Ralph Rossen and John Anderson in Red Wing Minnesota, employed a compression cuff designed by Anderson (named the Kabat-Rossen-Anderson (KRA) apparatus) that enabled complete arrest of CBF within two heartbeats (Rossen et al., 1943). These "Red Wing experiments" demonstrated strikingly rapid loss of consciousness (~ 4-10s) in otherwise healthy adult men. While periods of cerebral circulation arrest were luckily short and minimized any potential for development of permanent injury, these early studies in animals and humans emphasized how quickly neurons respond to low nutrient environments, and specifically to loss of substrates (oxygen and glucose) central to ATP production in neurons.

The largest proportion of ATP consumption appears to be in neurons for the maintenance of neurotransmission (Mergenthaler et al., 2013). This is supported by the enrichment of mitochondria at synapses where presynaptic vesicle recycling and postsynaptic sodium-potassium (Na^+ / K^+) ATPases hydrolyze ATP for the maintenance of electrochemical gradients and synaptic activity (Magistretti and Allaman, 2015; Mergenthaler et al., 2013). Additionally, energy-consuming clearance of neurotransmitters from the extracellular space by both neurons and glia can be severely impaired by low levels of ATP. Rapid loss of consciousness during Red Wing experiments could thus be a result of the shutdown of energy-

expensive cortical activity in the seconds following a precipitous drop in CBF (discussed in upcoming sections).

Beyond the rapid consequences to consciousness, early studies by Kabat and colleagues found that prolonged CBF arrest (≥ 8 minutes, using pressure cuff like the KRA apparatus) inevitably resulted in long term behavioral deficits or death in dogs (Kabat et al., 1941). In this model, follow up studies showed that brains subjected to ≥ 8 minutes of anoxia were further characterized by severe damage throughout most of the cerebral cortex, cerebellum, and brainstem (GRENELL, 1946). Although these early studies induced cerebral ischemia on a *global* scale, the immediate (~minutes) processes that occur are likely similar in brain regions during focal ischemia that are reliant on the blocked vasculature. This rapid development of neuronal injury residing near the occluded vessel(s) indicates that, by the time a stroke is confirmed in patients (often hours−days after onset), the initial core of an ischemic lesion is largely established and includes necrotic or unsalvageable tissue. Therefore, it is important that interventions target mechanisms of secondary injury to prevent the recruitment of neurons into the largely irreparable core of the infarction, when administered at later time points after ischemic stroke.

1.2.2 The ischemic cascade

In the 1950s the combined discoveries that glutamate elicited depolarization of neurons (CURTIS et al., 1959) and was toxic to cells led to the concept of injury induced by excessive excitation, or excitotoxicity (Lai et al., 2014). The discovery of excitotoxicity reshaped the stroke field and initiated development of drugs targeting key neurotoxic sequelae of ischemia on the cellular level. Today, it is largely accepted that excitotoxicity, commonly referred to as

the “ischemic cascade” in stroke research, is a fundamental mechanism behind neuronal death; as a result, extensive research focuses on targeting mechanisms that either limit glutamate and/or downstream effectors in the excitotoxic cascade (Lai et al., 2014; Wu and Tymianski, 2018), as described below.

1.2.3 Contributions of glutamate

In 1959, Van Harreveld reported the first link between glutamate toxicity and ischemic stroke damage by identifying the presence of glutamate in brain extracts taken a few minutes after circulatory arrest (Harreveld, 1959). Later work employing micro-dialysis techniques, revealed that after 10-minutes of complete cerebral ischemia in rats, extracellular glutamate had increased by 8-fold compared to baseline levels (Benveniste et al., 1984). Over the next two decades, multiple studies confirmed that glutamate rapidly increased in the brain after ischemia (Dawson et al., 2000; Mitani et al., 1990) and thus the development of drugs targeting this “first-responder” was thought to be the best strategy for improving stroke treatments.

1.2.4 Targeting glutamate release

In vivo glutamate release mechanisms including calcium (Ca^{2+})-dependent vesicular release (Drejer et al., 1985) and reversed operation of glutamate transporters (Rossi et al., 2000) have been proposed as primary mechanisms involved in excitotoxic glutamate accumulation. However, the relative importance of these different mechanisms depends on the *in vitro* model or degree of ischemia. In cultured cells, blockade of voltage-gated sodium (Na_v) channels using tetrodotoxin (TTX) inhibits vesicular glutamate release and also reduces neuronal death induced by hypoxia (Lai et al., 2014 and Smith et al., 1993). Thus, it was proposed that hyperexcitability and action potential mediated vesicular release (Benveniste et al., 1984;

Dawson et al., 2000) were mainly involved in neuron demise. This led to the development of drugs targeting synaptic release mechanisms, including Na_v blockers and N-type Ca^{2+} channel antagonists, which effectively reduced glutamate levels and was cerebroprotective *in vivo* when given prior to or shortly after (15-60min) experimental ischemia (Gaspary et al., 1994; Okiyama et al., 1995; Smith et al., 1993). Unfortunately, subsequent human trials with these new drugs, administered within a 12-hour treatment window post stroke onset, showed no significant improvement and/or had severe side-effects that prevented their progression beyond Phase II or III status (Lai et al., 2014, 2011).

In addition to synaptic glutamate release, impairment or reversal of glutamate uptake by neurons and glia has been proposed to contribute to ischemic cell death (Rossi et al., 2000). Excitatory amino acid transporters (EAATs) are located on both neurons and glia are are responsible for the clearance of extracellular glutamate from synaptic and extrasynaptic sites during neurotransmission. EAATs rely on the electrochemical gradient of largely Na^+, but also protons (H^+) and K^+, to move one molecule of glutamate into the cytosolic contents (three Na^+ and one H^+ in and one K^+ out) (Kandel, 2013). The massive disruption or complete breakdown of ionic gradients in hypoxic, ischemic, or other pathologic conditions (discussed in subsequent sections) may thus promote reversal of EAATs leading to glutamate accumulation and further excitotoxic effects. While further studies are needed to determine the role of EAAT-mediated glutamate accumulation in conditions of low ATP availability, current compounds that target EAATs also prevent essential synaptic and extrasynaptic clearance functions of these transporters and thus are not desirable for further trials in human stroke. Interventions designed to prevent only reverse transport, without preventing normal clearance, may hold some

promise for reducing glutamate and protecting rat hippocampal neurons from oxygen-glucose deprivation damage (Colleoni et al., 2008).

While the mechanisms and contributions of glutamate are not yet resolved, the above studies suggest that indeed glutamate does accumulate after ischemia and is in part mediated by vesicular release and/or reverse transport of EAATs. Additionally, they provide evidence that targeting glutamate release can be protective in cell culture and animal models. However, neuroprotection was highly dependent on the experiment of choice; including the duration of ischemia (or oxygen-glucose deprivation, OGD *in vitro*) and the time-course of drug administration (prior to or shortly after stroke onset and the duration of drug delivery). Furthermore, many questions remain with regards to the duration and localization of detected glutamate increases. In *in vivo* studies, glutamate levels were sampled on minute-to-minute time scales which lack sufficient temporal resolution and also provide very little spatial resolve—both of which may offer further insight into physiological mechanisms of the developing injury. Hints that alternative or additional processes are involved in excitotoxic neuronal demise after stroke lies in the unsettling disconnect and translatability of pre-clinical to clinical benefits of drugs targeting glutamate.

1.2.5 Contributions of calcium (Ca^{2+}) and NMDARs

Glutamate activates postsynaptic receptors causing depolarization primarily via influx of Na^{+}, which was initially believed to be the primary driver of excitotoxicity in response to glutamate exposure. This was initially supported by findings that glutamate exposure induced acute cell swelling in somata and dendrites, locations enriched with Na^{+} channels and characterized by substantial depolarization (Lai et al., 2014). However, it was soon realized that Na^{+} removal

during glutamate challenge *in vitro* completely prevented acute swelling but did not prevent cell death ~24 hours later (Choi, 1987).

In addition to Na^+-driven depolarization, ionotropic glutamate receptor activation (described below) can increase membrane permeability to the divalent cation calcium (Ca^{2+}) which serves as an important second messenger in many cellular processes across virtually all cell types. In neurons, increased intracellular Ca^{2+} concentration ($[Ca^{2+}]_i$) is not only essential for presynaptic transmitter release, but is also involved in postsynaptic activity-dependent gene expression, activation of Ca^{2+}-sensitive ion channel conductance, and other cellular functions. Due to the role of Ca^{2+} in many cellular processes, cytosolic Ca^{2+} levels are normally tightly regulated (in the low nanomolar range) via intracellular sequestration and extrusion processes. Evidence from cytotoxicity in non-neuronal tissues, including the heart, muscles, and liver largely converge on cytoplasmic and nuclear events initiated by intracellular Ca^{2+} (Lai et al., 2014). The connection between glutamate, Ca^{2+}, and neuronal death were noted *in vitro* following exposure of rat cortical neurons to excitatory amino acids, including glutamate. In these studies, glutamate exposure resulted in intracellular Ca^{2+} dysregulation and neuronal death (Berdichevsky et al., 1983). Of note, the glutamate analog *N*-methyl-$_{DL}$-aspartate (NMDA) was the most potent activator for increasing intracellular Ca^{2+} concentrations which in turn identified the NMDA receptor's (NMDAR) involvement in the excitotoxic injury process (Berdichevsky et al., 1983; Lai et al., 2014). Ensuing studies confirmed the role of intracellular Ca^{2+} entry *in vitro* by demonstrating that extracellular removal of this cation during glutamate exposure could prevent the occurrence of delayed cell death in the wake of substrate removal (Choi, 1987). These studies underscore Ca^{2+} influx and identify ionotropic

glutamate receptors, namely the NMDAR, as key mediators of excitotoxicity along the ischemic cascade.

The majority of excitatory neurotransmission is mediated by glutamate and its target metabotropic and ionotropic receptor families. There are three main families of ionotropic glutamate receptors including α-amino-3-hydroxy-5-methyl-4-isoxazole propionic acid (AMPA), kainate, and NMDA receptors containing GluN1, GluN2A-D, and GluN3A-B subunits. Compared to other glutamate receptors, the NMDAR has unique biophysical properties thus positioning these channels as noteworthy mediators for numerous neuronal processes. Exemplifying their fundamental role in proper brain function, NMDAR hyper or hypo-activation is implicated in a multitude of disease states including Alzheimer's disease, depression, schizophrenia, other neurological disorders, as well as excitotoxic injury mechanisms.

In conditions of energy depletion, insufficient pumping of Na^+/ K^+ against their electrochemical gradients causes neuronal depolarization and neurotransmitter release, including glutamate. These "excitotoxic" conditions set the stage for increased NMDAR cation permeability that requires ligand-binding and relief of magnesium (Mg^{2+}) blockade from within the channel pore. Opening of NMDARs is thus accomplished via depolarizing Na^+ influx, (e.g. through AMPARs, and other cation/ Na^+ permeable channels) which liberates Mg^{2+} from the NMDAR channel only when glutamate and co-agonist (i.e. D-serine/glycine) are both present. While NMDARs are nonselective cation channels, they are distinctively highly permeable to Ca^{2+} and thus crucial intermediaries of activity-dependent cellular tasks

like hippocampal-dependent learning, for example. Furthermore, recent studies have shown that NMDARs can exert metabotropic functions via their C-terminal cytosolic domains, capable of recruiting "death complexes" of proteins (Tu et al., 2010) even when Ca^{2+} influx is prevented (using potent NMDAR antagonists like MK-801, described next) (Weilinger et al., 2016).

MK801 is an uncompetitive NMDAR antagonist that has been widely studied and consistently demonstrated to serve neuroprotective roles by reducing infarct expansion after ischemia and preventing neuronal death *in vitro* (Lai et al., 2011). However, like the failure of drugs targeting glutamate release mechanisms, clinical testing of NMDAR antagonists (especially competitive antagonists) was unsuccessful. In addition to the development of severe side-effects that included nausea, vomiting, cardiovascular, and psychomimetic effects (Wu and Tymianski, 2018), NMDAR blockade was also associated with increased mortality resulting from infarction in acute ischemic stroke patients (Lai et al., 2014, 2011).

While initial translation failures of drugs targeting excitotoxic mechanisms after stroke in humans are multi-factorial (Gladstone et al., 2002), it is largely believed that these failures are due to the pathophysiology of glutamate release during the proposed ischemic cascade. Specifically, it is widely assumed that glutamate release occurs *only* in rapid succession (minutes) following occlusion onset and thus has already activated NMDAR-mediated cell death signaling cascades by the time a patient arrives at the hospital (Lai et al., 2014; Wu and Tymianski, 2018). Another train of thought emerging from failed clinical tests developed alongside modern techniques in animals identifying and elucidating distinct NMDAR subtypes

and their role in opposing cellular processes. This suggests that complete and nonspecific blockade of NMDARs may actually be detrimental to normal neuronal function as well as survival and repair mechanisms essential for brain recovery after injury (Wu and Tymianski, 2018). Combined with prior assumptions about glutamate time courses, the major focus of pre-clinical stroke research has shifted neuroprotective efforts towards identifying and targeting specific intracellular signaling cascades to either enhance cell survival and/or inhibit cell death pathways that are downstream of NMDAR activation. These efforts are important for the development of specific interventions with less side-effects as well as clarifying steps in the death process of neurons. However, given that ischemic stroke patients with worsening injury still have elevations in glutamate in their CSF (Berdichevsky, 1983) observations that substantial brain injury can still progress over a period of days or more in some individuals; the assumption that excitotoxicity has ran its course by the time a patient reaches the hospital may be incorrect.

1.3 Spreading depolarization (SD): a new target for stroke intervention

Over the last four decades studies in animals and humans have revealed important excitotoxic factors that contribute to rapid brain injury upon loss of metabolic substrate supply. However, only relatively recently has detection of a long-known, but usually ignored physiological phenomenon emerged as an important contributor to human brain injury (Dohmen et al., 2008; Dreier et al., 2006; Fabricius et al., 2006; Strong et al., 2002). This phenomenon called *spreading depolarization* (SD) is characterized by many cellular disruptions discussed previously under the umbrella term of "excitotoxicity," and could thus be an important new candidate for neuroprotective strategies.

1.3.1 SD Terminology

Over the course of this dissertation project, coordinated efforts by the COSBID consortium have been underway with a main goal of refocusing and uniting investigators in the SD field (Hartings et al., 2017). Since Leão's initial reports of SD conducted in 1944-1947, a growing division amongst researchers seems to have been exacerbated by terminology. As discussed previously (see Introduction), Leão described the phenomenon of SD as a "spreading depression" that can be initiated in the healthy cortex, as exemplified by migraine aura. Subsequent work examining brain physiology after stroke, asphyxiation, cardiac arrest, or other injury demonstrated that cortical depression after SD is less obvious or even absent (due to the loss of cortical potentials shortly after ischemia *in vivo*). This led to the development of terms like: "anoxic depolarization" (describing SD that occurred in response to complete substrate deprivation, like anoxia or OGD) and "peri-infarct depolarization" (SDs that erupted along the rim of an infarcted brain region). While these terms did provide insight into the conditions that initiated SD, they divided investigators in the field with regards to mechanisms of SD in different brain states. As such COSBID promoted the idea that massive tissue depolarization and resulting consequences occur along a continuum and depend on the metabolic status of tissue in which events propagated (Hartings et al., 2017). In this dissertation, *spreading depolarization* has will be used to describe the overall phenomenon of SD, but this terminology can also be used with specific modifiers that provide more information. Examples include *transient* (SDs that are short-lasting and do not cause damage), *prolonged* (SDs that are longer in duration and may indicate underlying tissue dysfunction), *persistent* (depolarization that does not recover until conditions change) or *terminal* (depolarization that cannot recover and indicate tissue injury). These modifiers have been

described in a recent review by COSBID (Hartings et al., 2017) in hopes of unifying the field of SD researchers and are thus used throughout this dissertation work.

1.3.2 Spreading Depolarization (SD)

SD is a slowly progressing (in mm min^{-1}) wave of depolarization that occurs with high incidence after stroke, acute brain injuries, and during migraine. Originally described as "spreading depression," SD was discovered in 1944 by the Brazilian neurophysiologist Aristides Leão while examining seizure activity in the rabbit cortex (Leao, 1944). In this initial report, Leão applied a local stimulus to the exposed brain and, instead of eliciting a seizure, observed depression of cortical activity in the alternating current (AC) range (> 0.5 Hz) that progressed in a spreading fashion and enveloping in all directions from the stimulated region. In follow-up studies, Leão noted the same spreading depression in response to asphyxiation and hypothesized that this phenomenon could play a role in pathologies including cerebral ischemia and migraine (LEAO, 1947; Leao and Morison, 1945). Indeed, Leão noted a large extracellular depolarization a*fter* non-spreading suppression of cortical activity in the ischemic cortex. Today, we know that Leão's "spreading depression" of spontaneous and evoked activity is one *consequence* of spreading depolarization ((Hartings et al., 2017).

Mounting evidence suggests that SD could be an evolutionary conserved and/or an intrinsic property of nervous tissue that is tightly packed, though further studies are needed to confirm this notion. Thus far, SD has been detected in gray matter in vertebrates (amphibians, birds, and mammals) and invertebrates alike. In vertebrates, central nervous system (CNS) structures including the cortex (Leao, 1944), hippocampus (Müller and Somjen, 2000) brain stem (Karunasinghe and Lipski, 2013), spinal cord (van HARREVELD, 1946; HARREVELD and

HAWES, 1946), striatum (Bureš and Hartman, 1967), and retina (Gorelova and Bures, 1983) all support propagation of the SD wave. Depending on the tissue cytoarchitecture (e.g. glia-to-neuron and intra- to extracellular space ratios, energetic demands of different cell types, capillary support, etc.), certain brain regions are more sensitive or resistant to SD initiation and/or propagation. This variability in brain region vulnerability to cerebral oxygen and/or glucose deprivation was seen in many studies prior to Leão's observations of SD following ischemia in 1947. In a review by Hoff et al. in 1945, authors highlighted that similar cellular changes were observed in the brain across seemingly different causes of death (i.e. ischemia, anoxia, asphyxia, hypoglycemia, etc.), and that life-supporting brainstem centers (e.g. medulla) were more resistant while cognitive areas (cortical layers) were extremely susceptible to histopathological injury (HOFF et al., 1945). Perhaps this variable susceptibility to hypoxia-induced injury is related to changes in SD threshold across cytoarchitecturally different central nervous system (CNS) tissues.

Most studies have examined SD and its consequences in the context of injury. In the past decade, SD has been implicated as a causal event leading to the development of macular degeneration in the retina ((Yu et al., 2012). Mice with *Kv1.1* or *Scn1a* mutations (K^+ and Na^+ channel mutations, respectively) are prone to seizure-induced death via SD-initiation in the life-supporting centers in the brainstem. This relates to patient cases of sudden unexpected death in epilepsy (SUDEP) (Aiba and Noebels, 2015) and perhaps brainstem SD is involved in other disorders such as sudden infant death syndrome (SIDS). In the above cases, retina and brainstem SD are clearly implicated in tissue deterioration and/or death, however consequences of SD are not always detrimental to organisms. For example, in locusts SD has

been observed in the metathoracic ganglia and shuts down ventilatory central pattern generator (GCP) center activity that is responsible for ventilation. In this instance, respiratory depression after SD does not cause death but instead may serve as a potential survival mechanism for inducing coma in locusts in response to noxious stimuli (e.g. hypo- or hyperthermia, anoxia). The global reduction in the animal's metabolic rate preserves energy until the stimulus is removed (Rodgers et al., 2010, 2007). This supports the idea that not all instances of SD cause injury and/or indicate the presence of injured tissue; instead, SD could serve as a mechanism for suppressing neuronal over-excitability (as in seizure) or reducing metabolic expenditure in environments of possible injury (such as drowning or cardiac arrest).

1.3.3 SD initiation and propagation

There are numerous types of stimuli that can initiate SD in the CNS including electrical stimulation (Leao, 1944), ischemia (LEAO, 1947; Leao and Morison, 1945), chemical application (Leao and Morison, 1945), hypoxia (HARREVELD and HAWES, 1946), and others; therefore there has been much debate regarding contributions of K^+ and/or glutamate for SD induction (Somjen, 2001). However, Van Harreveld's "dual hypothesis" which incorporates both K^+ and glutamate's excitatory effects on neurotransmission to be main contributors involved in SD initiation and propagation is now usually accepted (van Harreveld, 1978; Hartings et al., 2017; Pietrobon and Moskowitz, 2014). Thus, extracellular K^+ elevations, activation of voltage-gated Na^+ and Ca^{2+} channels, presynaptic and regenerative glutamate release, and NMDAR activation are all thought to participate in propagation of depolarizing currents and feedforward extracellular accumulation of K^+ and glutamate during SD (Zhou et al., 2013). The relative contributions of K^+ and glutamate likely depend on the physiological or pathological inciting stimulus, as demonstrated by studies that pharmacologically

manipulate extracellular levels of K^+ or glutamate. For example, reducing action potential dependent glutamate release (using TTX, described previously) as well as NMDAR antagonists can prevent electrical stimulation induction of SD but are ineffective at blocking SD induced by ischemia (modeled as oxygen-glucose deprivation, OGD *in vitro*).

While many studies have focused on elucidating cellular mechanisms involved in SD initiation, reviewed in (Pietrobon and Moskowitz, 2014), it is likely that set of stimuli that converge on the synchronous depolarization of a critical volume of excitable tissue (Tang et al., 2014) can ignite SD. Propagation of SD is also likely influenced by the state of brain tissue and the intrinsic (e.g. genetics) and extrinsic (e.g. injury) factors that govern cortical excitability. Therefore, while the concentrations of extracellular K^+ required to trigger SD are around ~10-12 mM (Heinemann and Lux, 1977), tissue propensity for SD induction after ischemia is not only species-dependent (Nakamura et al., 2010) but also may vary from one individual to the next (as suggested by clinical data in (Dohmen et al., 2008; Woitzik et al., 2013)).

1.3.4 Ion changes during the DC shift

A hallmark of SD is the presence of a large shift in the extracellular slow direct current (DC; < 0.1 Hz) or near-DC potential (< 0.5 Hz) and was first described by Leão in 1947 (LEAO, 1947). At the onset of SD, increases in membrane permeability outmatch ATP-dependent processes involved in electrochemical gradient maintenance and results in net inward current and depolarization of neurons (Dreier, 2011; Somjen, 2001). This breakdown of ionic gradients combined with changes in tissue resistance changes give rise to the large (>2 mV) extracellular DC potential shift that can last for minutes or longer (Somjen, 2001). The extent of electrochemical gradient breakdown during SD is massive and results in near-complete

depolarization of neurons and glia (Somjen, 2001, 2002). In comparison, electrochemical gradients remain largely intact during normal synaptic communication where depolarization lasts on the order of milliseconds.

Historical debates have existed regarding mechanisms (as mentioned previously) and the relative time course of specific depolarizing currents during SD in different experimental models (i.e.SD in healthy versus compromised CNS tissues) and is beyond the scope of this dissertation work. However, there is consensus in the field that, regardless of the method used to generate SD, there are fundamental (and massive) ionic changes that are largely time-locked with the onset of the DC shift (but can outlast it) and variations in these mechanisms represent characteristics of SD along a continuum (Hartings et al., 2017). While exact measurements of ion concentrations are difficult due to technical limitations and the influence of intra- and extracellular volume changes during SD, disruption in Ca^{2+}, K^{+}, Na^{+}, H^{+}, Cl^{-}, HCO_3^{-} ion homeostasis have all been observed during SD (Hartings et al., 2017; Somjen, 2001). In general, SD is characterized by a sharp surge in extracellular $[K^{+}]_e$ (from ~3 to 40-75mM), and concomitant reductions in interstitial $[Ca^{2+}]_e$ (from 1.3 to <0.1mM), $[Cl]_e$ (from ~150 to 95mM), and $[Na^{+}]_e$ (from ~150 to ~60mM) (Hartings et al., 2017). The bulk changes in extracellular (and intracellular) ion concentrations (Table 1.1) are enabled by substantial increases in membrane permeability of neurons (and astrocytes) and thus contribute to depolarization during the DC shift of SD.

Table 1.1. Electrochemical gradient breakdown during SD (in paretheses) compared to baseline

Ion	Extracellular concentration (mM)	Intracellular concentration (mM)	Equilibrium potential[#] (mV)
[ac]Na^+	145-150 (~60)	10-12 (35)	+67
[bc]K^+	3-5 (40-75)	130-155 (~120)	-98
[cd]Ca^{2+}	1.3-1.5 (<0.1)	100 nM (~30μM)	+129
[acd]Cl^-	123-150 (95)	~4 (~100)	-90

[#]calculated from Nernst equation using 37°C. Resting concentrations based off calculations in Hille, 2001.

1.3.5 Metabolic demand of SD

Restoration of electrochemical gradients after SD requires tremendous ATP consumption, and the effectiveness of recovery is strongly influenced by underlying tissue metabolic status. Even in the well-perfused brain, activation of ATP-dependent pumps reset SD-induced ionic disturbances and results in ~50 – 70 % reduction of tissue ATP levels (Mies and Paschen, 1984; Takano et al., 2007), in some studies. Based on experimental evidence, recent calculations of Gibbs free energy release during electrochemical breakdown suggest that SD is the "largest disruption of homeostasis that is possible in living neural tissue" (Dreier et al., 2017; Dreier and Reiffurth, 2015), even more energetically demanding than seizures. This energetic burden can be met by increased cellular metabolism and increased delivery of oxygen and glucose (via cerebral perfusion *in vivo*) and thus does not cause permanent or overt neuronal injury (Harreveld, 1958; Nedergaard and Hansen, 1988) inn otherwise uninjured brain. On the contrary, in the injured human brain, spontaneous induction of SD (initiated by trauma or ischemia) has been shown to cause step-wise reductions in tissue glucose levels (indicative of increased metabolic demand) as well as corresponding increases in metabolic

byproducts (i.e. lactate) and further disruption of extracellular ion concentrations (i.e. K^+) (Rogers et al., 2016). This indicates that SD consequences are greatly influenced by the ability of brain tissue to meet energetic demands imposed by SD.

Previous work has demonstrated substantial changes in metabolic substrates and/or byproducts are time-locked with SD – versus gradual changes over time; and include increased glucose utilization (Mies and Paschen, 1984a; Takano et al., 2007). Protons (H^+) and lactate production (Kocher, 1989) and corresponding depletion of tissue O_2 (Takano et al., 2007) and glycogen stores (Seidel and Shuttleworth, 2011). These measurements indicate a high level of metabolism which can lead to (in some studies) a massive drop in cellular ATP concentrations (Mies and Paschen, 1984b). In the non-injured brain, these changes are transient and the only noticeable consequence to neurotransmission is the long-lasting cessation of brain activity that was originally described by Leão (Leao, 1944). Mechanisms of suppression during the large depolarization of SD include collapse of ion gradients and Na^+ - channel inactivation resulting in depolarization blockade (Kager et al., 2000). However, suppression of activity lasts longer (typically > 5 min) than the duration of depolarization and thus indicates the presence of other mechanisms that limit neuronal activity. More recently, it was found that a major metabolite of ATP breakdown, adenosine, is a key mediator of neuronal suppression after SD (Lindquist and Shuttleworth, 2012, 2016).

The majority of ATP consumption during SD likely results from the pumping activity of Na^+/K^+ ATPases that must rapidly hydrolyze ATP in order to counteract cation influx and recover resting membrane potentials. However, ATP-dependent Ca^{2+} buffering processes and

synaptic vesicle replenishment also add to ATP consumption after SD. All this ATP utilization can be monitored downstream via the production of adenosine levels that increase in a similar trajectory to other metabolic products, described above. During these processes ATP breakdown results in the production adenosine monophosphate (AMP) that can be further metabolized by 5' nucelotidases to form adenosine (Frenguelli, 2017). Accumulation of extracellular adenosine can then modulate neurotransmission via activation of adenosine 1 receptors (A_1R) which are highly expressed in the rodent brain (Dixon et al., 1996) and are located on both pre-and post-synaptic membranes (Boison et al., 2013). Coupling of A_1Rs to G-proteins inhibits the production of cyclic AMP (cAMP) which has downstream consequences of reducing synaptic release of most neurotransmitters, including glutamate. Evidence that A_1Rs are activated in response to SD is provided by experiments using the specific A_1R antagonist (DPCPX) that was found to greatly accelerate postsynaptic responses after SD in mouse brain slices and *in vivo* (Lindquist and Shuttleworth, 2012, 2014).

In metabolically compromised brain slices or after distal middle cerebral artery occlusion (dMCAo) in mice, adenosine accumulation during SD is pronounced compared to levels following SD in healthy brain tissue (Lindquist and Shuttleworth, 2014). In studies by Lindquist and Shuttleworth, SD-induced adenosine signals were again correlated with the duration of suppression of evoked and spontaneous cortical activity *in vivo*. Results from these studies further indicated that real-time energy production via glycolysis and oxidative phosphorylation greatly influenced the amount of adenosine that accumulates. Therefore, the duration of A_1R-mediated suppression of activity likely relates to the metabolic burden and the amount of ATP consumed for tissue recovery after SD. This is also indicated in humans

(discussed below) where worsening brain injury is characterized by progressively longer recovery of times cortical activity monitored using electrocorticography (ECoG) techniques (Hartings et al., 2017). Adenosine accumulation or the duration of A_1R-mediated suppression can thus serve as a read-out of SD metabolic burden.

1.3.6 SD in the human brain

As noted above, throughout Leão's investigation of SD, he hypothesized that SD may play an important role in human physiology including migraine, ischemia, and seizures (LEAO, 1947; Leao, 1944; Leao and Morison, 1945). However, it was not until 1977 that SD was first recorded in humans during stereotaxic brain surgery for focal epilepsy (amka et al., 1977). In this study, Sramka and colleagues saw that SD could be induced by KCl infusion into the caudate nucleus or hippocampus of humans, and the ensuing suppression of cortical activity after SD was considered diagnostically useful for "functional ablation" during epilepsy neurosurgery. Despite subsequent confirmation of SD in human brain slices, showing properties apparently identical to those well described in rodent tissues (Avoli et al., 1991; Petzold et al., 2005), the relevance to human physiology remained unclear until advancements in imaging and recording techniques enable detection of SD in the 2000s.

Evidence that SD was involved in migraine came prior to Leão's initial description by Karl Lashley in 1941 (LASHLEY, 1941). In documenting the spread of his own migraine aura across his visual cortex Lashley, unknowingly at the time, revealed a striking similarity to the slow rate of spread of SD. However, it was not until 2001 that the propagating blood flow response to SD was visualized using functional MRI (Hadjikhani et al., 2001). Today it is

becoming more generally accepted that SD in the adequately perfused visual cortex of migraine patients can manifest as a "scintillating scotoma" (LASHLEY, 1941) where excitatory transmitter release at the SD wave front is followed by depression of activity, both of which may contribute to visual acuity changes during aura.

It took 25 more years from its initial detection in humans, and close to 60 years from Leão's original description, to unequivocally electrically record spontaneous SDs in the injured human cortex by Anthony Strong and colleagues (Strong et al., 2002). This report changed the landscape for SD researchers and hinted that this phenomenon could play a large role in injury progression. A year later, SD investigators joined forces and formed the Co-Operative Studies on Brain Injury Depolarizations (COSBID) collaboration, with a mission to reveal the relevance of SD to human brain injury. Over the next 15, large research efforts organized by the COSID consortium have led to the identification of SD using subdural ECoG strip electrodes in a range of acute neurological conditions. From these intraoperatively placed strips, the SD hallmarks of a propagating shift in DC potential accompanied by suppression of high frequency activity has been recorded in 70-80% of aneurysmal subarachnoid hemorrhage patients (Dreier et al., 2006), 50-60% of severe traumatic brain injury (TBI) patients (Eriksen et al., 2019), and 60-70% of patients with intracerebral hemorrhage (Fabricius et al., 2006). Importantly, SD has been detected in nearly all patients with malignant hemispheric stroke (Dohmen et al., 2008; Woitzik et al., 2013).

1.3.7 SD after ischemic stroke

A little over ten years ago, Dohmen et al. and the COSBID group demonstrated that 1) SD occurs in high incidence in the human cortex after focal stroke and 2) SDs that occur in

temporal clusters were associated with poor ECoG recovery and further tissue deterioration (Dohmen et al., 2008). In the 16 patients included in this study, all had infarction of MCA that required decompressive brain surgery to avoid further intracranial pressure (ICP)-related injury. During surgery, investigators evaluated ECoG recordings from electrode strips placed near the infarct in viable penumbral tissue. Recordings began anywhere from 13 to 109 hours after individual stroke onset, and SD was detected in all patients that had ECoG strips located over peri-infarct brain regions. In the two patients without detectable SDs, ECoG strip were located over ischemic core regions and thus non-viable tissue. This indicates that SDs are occurring primarily in metabolically vulnerable tissues for days after stroke onset and during time periods of injury progression observed in CT scans.

1.3.8 SD incidence and relationship to injury progression

Prior to SD detection in the human stroke brain, it was generally assumed that spontaneous SDs occurred only up to 6 hours after occlusion in animal stroke models which suggested that the majority of cell death and infarct maturation manifesting at later time points (~24 hours) was due to other mechanisms, suggested by (Hartings et al., 2003). However, foundational work by Hartings et al. in 2003 revealed that, following permanent and transient MCAo, spontaneous SDs persisted through 24 hours after injury in the rat cortex (Hartings et al., 2003). Prolonged ECoG recordings further revealed that SD frequency increased in the acute hours (~ 6 hrs.) and again ~12 hours after stroke onset. Importantly, SDs were detected throughout lesion development (~24 hours) as measured by the loss of TTC staining over this same time period. Not only did this study highlight the connection between SD and stroke injury maturation, but also showed the ability of NMDAR-antagonists (Con-G; selective for NR2B-containing NMDAR subtypes) to limit infarct expansion when administered intrathecally

during this phase of secondary SD frequency increases (1 bolus) hours after stroke injury (administered ~8 hr. post MCAo).

1.4 Reevaluating mechanisms of the ischemic cascade in the context of SD

1.4.1 Rapid consequences at onset of ischemia

Early studies examining cell death processes at the initial onset of ischemia likely missed SD due to the lack of physiological techniques capable of detecting SD at the time. In 1932 Edgar Adrian and Sir Charles Sherrington shared the Nobel Prize for Physiology for the first recordings of neuronal electrical discharges; and the first recordings of cortical activity during cerebral anoxia in animals were being reported around this time (Sugar and Gerard, 1938). In these early studies by Sugar and Gerard, they noted that cortical activity recorded in the cat motor cortex was nearly absent within 10-20 seconds of bilateral carotid occlusion (Sugar and Gerard, 1938). Later studies defined cortical potentials in terms of blood flow where widespread suppression of cortical activity (observed in the 0.5-70Hz range of electrocorticography) developed (again within ~10-20s) upon the reduction of CBF below the threshold of 15-23 ml/100g/min (Hartings et al., 2017). If CBF is further limited to 5-10ml/100g/min, the suppression of cortical responses is inevitably followed (~2-5 min.) by massive tissue depolarization (Hartings et al., 2017) that can only be electrically recorded in the slow potential range. Importantly, these electrophysiologic consequences were noted in Leão's experiments in the rabbit cortex following global arrest of CBF (LEAO, 1947; Leao and Morison, 1945) where he demonstrated that, if ischemia was continued beyond the development of isoelectric cortical potentials, it was followed (~2-5 min. after occlusion) by the large DC potential shift indicative of SD. In these experiments, the negative voltage shift during SD lasted for the duration (up to 12 minutes) of circulation arrest (LEAO, 1947). This

may indicate that the rapid and damaging cellular consequences of the ischemic cascade are closely connected with SD, that erupts within minutes of stroke onset.

Whether or not injury results from SD in animal models is likely dependent on multiple related factors, but low cerebral blood supply is an obvious contributor to vulnerability (Dreier et al., 2018; Hartings et al., 2017). During the infamous Red Wing experiments in humans (mentioned previously) there was rapid loss of consciousness (4-10s) following pressure-induced occlusion of CBF but there were no overt signs of injury— perhaps because CBF arrest was not continued beyond 100s (Rossen et al., 1943) and thus likely did not trigger SD. It is interesting to note however, that one patient with a clinical history of migraine, did experience what he described as a migraine aura, perhaps due to increased SD susceptibility. In the context of studies that were being conducted in dogs also during this time (see above), the findings that only global CBF arrest lasting more than >8 minutes caused permanent behavioral deficits (or death) and/or pathological changes in neurons (GRENELL, 1946; Kabat et al., 1941); speculatively this could be due to the presence or absence of SD. In support this idea (and the critical role of SD in the induction of injury in the injured brain), experiments conducted in rats found that, in the absence of SD, severe focal ischemia (below 10% of baseline) did not itself result in histological pathology (Kaminogo et al., 1998). These results indicate that SD erupts following ischemia onset and the duration of electrochemical failure during SD and the overall capacity for tissue to increase blood supply to the affected region are main factors that contribute to brain death (Dreier et al., 2018; Hartings et al., 2017). These factors are likely important during subsequent SDs that initiate during the secondary phase of infarct maturation and increased SD frequency (Hartings et al., 2003). Such SDs have been

shown to ignite along the penumbra-core border (Nakamura et al., 2010; Strong et al., 2006) and can be due to pathological K^+ elevations (Petzold et al., 2005) or in response to supply-demand-mismatches (von Bornstädt et al., 2015).

Key experiments that further linked SD to secondary injury after ischemia were conducted by Busch and colleagues in 1996 (Busch et al., 1996). Here, SD was induced via repeated topical application of K^+ on the cortical surface after MCAO in rats and infarct expansion was monitored using DWI-MRI over this time. When compared to control animals, lesion expansion occurred in a step-wise fashion, with each additional SD confirmed by DC shifts in electrophysiological recordings. Furthermore, administration of the NMDAR antagonist MK801 blocked SD and prevented the expansion of ischemic injury. NMDAR antagonists can (in some instances) prevent SD initiation (discussed below) and could indicate that the ischemic cascade may be due primarily to excitotoxic mechanisms that are time-locked with, and caused by SD.

1.4.2 Mechanisms of injury during SD

A. The role of glutamate

As discussed above, decades of work have made a clear connection between glutamate and the induction of neuronal injury. In early work the ~ 8-fold increase in extracellular glutamate measured within ~ 10 minutes of global anemia (Benveniste et al., 1984) could be due to glutamate release during SD. Indeed, studies using micro-dialysis to measure interstitial glutamate levels found that it was not increased immediately after cardiac arrest in rats and did not increase until the onset of SD (confirmed by the presence of the DC shift) ~10 minutes after CBF arrest (Fabricius et al., 1993). Recently, it was demonstrated that upon occlusion of

the middle cerebral artery (MCA) there was an immediate ~60% *decrease* in extracellular glutamate that corresponded to the non-spreading loss of spontaneous cortical activity (i.e. > 0.5Hz range) (Hinzman et al., 2015). In that study, use of microelectrode glutamate arrays again tied glutamate with SD onset in the core region of the stroke.

Synaptic release appears to be a significant contributor to extracellular glutamate accumulation during SD and was demonstrated using the Zn^{2+}-sensitive fluorescent reporter (FluoZin3) (Carter et al., 2011). Zn^{2+} imaging enables indirect monitoring of vesicular transmitter release, as the cation Zn^{2+} is co-packaged into glutamatergic presynaptic vesicles via the ZNT3 transporter (Cole et al., 1999). Utilizing FluoZin3 fluorescence as a surrogate read-out of synaptic glutamate release (Qian and Noebels, 2005), studies in brain slices (using K^+ microinjection for SD initiation) demonstrated that episodic glutamate release occurred only in tight relationship to SD (Carter et al., 2011). Additionally, oxygen-glucose deprivation (OGD) triggering of SD in this study showed fluorescence increases only upon onset of electrochemical failure (DC shift). These studies provide further evidence that glutamate increases only in synchrony with SD in the aftermath of stroke.

In order to intervene with glutamate-mediated toxicity in ischemic core region, therapies would need to be preventative and/or administered almost must begin immediately after infarction in order to protect neurons, an approach likely not suitable for the vast majority of ischemic stroke patients. While this may suggest that indeed glutamate-mediated excitotoxicity is over by the time a patient reaches the hospital, animal and human studies have shown that SDs can still occur days after initial ictus. SDs could theoretically explain why clinical testing of glutamate-

targeting drugs were unsuccessful—i.e. interventions were administered too late to prevent initial injury in the core and stopped prior to secondary infarct maturation during the delayed phase of increased SD incidence. Therefore, studies are still needed to identify cellular mechanisms that can be targeted in order to limit excitotoxic consequences during SD in the injured brain.

Subsequent microelectrode recordings strongly support the idea of time-locked glutamate accumulation, strictly matching SD. Enzyme-coated microelectrodes had a much higher time resolution than previous microdialysis methods and allowed clear demonstration of glutamate kinetics during single SDs after focal ischemia. In addition to examining SD onset in the first minutes of occlusion, spontaneous SDs igniting from penumbral regions of the MCA watershed are also temporally locked with increases in glutamate signals; the duration of which positively correlate to the duration of nearby recorded DC shifts (Hinzman et al., 2015). Moreover, brain regions proximal to the occlusion site exhibited prolonged and/or terminal SDs that were associated with long-lasting glutamate signals (>300 seconds). These studies provide a compelling link between glutamate toxicity and SD in animal stroke models and suggest that these periods of excitotoxicity may also be important contributors to injury in human ischemic stroke.

There is evidence that increased glutamate levels persist during infarct maturation in acute ischemic stroke patients. Using micro-dialysis to measure CSF glutamate content over 24-48 hours after infarct onset, Davalos and colleagues identified elevations of transmitter in patients with progressing, but not stable, ischemic stroke (Dávalos et al., 1997). However, likely due

to unsuccessful clinical trials at the time of this study (mentioned previously), this report also acknowledged that the ischemic cascade could still be "fully triggered" at the time points monitored (Dávalos et al., 1997). Glutamate elevations could have thus been interpreted as a reflection of more severe-grade lesions; as such, interventions pursuing glutamate release in progressing stroke patients were not well justified. However, since SDs have been detected in most patients with progressing infarction (using subdural electrodes placed during neurosurgical procedures), SD could theoretically underlie CSF glutamate increases from prior studies. This suggests that discrete and infrequent periods of ongoing SD-mediated glutamate excitotoxicity mediate delayed lesion development after stroke. Studies that examine mechanisms of extracellular glutamate accumulation are thus necessary in order to reduce deleterious consequences of SD and widen therapeutic opportunities after ischemic stroke.

B. The role of NMDARs and Ca^{2+}

Neuronal ion gradients remain largely intact during normal physiological activity and thus intracellular Ca^{2+} levels are maintained in the low nanomolar range. During SD, altered ion channel conductance and increased permeability to Ca^{2+} can lead to marked decreases in extracellular Ca^{2+} concentrations, measured using ion-sensitive electrodes, and is presumably due to substantial influx into neurons (Somjen, 2001). This was confirmed in brain slice preparations using single cell loading of a low-affinity organic indicator (Fura-6F) to estimate intracellular Ca^{2+} load in hippocampal pyramidal neurons (Dietz et al., 2008). In this study, it was estimated that intracellular Ca^{2+} concentrations can reach ~10 – 25μM in neurons during SD (initiated by K^+ microinjection) but do not cause injury in healthy brain slices. However,

irrecoverable neuronal Ca^{2+} loading was observed during SD induced by OGD (Dietz et al., 2008).

Follow-up studies demonstrated that NMDAR-mediated cation influx during the late-phase of the DC shift was a main contributor to irrecoverable Ca^{2+} loading and acute injury during SD in metabolically compromised neurons (induced by brief dialysis of neurotoxic sodium azide) (Aiba and Shuttleworth, 2012). As described previously, the voltage-dependence of NMDARs is conferred by Mg^{2+} block within the ion channel pore that reduces open channel probability until the presence of coincident depolarization and glutamate (and co-agonist D-serine or glycine) binding (Retchless et al., 2012). Massive postsynaptic depolarization combined with significant increases in presynaptic glutamate release during SD thus produce the ideal conditions for sustained opening of NMDARs (Aiba and Shuttleworth, 2012). This late component of SD-mediated Ca^{2+} dysregulation is an important contributor to acute injury as focal application of the competitive NMDAR antagonist APV can alleviate intracellular Ca^{2+} accumulation during SD and prevent acute indicators of neuronal injury (Aiba and Shuttleworth, 2012). These studies highlight that targeting intracellular Ca^{2+} loading is a potential neuroprotective strategy for limiting deleterious consequences of SD in metabolically compromised brain.

1.5 Potential beneficial outcomes of SD

While this section focuses largely on adaptive mechanisms in the brain that have been shown to reduce injury after stroke, it is important to note that SD has been implicated in not only

protective preconditioning (described below) but many other processes that may be beneficial to functional recovery after stroke (Dreier, 2011; Nakamura et al., 2010).

1.5.1 Concept of conditioning

A well-studied strategy for eliciting protection or tolerance against ischemia-induced damage is the concept of conditioning. Conditioning refers to protective mechanisms that occur in response to the application of a detrimental stimulus that is below the threshold of initiating cell death (Shen et al., 2016; Zhao, 2009). There are many stimuli capable of inducing tolerance including hypoxia, ischemia, anesthetics, inflammatory mediators, hypo- and hyperthermia, sleep deprivation, and SD (Dirnagl et al., 2003; Pincherle et al., 2018; Shen et al., 2017). Additionally, since cell death signaling cascades can be similar in many cell types tolerance can be induced by one trigger and provide protection against other insults (i.e. cross-tolerance) (Dirnagl et al., 2003). In general, there are two main types of conditioning: pre- and post-conditioning. Preconditioning refers to tolerance mechanisms initiated prior to injurious stimulation, while postconditioning can be induced up to two days after prior insult (Burda et al., 2009; Zhao, 2009).

1.5.2 Preconditioning

Experiments on conditioning began in the 1950's and largely focused on ischemia-reperfusion injury in the heart (SEWELL et al., 1955). Early studies in dogs identified that brief ischemic events protected the myocardium from subsequent prolonged ischemia (Murry et al., 2018), thus generating the concept of protection induced by *pre*conditioning. In these studies, ischemic preconditioning was found to delay cell death after myocardial infarction and increase the volume of salvageable tissue during reperfusion therapies (Meldrum, 1997; Murry

et al., 2018). Over the course of the next few decades, extensive research into the cellular mechanisms that confer protection to the heart led to clinical trials applying ischemic preconditioning for myocardial protection prior to planned cardiac surgical procedures or in adjunct with reperfusion therapies (Dirnagl et al., 2003; Iliodromitis et al., 2007; Thijssen et al., 2016; Yellon and Dana, 2000).

Preconditioning in the brain was reported as early as 1964 in a report by Dahl and colleagues. In that study, pre-exposure to anoxia enhanced survival times during subsequent prolonged anoxia in rats (Dahl and Balfour, 1964). It was also noted that cerebral ATP concentrations decreased slower while lactate production was enhanced in pre-exposed animals; leading to the hypothesis that preconditioning altered cellular metabolism to protect against subsequent hypoxic injury (Dahl and Balfour, 1964). Hypoxia-induced tolerance was also confirmed *ex vivo* in rat hippocampal slices, where brief (~5 minute) exposure to hypoxic conditions delayed the loss of evoked synaptic activity during subsequent hypoxic conditions (loss at ~16 min. compared to ~13 min. in slices without preconditioning (Schurr et al., 1986). Subsequent work identified that ischemic preconditioning corresponded to an increase in proteins involved in cellular tolerance (i.e. heat shock proteins (HSP)) and was associated with reduced infarct sizes in rats following MCAo (48 hours later) (Simon et al., 1993). This was further examined in more depth by Stenzel-Poore et al. using combined *in vivo* and *in vitro* approaches to evaluate the genomic response to cerebral ischemia using DNA oligonucleotide microarrays (Stenzel-Poore et al., 2003). Here, prior preconditioning "reprogrammed" cellular responses to damaging ischemia, where instead of upregulating gens involved in immune responses and apoptosis, there was a downregulation of genes that overall shifted cellular profiles towards

dampened cellular activity. For example, genes involved in energy utilization were downregulated including those for ion-channel activity (e.g. voltage-gated potassium channels) and proteins involved in glucose oxidation (aldo-keto reductase and alcohol dehydrogenase enzymes), which could reflect reduced or more efficient cellular metabolism (Dirnagl et al., 2003; Pincherle et al., 2018; Stenzel-Poore et al., 2003). These transcriptional responses are similarly observed in hypoxia-tolerant species and reduce energy expenditure to adapt to environments with limited oxygen availability (Dirnagl et al., 2003; Stenzel-Poore et al., 2003).

In addition to the shift in metabolic profiles and inflammatory mediators, other cellular responses have been identified following ischemic preconditioning including restorative mechanisms (neurogenesis (Lee et al., 2007) and angiogenesis (Gustavsson et al., 2006), reductions in excitatory transmission (van Rensburg et al., 2009), and adenosine (specifically activation of A1 receptors) (Dirnagl et al., 2003; Heurteaux et al., 1995; Pincherle et al., 2018).

1.5.3 Postconditioning

There is evidence in humans that transient ischemic events (such as transient ischemic attacks, TIA) are associated with reduced infarct size (Wang et al., 2017; Weih et al., 1999) and morbidity (Esposito et al., 2015) after subsequent ischemic stroke, and further support the concept of preconditioning. However, translation of preconditioning to clinical practice is likely not feasible for the general population due to the unpredictable nature of stroke injury. Recent studies have shown that tolerance can be induced *after* injury (i.e. postconditioning) and may be important for neuroprotection in the days after ischemic stroke (Dirnagl et al., 2003; Pincherle et al., 2018; Zhao, 2009). This was first noted in the heart after coronary artery

occlusion and reperfusion in experiments by Sewell et al. in 1955 (SEWELL et al., 1955) but has gained interest over the past 20 years as a novel approach for reducing brain injury after stroke (Vetrovoy et al., 2017; Zhao, 2009). In animal stroke models, postconditioning can reduce infarct sizes following focal and global ischemia (Zhao, 2009) and can also reduce cell death *in vitro* in the aftermath of OGD exposure (Pignataro et al., 2009). Additionally, postconditioning is effective using different stimuli including intermittent reperfusion (during transient occlusions), ischemia or hypoxia, or administration of neurotoxic agents (Zhao, 2009). While more studies are needed to examine mechanisms of endogenous protection elicited by postconditioning, evidence thus far suggests that cellular responses are similar to those induced via preconditioning.

1.5.4 The role of SD in conditioning

As mentioned above, preconditioning can be induced by a number of triggers, including SD. This was first demonstrated by Kobayashi et al. in 1995 where application of KCl (2hrs; resulting in ~10 SDs) reduced the number of dead cells in the ipsilateral cortex (versus saline on the opposite hemisphere) during subsequent (24hrs. later) bilateral forebrain ischemia in rats (Kobayashi et al., 1995). This protection was further confirmed following MCAO induction 3 days after SD preconditioning and was related to increases in brain-derived neurotrophic factor (BDNF) mRNA after repetitive SDs (2hrs. of KCl (~10 SDs) without subsequent MCAO) (Matsushima et al., 1998). SD-induced BDNF upregulation was further shown to be an important contributor to protection as heterozygous mice with reduced BDNF levels had no benefit of SD preconditioning on infarct size after focal ischemia (Yanamoto et al., 2004).

Interestingly, SD alone (without exposure to subsequent ischemia) can also induce many similar changes observed in response to ischemic preconditioning (described previously) and include genetic reprogramming (Shen et al., 2017, 2016), neurogenesis (Urbach et al., 2016), adenosine accumulation and A_1R activation (Lindquist and Shuttleworth, 2012), specific reductions in excitatory transmission (Sawant-Pokam et al., 2017), and upregulation of inflammatory pathways (Eising et al., 2017). This begs the question as to whether protective effects of ischemic preconditioning are actually due to SD induced by another stimulus (i.e. oxygen and/or glucose deprivation); and further suggest that not every SD is detrimental and, on the other hand, might actual promote recovery and repair mechanisms in the aftermath of injury.

Issues arise when it comes to SD and postconditioning mechanisms after stroke. To my knowledge there have been no studies examining SD postconditioning after stroke which may largely stem from decades of research that clearly show that exogenous induction of SD in the injured brain leads to stepwise infarct progression in animal stroke models (Busch et al., 1996).

On the other side of the coin, the stimuli employed during postconditioning studies) to induce endogenous protection after stroke (e.g. ischemia or hypoxia) are also likely to initiate SD. For example, subtle mismatches in neurovascular coupling (e.g. transient dips in tissue oxygen or increased cortical activity) can ignite SD in penumbral zones after MCAO in mice and may predispose the onset of SD in human stroke patients (von Bornstädt et al., 2015). Studies are thus needed to determine if tolerance to injury requires SD or if subthreshold stimuli are sufficient.

From SD preconditioning studies and other previous work (Nedergaard and Hansen, 1988) it is clear that SD is not always detrimental to brain tissue. Even in the injured brain, confirmation of SD (via ECoG recordings) does not reliably guarantee injury progression. In the foundational study conducted by Dohmen and colleagues (described previously) it was noted that high SD incidences did not necessarily indicate injury progression in all malignant ischemic stroke patients (Dohmen et al., 2008). Illustrating this point, the authors highlight one patient case where 40 DC shifts were detected in the ICU but there was no corresponding infarct growth detected in CT scans taken 4 months post stroke. Additionally, this patient exhibited one of the better prognoses according to the extend Glasgow Outcome (eGOS) scale at 6 months. On the other hand, another patient with 14 SDs exhibited progressively worse ECoG recovery with each event that translated to lesion progression during CT follow-up approximately one week later. While real caveats exist with regards to initial infarct severity, age, location of the ECoG strip, etc., it remains unclear whether all SDs contribute to poor outcomes after stroke, and importantly, whether pharmacologically blocking SDs will prevent any possible neuroprotective benefits.

1.6 Rationale for targeting SD consequences

Prospective clinical studies are needed to demonstrate better patient prognoses when SD is blocked. This poses a challenge as there are many obstacles which technical issues for monitoring SD in humans; which is currently restricted to ECoG strips placed directly on the brain during essential surgical procedures and thus limits studies to severely injured patients that may not benefit from interventions). Moreover, ECoG recordings only provide

information from tissue in the electrode proximity and elimination of SD from one recording site may detect other SDs at different locations.

Accumulating evidence that recognizes potential benefits of SD make navigating the clinical setting even more challenging and thus alternative approaches are needed that limit damaging consequences of SD without preventing theoretical benefits of propagation into remote brain regions. In 2012, the COSBID group published large retrospective study that explored the effect of SD incidence with respect to the analgesics and sedatives administered to brain injured patients in the ICU (Hertle et al., 2012). Out of 6 medications, the only drug found to significantly reduce the odds ratio for SD occurrence was ketamine. Ketamine is a dissociative anesthetic that antagonizes NMDARs and has been previously shown to inhibit SD in animal models (Hernández-Cáceres et al., 1987; Marrannes et al., 1988; Sánchez-Porras et al., 2014) and in case reports (Sakowitz et al., 2009; Schiefecker et al., 2015) and more recently in a crossover prospective study in brain injured patients (Carlson et al., 2018).

The high doses of ketamine that are required to block SD are likely well above those that prevent normal synaptic activation of NMDARs (Pietrobon and Moskowitz, 2014). This is further augmented in brain injury where pathological elevations in extracellular K^+ have been shown to reduce efficacy of NMDAR blockade of SD (Petzold et al., 2005). Therefore, in addition to not preventing any benefits of SD in remote brain regions, high dose ketamine may further augment tissue injury after ischemia (as seen with previous NMDAR antagonists) by preventing cell-survival cascades that depend on NMDAR activity. Whether ketamine can

limit excitotoxic consequences of SD in vulnerable brain regions, without preventing remote propagation, is unknown.

1.7 Goals of this study

This dissertation work examines mechanisms of neuronal injury associated with SD in brain slices and *in vivo* after stroke. The overall hypothesis is that extracellular glutamate accumulation and NMDAR-mediated Ca^{2+} influx underlie neuronal injury processes in vulnerable tissue after passage of the SD wave front. Therefore, the degree of basal tissue metabolic compromise increases deleterious consequences of SD and thus determines whether neurons will recover (Figure 1.1). Specifically, these key excitotoxic mediators of injury (extracellular glutamate and intracellular neuronal Ca^{2+} loading via NMDARs) are expected to be prolonged when neurons have impaired metabolism prior to SD. An additional goal of this project is to test ketamine's efficacy in reducing excitotoxic consequences, as opposed to outright block, of SD. Completion of these studies will provide the first evidence that limiting deleterious consequences of SD can be achieved using lower concentrations/doses of NMDAR antagonists like ketamine. These findings could theoretically benefit ICU clinicians with regards to intervention or sedation decision-making in patients at-risk for SDs and secondary lesion progression.

Figure 1.1

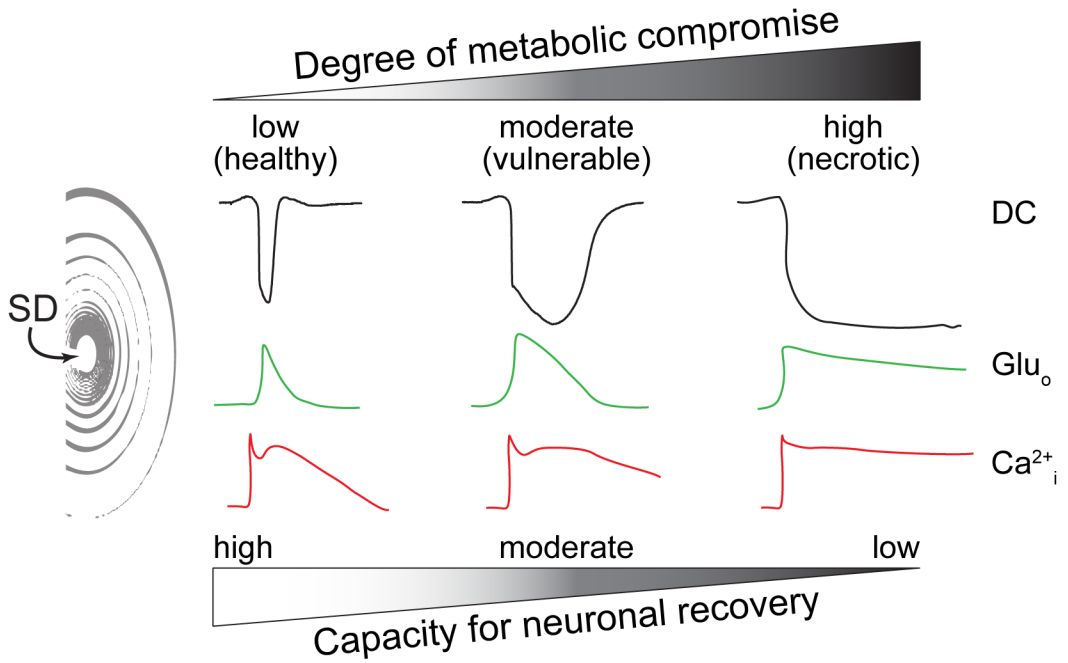

Figure 1.1. Specific aims of study. Experiments in this dissertation will test the overall hypothesis that extended glutamate release and NMDAR-mediated Ca^{2+} loading underlie excitotoxic neuronal injury in metabolically compromised brain. Specific Aims 1&2 will examine the influence of metabolic capacity on extracellular glutamate (Glu_o) increases and intracellular neuronal Ca^{2+} (Ca^{2+}_i) loading during SD; using electrophysiology and fluorescence imaging techniques in brain slices. A novel model of substrate restriction will also be employed to increase neuronal susceptibility to damaging effects of SD but does not alone cause injury (moderate/vulnerable). In these studies, SD is generated from a distant location within the slice and the duration of SD-induced DC potential changes, glutamate, and Ca^{2+} are expected to increase with the degree of initial brain slice compromise. Findings from specific aims 1 & 2 will characterize excitotoxic consequences of SD in well-controlled brain slices and test whether clinically approved NMDAR blockers (e.g. ketamine) can modulate these indicators of potential injury. Specific Aim 3 will examine contributions of excitotoxic SD consequences *in vivo* after focal ischemia. Electrophysiology and fluorescent reporters of glutamate and Ca^{2+}, initially characterized in slice, will be utilized to monitor SD evoked at a distant location from the infarcted vessel. After passage of the SD wave front, glutamate and NMDAR-mediated Ca^{2+} increases are expected to be prolonged in (vulnerable) peri-infarct tissues compared to remote brain with adequate residual flow (low degree of compromise). Successful completion of study aims will characterize cellular-mediators involved in SD-mediated tissue deterioration. This would provide an alternative clinical approach to targeting SD *consequences* rather than *initiation.*

1.7.1 General experimental models

In the course of this work, a novel brain slice model was developed, which may better recapitulate consequences of SD in penumbral brain regions, as opposed to current methods

that rely on OGD. This model was then further characterized and used to answer questions regarding how otherwise viable neurons may succumb to SD injury. After characterization in brain slices, final studies evaluated SD-mediated excitotoxicity *in vivo* after dMCAo, and these experiments included tests of whether the protective effects of ketamine seen in brain slices were seen in penumbral brain regions *in vivo* while still enabling SD propagation in remote locations.

1.7.2 Chapter 2: Does ketamine work to limit deleterious consequences in brain slices without blocking SD?

In Chapter 2, experiments were designed to test the hypothesis that deleterious effects of SD could be limited using concentrations of ketamine that do not prevent SD outright. A novel brain slice model of metabolic compromise, electrophysiology, and imaging of neuronal Ca^{2+} loading were techniques utilized to study consequences of SD that occur in vulnerable neurons. This model, referred to as a "vulnerable" recording conditions, was employed to more closely examine processes in the wake of SD that promote the transition from viable to injured (or impaired) neurons.

1.7.3 Chapter 3: Do brain slice models of stroke (OGD or hypoxia) adequately recapitulate SD consequences that are observed in vulnerable brain regions? What factors increase SD vulnerability?

The main goal of Chapter 3 studies was to examine in more detail the brain slice model of compromise employed in studies from Chapter 2. The overall hypothesis of this study is that vulnerable brain slices are mildly impaired at baseline prior to SD, but the additional hit of a more metabolically burdensome SD is what causes neuronal demise.

Experiments evaluated basal metabolic capacity of vulnerable brain slices using electrophysiologically, oxygen measurements, and imaging read-outs. In addition to these techniques, extracellular glutamate fluorescence imaging during SD was used to test the hypothesis that neurons are exposed to excitotoxic levels of glutamate for prolonged durations in vulnerable conditions—which suggests an increased burden of the SD. Additional techniques including immunohistochemistry and intrinsic optical imaging (IOS) were also employed to evaluate structural changes that occur after SD in vulnerable conditions.

1.7.4 Chapter 4: Are low doses of ketamine effective at reducing excitotoxic consequences of SD in vivo after stroke?

The main objective of Chapter 4 was to test mechanisms of SD-mediated consequences *in vivo* after stroke in mice. Experiments tested the hypothesis that a low dose of ketamine, without blocking SD, could limit deleterious effects of SD— especially in penumbral brain regions that have been thought to gain the least protection from NMDAR antagonist administration.

Initial methods used in this chapter will employ electrophysiology (for monitoring of DC shifts and spontaneous cortical activity (ECoG)) and laser speckle contrast imaging (LSCI) monitoring of cerebral blood flow after surgical induction of a dMCAo. Follow-up studies will utilize fluorescence imaging techniques of Ca^{2+} and glutamate during SD. The overall hypothesis for this study brain regions more proximal to the occlusion site (i.e. penumbra) is vulnerable to injury due to increased excitotoxic burden of SD and ketamine can reduce these damaging consequences.

2. Ketamine reduces deleterious consequences of spreading depolarizations

Katelyn M. Reinhart & C. William Shuttleworth
Department of Neurosciences, University of New Mexico School of Medicine.

Corresponding Author:
C. W. Shuttleworth, Ph.D.
Department of Neurosciences, MSC08 4740
1 University of New Mexico
Albuquerque, NM 87131
(505) 272 5826
bshuttleworth@salud.unm.edu

2.1 Abstract

Recent work has implicated spreading depolarization (SD) as a key contributor the progression of acute brain injuries, however development of interventions selectively targeting SDs has lagged behind. Initial clinical intervention efforts have focused on observations that relatively high doses of the sedative agent ketamine can completely suppress SD. However blocking propagation of SD could theoretically prevent beneficial effects of SD in surrounding brain regions. Selective targeting of deleterious consequences of SD (rather than abolition) could be a useful adjunct approach, and be achieved with lower ketamine concentrations. We utilized a brain slice model to test whether deleterious consequences of SD could be prevented by ketamine, using concentrations that did not prevent the initiation and propagation of SD. Studies were conducted using murine brain slices, with focal KCl as an SD stimulus. Consequences of SD were assessed with electrophysiological and imaging measures of ionic and synaptic recovery. Under control conditions, ketamine (up to 30μM) did not prevent SD, but significantly reduced the duration of neuronal Ca^{2+} loading, and the duration of associated extracellular potential shifts. Recovery of postsynaptic potentials after SD, was also significantly accelerated. When SD was evoked on a background of mild metabolic compromise, neuronal recovery was substantially impaired. Under compromised conditions, the same concentrations of ketamine reduced ionic and metabolic loading during SD, sufficient to preserve function after repetitive SDs. These results suggest that low concentrations of ketamine could be utilized to prevent damaging consequences of SD, while not blocking them outright and preserving potentially protective effects of SD.

Keywords: Spreading depression; brain slice; excitotoxicity; metabolic compromise; NMDA receptor; calcium loading; neuronal injury; excitatory postsynaptic potentials.

2.2 Introduction

Spreading depolarization (SD) is a slowly propagating wave (2- 4 mm min^{-1}) of near-complete neuronal and glial depolarization that has gained renewed interest as an important contributor to the progression of acute brain injuries (Lauritzen et al., 2011, Dreier et al., 2017, Hartings et al., 2017). SD can be initiated by stimuli that cause synchronous depolarization of a critical volume of brain tissue (Tang et al., 2014), and SD propagation across the brain is propelled by feed-forward release of glutamate and/or K^+ (Somjen, 2001). In injured brain, the initiating depolarization is caused by ischemia, trauma, or other energetic supply-demand mismatches (von Bornstadt et al., 2015). The extent of ionic loading accompanying SD is extreme, with intracellular Ca^{2+} loads continuously exceeding 10s of micromolar for more than a minute (Somjen, 2001, Dietz et al., 2008). As such, the metabolic costs to recover from SD are much more demanding than other brain phenomena, such as seizures (Dreier et al., 2013), and thus are particularly challenging for the injured brain (Hartings et al., 2017).

Whether or not injury occurs after SD depends greatly on the capacity of tissues to re-establish ionic gradients in the aftermath of SD. This capacity is governed by the degree of ionic loading during SDs, the baseline metabolic capacity, and the ability of a region to profoundly increase blood flow to match energy demands after SD (Dreier, 2011). This is exemplified during SD in the healthy brain (e.g. migraine aura), where metabolic and vascular perfusion reserves are adequate, and thus SD does not result in any permanent damage (Nedergaard and Hansen,

1988). In contrast, SDs that spontaneously occur following stroke (Dohmen et al., 2008), trauma (Hartings et al., 2011), or subarachnoid hemorrhage (Dreier et al., 2009) can underlie stepwise progression of injury (Busch et al., 1996, Hartings et al., 2003, Hartings et al., 2017).

The development of clinical interventions for SD has lagged behind efforts to demonstrate their incidence in different pathologic conditions. Initial efforts have concentrated on the application of agents such as NMDA receptor (NMDAR) antagonists that block the initiation and propagation of SD. The dissociative anesthetic ketamine is an NMDAR antagonist that prevents SD in animal models (Hernandez-Caceres et al., 1987, Marrannes et al., 1988) and shows effectiveness in case reports (Sakowitz et al., 2009, Schiefecker et al., 2015). A retrospective review of medications used in the intensive care unit (ICU) also shows that ketamine infusion can reduce the frequency of SDs in brain injured patients (Hertle et al., 2012). Prospective studies of ketamine would be useful to determine whether a reduction in SD frequency is associated with improved outcomes in the clinic. However, such studies are complicated by two potential problems. First, the high ketamine concentrations used to suppress SD also result in substantial sedation with attendant increases in risk of ICU complications (Abou-Chebl et al., 2010, Nichols et al., 2010). Secondly, SDs propagate widely in injured brain, including through tissue that may be distant from an injury core where intact metabolic capacity is retained. It is possible that SDs invading these distant regions cause protective preconditioning (Yanamoto et al., 2004, Viggiano et al., 2016), adaptive synaptic plasticity (Faraguna et al., 2010), and/or neurogenesis (Urbach et al., 2017) that may be beneficial to functional recovery (Nakamura et al., 2010, Dreier, 2011) These theoretical issues require further study, but suggest that different approaches to selectively target the

deleterious consequences of SD could be a useful adjunct to the current focus on global block of SD events.

We tested here whether deleterious effects of SD could be limited by lower concentrations of ketamine that do not prevent SD outright. Our findings with measurements of Ca^{2+} loading and a model of metabolic vulnerability indicate that ketamine can be protective without blocking SD, and support a possible significant modification of therapeutic strategies for SD, based on blocking consequences of SD rather than incidence.

2.3 Materials and Methods

2.3.1. Animals and Preparations

All animal procedures were performed in accordance with protocols approved by the UNM Health Sciences Center Institutional Animal Care and Use Committee. Adult (4-8 weeks) male and female mice (C57Bl/6 and/or GCaMP5G) were used for all experiments. For Ca^{2+} imaging experiments, homozygous mice expressing the floxxed calcium indicator GCaMP5G under the CAG promoter (Gee et al., 2014) were purchased from The Jackson Laboratory (Stock No: 024477, B6;129S6-*Polr2a*$^{tm1(CAG\text{-}GCaMP5g,\text{-}tdTomato)Tvrd}$/J), and bred with homozygous mice expressing Cre Recombinase under the CamK2a promoter (B6.Cg-Tg(Camk2a-cre)T29-1Stl/J, Jax Stock No: 005359). Offspring were utilized in experiments and had robust GCaMP5G expression in hippocampal pyramidal neurons (Wang et al., 2013).

Acute brain slices were prepared as previously described (Shuttleworth et al., 2003). Briefly, animals were deeply anaesthetized with 0.15mL (s.c.) injection of ketamine-xylazine (85 and 15 mg ml^{-1}, respectively), decapitated, and brains were quickly removed into 150 mL

oxygenated ice-cold cutting solution (in mM): sucrose, 220; $NaHCO_3$, 26; KCl, 3; NaH_2PO_4, 1.5; $MgSO_4$, 6; glucose, 10; $CaCl_2$ 0.2; equilibrated with 95% O_2/5% CO_2 supplemented with 0.2 ml ketamine (100 mg/ml, Putney Inc., Portland, ME), to limit excitotoxicity during the slice preparation as described in (Aitken et al., 1995). Coronal cortico-hippocampal slices (350 μm) were prepared with a Pelco 102 Vibratome (Ted Pella, Inc., Redding, CA), hemisected, and then allowed to recover in artificial cerebrospinal fluid (aCSF; containing (in mM): NaCl, 126; $NaHCO_3$, 26; glucose, 10; KCl, 3; $CaCl_2$, 2, NaH_2PO_4, 1.5; $MgSO_4$, 1; equilibrated with 95% O_2/ 5% CO_2), at 35°C for 60 min. After 1h, the holding aCSF was replaced with chilled (20°C) aCSF and slices were allowed to equilibrate to room temperature until the start of recording sessions. These incubations and exchanges served to ensure effective wash out of residual ketamine from slices, as previously established with responsiveness to glutamate and NMDA (Shuttleworth et al., 2003, Hoskison and Shuttleworth, 2006, Vander Jagt et al., 2008).

2.3.2 Generation of SD

Individual brain slices were transferred to a submersion recording chamber with nylon slice supports (RC-27L, Warner Instruments, Hamden, CT), and continuously super fused with oxygenated (95% O_2/95% CO_2) aCSF at 2.2 ml min^{-1}. Bath temperature was maintained at 32°C by an inline heater assembly (TC-344B, Warner Instruments). After placement of electrodes into the slice (See Electrophysiology methods) slices were allowed 20 minutes for equilibration. As described below (Results), modified aCSF with elevated K^+ (8mM) was used for most experiments, in order to increase ability of single slices to support repetitive SDs and enable rigorous testing of drug effects (Funke et al., 2009, Zhang et al., 2015). SDs were evoked by pressure microinjection (40ms, 30 psi; Picospritzer; Parker Hannifin, OH, USA) of KCl (1M) via a glass micropipette ~3 MΩ) placed in hippocampal CA1 stratum radiatum.

Repetitive SDs were initiated in each slice at 15 minute intervals to allow for full recovery between events. In experiments assessing the effect of ketamine antagonism during repetitive SDs (Figures 2.2-4 & Supplementary Figures), antagonist wash-in commenced following the second of two control SDs, and the second control SD was used for analyses (Footitt and Newberry, 1998). SD initiation and propagation, as well as slice viability (see Metabolic Challenge below), were examined by monitoring intrinsic optical signals (IOS) of submerged brain slices trans-illuminated with visible light (≥ 600nm) and collected using a 4X objective (Olympus, 0.10 NA). IOS data were captured at 0.5 Hz using a cooled CCD camera (Imago, Till Photonics) and analyzed with TillVision software (TillPhotonics, version 4.01). Data analysis involved normalizing transmitted light to baseline and expressing IOS as percent change in transmission ($\Delta T/T_0 \times 100$) (Anderson and Andrew, 2002).

2.3.3 Electrophysiology

Extracellular recordings were acquired (1-10kHz) with an Axon MultiClamp 700A amplifier, digitized (Digidata 1332), and recorded using pCLAMP10.2 software (Molecular Devices, Sunnyvale, CA, USA). Glass recording microelectrodes were filled with aCSF (tip resistance ~3MΩ) and positioned at a depth of 50–100 μm in the CA1 stratum radiatum ≥200 μm from the KCl-filled glass ejection micropipettes. The durations of SDs were calculated from the extracellular potential shift ("DC shift" (Somjen, 2001)), measured at 20% of the peak maximum to 80% recovery. In experiments assessing synaptic recovery after SD, a concentric bipolar electrode (FHC, Bowdoin, ME, USA) was placed on the slice surface ofCA1 stratum radiatum, between the KCl ejection micropipette and recording electrode, for stimulation of Schaffer collateral inputs. Excitatory postsynaptic potentials (EPSPs) were recorded using test pulses (50 μs, 0.1Hz) delivered at intensities (80 – 400 μA) that gave 40 - 60% of the maximum

EPSP amplitude. DC shifts and EPSPs were analyzed using Clampfit 10.2 software (Molecular Devices, Sunnyvale, CA, USA). Postsynaptic potentials were resolved from gap-free recordings with a high-pass filter (1 Hz cut-off). The duration of EPSP suppression after a single SD was measured from the time of the maximum negative potential of the DC shift to the time at which postsynaptic potentials first reached ≥ 50% of baseline values.

2.3.4 Fluorescence Imaging

Neuronal Ca^{2+} dynamics during SD reported by GCaMP5G were imaged with a 20X water-immersion objective (Olympus, 0.5 NA) and analyzed in TillPhotonics, version 4.01 software (Till Photonics GmBH, NY). GCaMP5G was excited at 480nm using a monochromator (Polychrome V, 2Hz); emission signals were passed through a dichroic mirror (515 DCLP) and captured using a cooled CCD camera (Imago, Till Photonics). Total Ca^{2+} accumulation in specific regions of interest during SD were calculated (GraphPad Prism 7.03) as the integral of the signals for 120 seconds or 200s following the peak of the SD transient. The duration of Ca^{2+} during SD was measured from the initial positive peak amplitude to the time point where fluorescence returned to ≤ 5% of baseline levels.

Autofluorescence signals during SD that could contaminate Ca^{2+} signals were evaluated in wild-type brain slices not expressing GCaMP5G. A small, but long-lasting (>200s) fluorescence decrease was observed, as described previously and attributed to flavoprotein autofluorescence (Shuttleworth, 2010). Autofluorescence decreases were similar in both somatic and dendritic compartments (-3.0 ± 0.9 and -2.3 ± 0.9 $\Delta F/F_0$ (%) decrease at 160s after SD for stratum pyramidale and stratum radiatum, respectively; n=3, Supplementary Figure

2.2B). Ca^{2+} signals were therefore corrected for background and autofluorescence changes during SD, and expressed as percent change from baseline values ($\Delta F/F_0 \times 100$).

2.3.5. Metabolic challenge

Under control conditions, slices are normally held 0.5mm above the coverslip floor of the recording chamber to ensure continuous flow of aCSF on both sides of the slice. This is considered a nominally-healthy condition for the current study (see discussion in Frenguelli, 2017). However, in some experiments, we reduced aCSF flow to the bottom side of the slice, in order to intentionally reduce metabolic capacity and increase vulnerability to SD. This was accomplished by inverting the slice support insert (SS-3, Warner Instruments), to remove the flow channel under the slice. As opposed to complete oxygen-glucose deprivation, this partial metabolic compromise did not spontaneously initiate SD in any preparation (n = 44). Slice recovery after SD was evaluated from 1) intrinsic optical signals (Anderson and Andrew, 2002) 2) the ability of the tissue to generate a second SD (Koroleva and Bures, 1996) and 3) electrophysiologically with evoked extracellular postsynaptic potentials (Lindquist and Shuttleworth, 2012).

2.3.6 Drugs

Ketamine (100 mg/ml, racemic: R (-)/S (+)) was purchased from Putney, Inc. (Portland, ME), and solutions containing ketamine were prepared daily. All other chemicals were obtained from Sigma-Aldrich (St. Louis, MO, USA).

2.3.7 Statistical analysis

Data are reported as mean ± SEM. Statistical analyses (repeated measure one-way analysis of variance (ANOVA), paired and unpaired t-tests) were calculated using GraphPad Prism (version 7.03; La Jolla, CA). Statistical significance was determined by *P* values < 0.05, with Bonferroni correction during multiple comparisons.

Figure 2.1

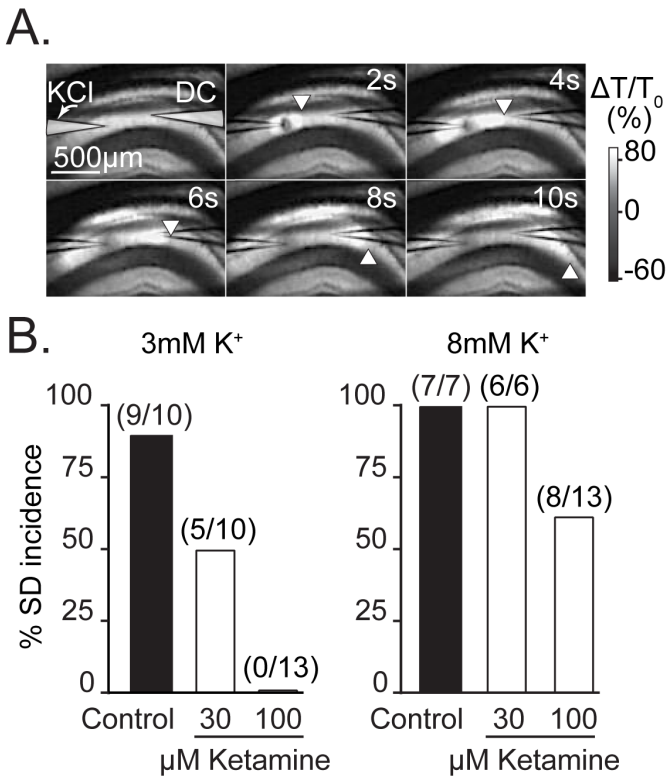

Figure 1. Basal extracellular K^+ influences sensitivity to ketamine. **A**: Representative intrinsic optical signals showing SD propagation through the hippocampal CA1 region of a brain slice. SD was triggered by micro injection of KCl from a micropipette on the left (*labeled "KCl"*) and SD is visualized as a slowly-propagating wave of increased light transmission. The location of the advancing wavefront is marked by *white arrowheads* and a second microelectrode (*labeled "DC"*) was used to confirm electrical responses of SD coincident with arrival of the optical signal (not shown). The upper right-hand values indicate time, in seconds, relative to the triggering of the KCl stimulus pulse. **B:** Effect of ketamine exposures on SD incidence under two different recording conditions (3mM vs 8mM bathing K^+). Ketamine more potently prevented SD incidence in the lower basal K^+ recording conditions. Values in parentheses indicate number of preparations.

2.4 Results

2.4.1 Ketamine can reduce rate and duration of SD

We first examined the concentration-dependence of ketamine block of SD in brain slices (**Figure 2.1**). Under standard recording conditions (3mM K^+ aCSF, see Methods), 100μM ketamine invariably abolished SD. Consistent with previous observations using other NMDAR antagonists, the effectiveness of SD block was reduced by moderate elevations of baseline extracellular K^+ that are similar to elevations in peri-infarct tissues *in vivo* (Petzold et al., 2005). From these initial experiments, we selected the highest concentration of ketamine that did not block SD for subsequent studies (30μM, 8mM K^+ aCSF).

Figure 2.2 shows the time-dependent inhibition of SD propagation rate by ketamine. In these experiments, ketamine (10 minutes pre-exposure, and maintained throughout the experiment) immediately slowed SD propagation rate compared to that of control SDs initiated within the same slice, but the maximum effect was observed by the second SD following drug exposure (Figure 2.2B). In a separate set of experiments, brain slices were pre-exposed to ketamine for extended incubation times (> 3hrs) prior to recording sessions. In these preparations, the maximal slowing was achieved on the first SD trial in ketamine (3.4 ± 0.2 vs. 5.1 ± 0.3 mm min^{-1} for the first SD in ketamine during acute exposures (shown in Figure 2.2B)) and was not enhanced with successive stimulations (**Supplementary Figure 2.1A**; P = 0.27 for first vs. third SD in ketamine

Figure 2.2

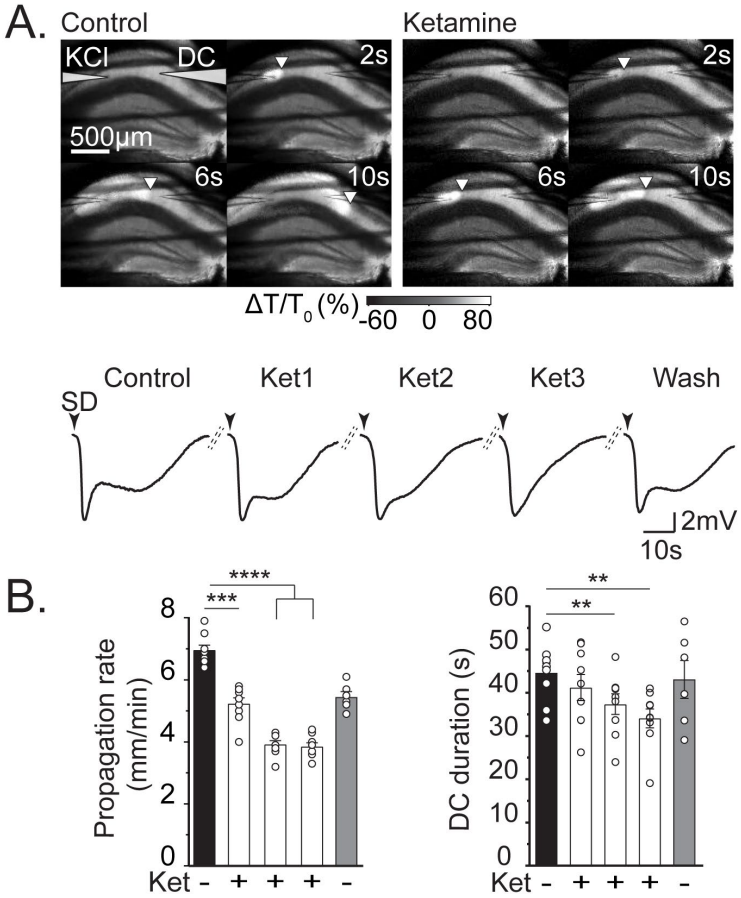

Figure 2. Ketamine reduced SD propagation rate and DC shift duration. **A**: Representative example of the effect of ketamine wash-in, during a series of repetitive SDs. Top panels show intrinsic optical signal changes to track SD propagation (as described in Figure 1) in control conditions (*left*), and during the third SD evoked in the presence of 30μM ketamine (*right*). Note the delayed propagation of the SD wavefront in ketamine. The traces show DC potential recordings during this sequence of SDs in the same slice. *Black arrowheads* indicate DC shift onset, and *dashed lines* represent 15 minutes recovery between stimulations. The duration of the DC shift of SD was progressively reduced, and then largely recovered after ketamine washout. **B**: Summary data from 6 preparations as shown in A (*white symbols*), demonstrating progressive decreases in both propagation rate and DC duration with partial recovery upon ketamine wash out (*gray bar*, n=3). *Black symbols* (n=3) represent DC shift data and propagation rate from separate experiments shown in Figure 4. *P<.05, **P<0.01, ***P<0.001, **** P<0.0001.

When recorded in the CA1 dendritic subfield, DC potential changes during SD have a prominent "inverted saddle-like" shape with a slower secondary phase involving NMDAR activation (Marrannes et al., 1988, Somjen, 2001, Aiba and Shuttleworth, 2012). SD duration

was progressively reduced following acute ketamine exposures and reversed following wash out (Figure 2.2). Similar to effects on propagation rate, DC durations following long ketamine pre-exposures (> 3hrs, Supplementary Figure 2.1A), were maximally reduced upon the first SD trial (27.1 ± 2.2 vs. 41.2 ± 3.0s for the first SD in ketamine during acute exposures (shown in Figure 2.2B)), and were not enhanced by successive SDs in ketamine (Supplementary Figure 2.1A; P = 0.51 for first vs. third SD in ketamine).

Separate time-matched control studies verified that effects seen with ketamine on DC shift duration were not due to spontaneous rundown over time (Supplementary Figure 2.1B). Similarly, propagation rate showed no change during repetitive SDs in these control studies (Supplementary Figure 2.1B). A small decrease (~13%) in the amplitude of DC potential shifts was noted during repetitive SDs in ketamine (data not shown, control: 8.85 ± 0.43 mV vs. third ketamine trial: 7.71 ± 0.33 mV, n=6, P=0.02). However, time-matched control experiments (i.e. without ketamine) showed the same degree of run down, implying that this was not due to ketamine itself (data not shown, ~13% decrease; durations of second vs. fifth SD: 7.65 ± 0.78 mV vs. 6.37 ± 0.70 mV, P=0.01, n=8).

2.4.2 Ketamine reduces neuronal Ca^{2+} accumulation and accelerates postsynaptic recovery

Ionic disruption is massive during SD, and NMDAR activation is largely responsible for extended neuronal Ca^{2+} influx during the DC shift (See Introduction). We next tested whether ketamine reduced neuronal Ca^{2+} accumulation following SD (**Figure 2.3**). Since the maximum effect of ketamine was observed with successive SD stimulations, the 3rd SD following

Figure 2.3

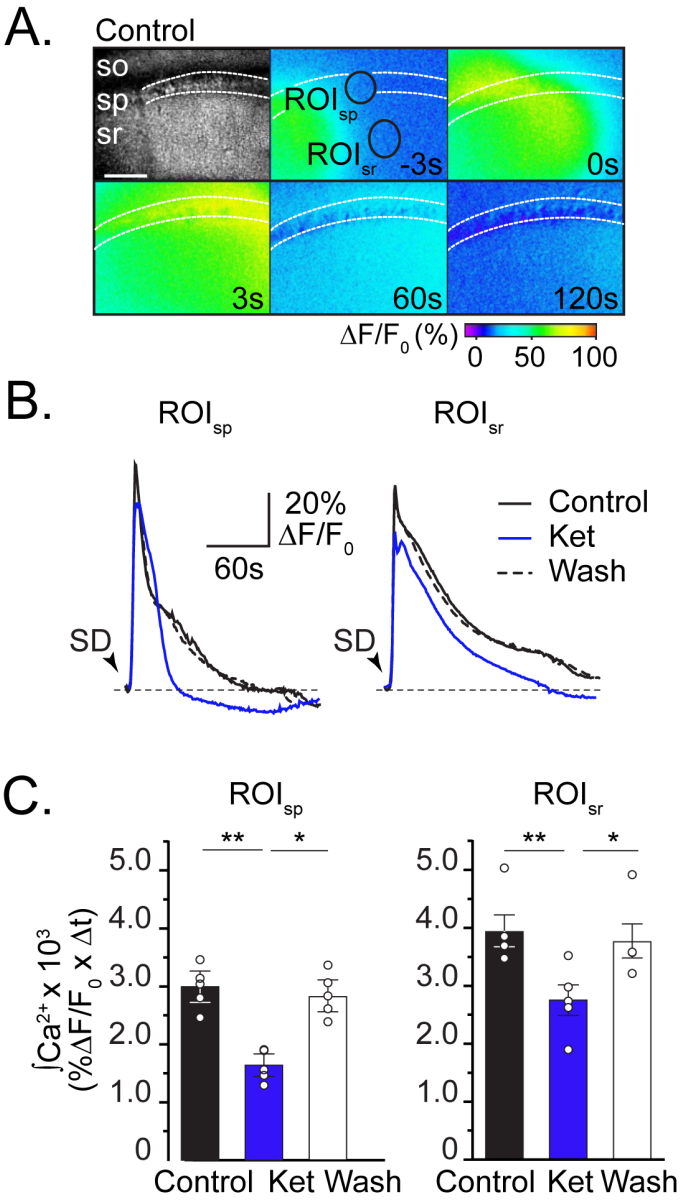

Figure 3. Ketamine reduces neuronal intracellular Ca^{2+} accumulation during SD.
A: Top left panel: Transmitted light image, showing stratum oriens (so), stratum pyramidale (sp), stratum radiatum (sr) in area CA1. Pseudo colored images show GCaMP5G fluorescence collected during SD in control conditions. Numbers in each frame indicate time (in seconds) in relation to the peak Ca^{2+} transient in regions of interest corresponding predominately to pyramidal cell somata (*ROI_s*) and CA1 dendritic regions (*ROI_d*). Scale bar = 100μm. **B**: Data extracted from ROI_s and ROI_d show that Ca^{2+} transients during SD in ketamine (*blue*) recover faster than control (*black*), and are reversible after ketamine wash out (*dashed*). *Gray traces* in each plot represent autofluorescence (AF) decreases in somata and dendrite regions during SD in a brain slice not expressing GCaMP5G. *Black arrowheads* indicate SD onset. **C**: Summary data (n=5), show that ketamine reversibly and reliably reduces total neuronal Ca^{2+} accumulation in both ROIs (integrals of 120s transients; see Methods). *P<.05, **P<0.01, ***P<0.001.

ketamine was used for experiments in Figures 2.3 & 2.4. Figure 2.3A shows large intracellular

neuronal Ca^{2+} (GCaMP5G) transients during a control SD. Ca^{2+} rapidly increases during the

SD wave front and returns to ≤5% baseline levels by ~2.5 minutes (Figure 2.3B). Ca^{2+} transients in pyramidal cell body regions (stratum pyramidale) had increased peak amplitudes compared to signals in dendrites (stratum radiatum), however Ca^{2+} elevations in dendrites were slightly longer in duration (**Supplementary Figure 2.2A)**. This resulted in an overall increase in *total* Ca^{2+} accumulation during control SDs in dendrites compared to cell bodies (black bars in Figure 2.3C, P=0.04) Ketamine reduced the peak amplitude and duration of Ca^{2+} transients (Supplementary Figure 2.2A). The rapid resolution of SD-induced Ca^{2+} transients in ketamine (Figure 2.3B) reveals a small, reversible underlying fluorescence decrease. Since these signals have been corrected for autofluorescence dynamics during SD (see Methods), residual undershoots revealed in ketamine are likely contributed to by light scattering changes during SD. Ketamine attenuated *total* Ca^{2+} accumulation during SD in stratum pyramidale and radiatum (Figure 2.3 B&C). These data support the hypothesis that ketamine reduces the DC shift duration during SD, and thereby results in reduced intracellular Ca^{2+} dysregulation in neurons.

One consequence of SD is a long-lasting suppression of spontaneous and evoked synaptic transmission (Leao, 1944, Lindquist and Shuttleworth, 2012, 2017). We therefore determined whether shorter DC shifts and reduced neuronal Ca^{2+} dysregulation in ketamine were associated with accelerated synaptic recovery after SD. **Figure 2.4** shows that ketamine reliably accelerated the recovery of evoked excitatory postsynaptic potentials (EPSPs) by ~25% compared to within-slice controls. Separate time-matched control experiments

confirmed that changes in EPSP recovery time were due to antagonist exposure, rather than any other spontaneous changes. Together with Figures 2.2 & 2.3, these data suggest that (without blocking SD), ketamine can reduce SD propagation, duration, and ionic dysregulation thus enabling faster recovery of synaptic activity.

2.4.3 Ketamine improves recovery in metabolically vulnerable brain slices

We next examined whether ketamine, at a concentration that does not block the initiation or propagation of SD (i.e. 30μM), can significantly protect against deleterious consequences of

Figure 2.4

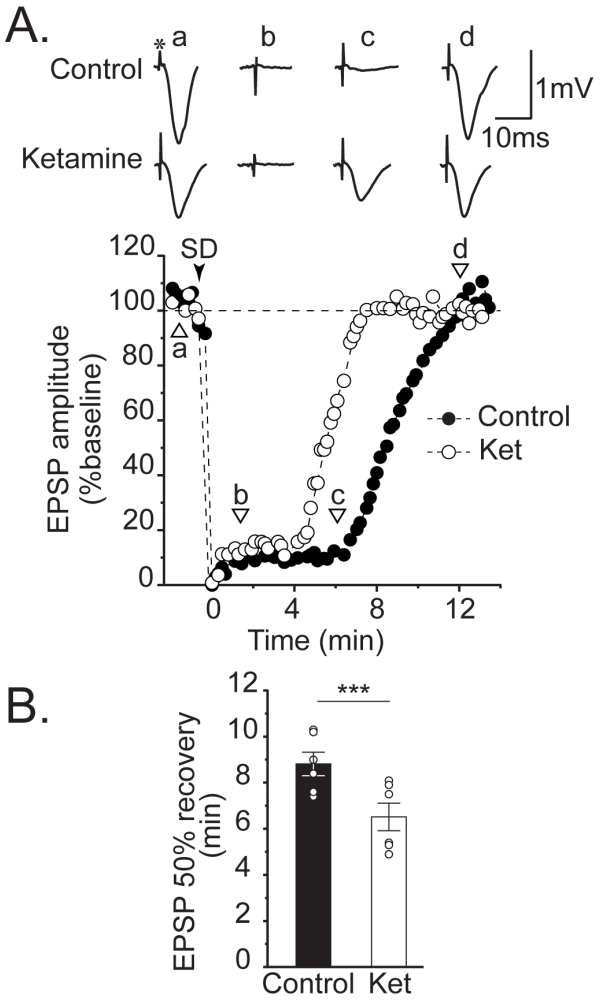

Figure 4. Ketamine accelerates recovery of evoked postsynaptic potentials after SD.

A: Representative example of suppression and recovery of evoked excitatory postsynaptic potentials (EPSPs) after SD. Control EPSPs (a) were abolished after SD (b,c), and slowly recovered to baseline amplitudes after ~12 min (d). The *asterisk* above control (a) trace indicates the bipolar stimulus artifact. The full time course of EPSP suppression and recovery in this same slice is plotted below (*filled circles*). SD onset indicated by *black arrowhead*. Ketamine (30μM) did not prevent EPSP suppression, but significantly accelerated recovery rate (*lower* set of traces, and *empty circles* in plot). **B**: Summary data from 6 such experiments. The effect of ketamine on DC shift duration in this data set was consistent with prior observations in Figure 2 (45.9 ± 2.3 vs. 35.7 ± 1.1 s for control and ketamine, respectively; P = 0.0026). *** P<0.001

SD in metabolically vulnerable brain slices. As described above (Methods), partial reduction in metabolic substrate availability was achieved by restriction of aCSF flow under brain slices. As opposed to complete oxygen-glucose deprivation approaches, this partial metabolic compromise did not spontaneously initiate SD in any preparation tested (n = 44), but greatly impaired recovery after SD.

Figure 2.5 shows ketamine reduced excessive Ca^{2+} loading in vulnerable tissues, and was associated with significantly improved functional recovery. SD-induced Ca^{2+} transients were noticeably prolonged in vulnerable tissues, consistent with previous observations (Aiba and Shuttleworth, 2012), with residual intracellular Ca^{2+} remaining ~20-30% above baseline ~3.5 minutes after SD (Supplementary Figure 2.2C). Ketamine pre-exposure significantly reduced the integral of Ca^{2+} transients in both somatic and dendritic compartments (Figure 2.5B), and enabled generation of a second SD in vulnerable slices (Figure 2.5C). Likewise, recovery of EPSPs was substantially delayed after SD in vulnerable tissues, and ketamine enabled EPSPs to return to ~60% of baseline amplitude responses after SD (Figure 2.5D).

Figure 2.5

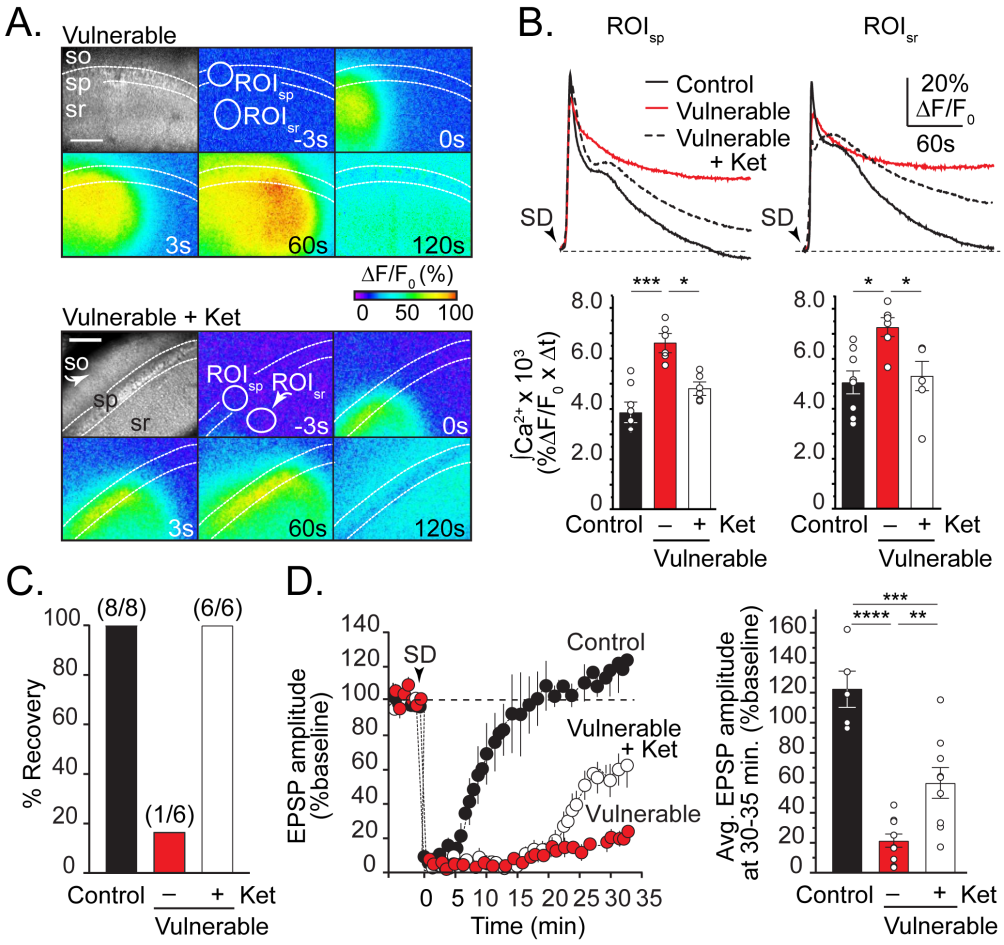

Figure 5. Ketamine improves recovery of neuronal Ca^{2+} loading and promotes functional recovery after SD in vulnerable brain slices. A: Top montage: GCaMP5G imaging in vulnerable brain slices show considerably prolonged Ca^{2+} elevations compared to control conditions (compare with Figure 4). Lower montage shows reduced intracellular Ca^{2+} 120s after SD in ketamine.Scale bar =100µm. **B**: Plots show Ca^{2+} transients from somatic and dendritic ROIs (*white circles* in A) during SD in control (*black*), vulnerable (*red*), and vulnerable + ketamine (*dashed*). Summary data of Ca^{2+} transient integrals from a set of such experiments confirm beneficial effects of ketamine (control, n=9; vulnerable, n=6; vulnerable + ketamine, n=6).**C:** Data from experiments in B, showing vulnerable slices exposed to ketamine recovered the ability to generate a second SD. Values in parentheses indicate number of preparations. **D**: Summary data of EPSP amplitude suppression and recovery after SD in control (*black*, n=5), vulnerable (*red*, n=10), and vulnerable with ketamine (*white*, n=9). *Black arrowhead* indicates SD onset and loss of postsynaptic responses. **P<0.01,***P<0.001, ****P<0.0001.

Figure 2.6

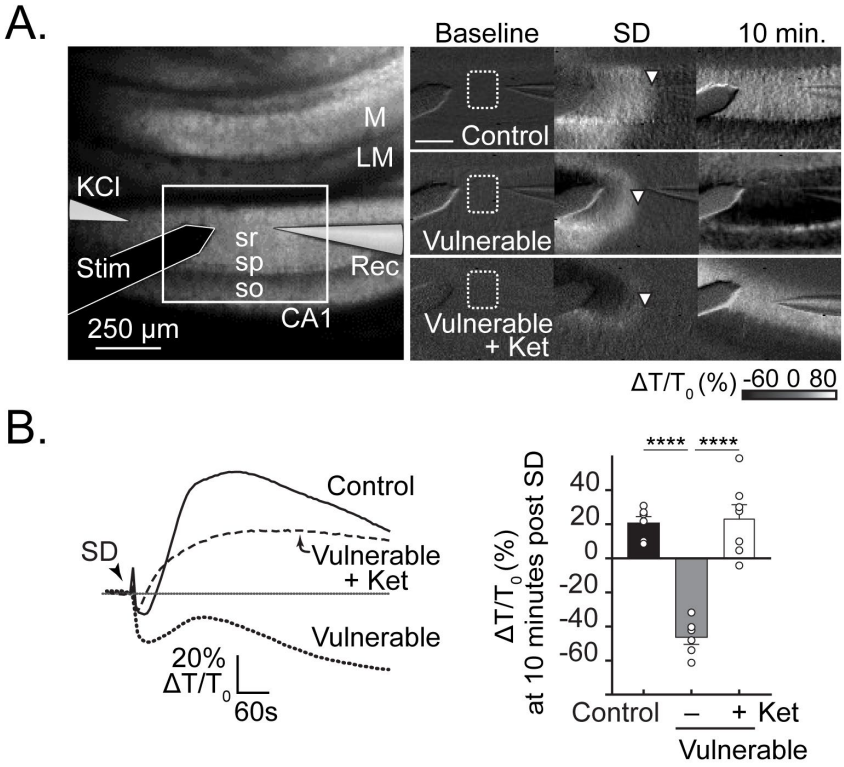

Figure 6. Ketamine protects against structural disruption after SD in vulnerable slices. **A**: Left hand panel shows the arrangement of recording electrodes on a transmitted light image. The *white box* outlines the imaging area shown in panels on the right; so, stratum oriens; sp, stratum pyramidale; sr, stratum radiatum; LM, stratum lacunosum moleculare; M, molecular layer of dentate gyrus. The set of images on the right show representative light transmittance (intrinsic optical) changes at baseline, during SD, and 10 minutes after SD in brain slices recorded under three different conditions; control, vulnerable, and vulnerable + ketamine. Note the difference in light transmission seen at the 10-minute time point after SD. *White arrowheads* indicate the wave front of SD. Scale bar = 250 µm. **B:** Signals extracted from the three representative examples shown in A (*traces* on left*)*, and summary data (n= 6-7, right hand panel) at 10 minutes after SD in these studies. These population data confirm substantially decreased light transmittance after SD vulnerable slices, and prevention by ketamine. ****P<0.0001.

Figure 2.6 shows the effects of metabolic compromise on intrinsic optical signals (IOS) during SD, and optical signals associated with ketamine protection. Under control conditions, a prominent light transmission increase is observed that recovers towards baseline. In contrast, SD in metabolically compromised conditions was invariably followed by a sustained decrease in IOS signals (~45% $\Delta T/T_0$; Figure 2.6A&B). Previous reports have attributed IOS decreases in metabolically compromised conditions to a combination of factors, including dendritic

disruption and swelling of intracellular organelles (Obeidat and Andrew, 1998, Fayuk et al., 2002), and persistent astrocyte swelling observed in vulnerable tissues could also contribute (Risher et al., 2012). In the present study, ketamine effectively prevented decreased IOS signals associated with lack of functional recovery in vulnerable slices (see Figure 2.5). Thus, prolonged IOS decreases were prevented in almost all vulnerable preparations (Figure 2.6B). Together these findings support a role for extended NMDAR-dependent Ca^{2+} influx into neurons during SD in vulnerable tissues (Aiba and Shuttleworth, 2012), and suggest that sub-maximal concentrations of NMDAR antagonists can target this process to enable better functional recovery.

2.5 Discussion

2.5.1 General

The main new finding of the study is the demonstration that ketamine can be protective against SD-induced injury, even at concentrations that are insufficient to block the initiation or propagation of the SD event itself. Ketamine was able to significantly improve recovery from ionic loading of SD and was shown to be sufficient to protect tissues from SDs in a model of metabolic vulnerability. These beneficial effects provide support for the notion that targeting consequences of SD could be effective in injured brain, as an adjunct or alternative to interventions intended to completely abolish SD events.

2.5.2 Mechanisms of ketamine actions

We focused on the NMDAR antagonist ketamine because of its current use in clinical settings and because of reports that ketamine sedation in the ICU was associated with reduced frequency of SD events (Sakowitz et al., 2009, Hertle et al., 2012, Schiefecker et al., 2015). In

order to preserve NMDAR availability and potential beneficial outcomes of SD (see Introduction), we determined concentrations of ketamine that kept SD intact in healthy brain slices (Figure 2.1). Ketamine's ability to block SD, even with high concentrations, was reduced when basal extracellular K^+ was moderately increased. As previously discussed (Petzold et al., 2005), these K^+ elevations may be similar to pathological ionic disturbances in peri-infarct tissues in animals (Nedergaard and Hansen, 1993) and in brain injured patients (Rogers et al., 2017). The ketamine concentration selected for most studies here (30μM, Figures 2.2-6) allowed for repetitive SD initiation, while presumably leaving a portion of NMDARs available (Izumi and Zorumski, 2014, Khlestova et al., 2016). Since ketamine competes with Mg^{2+} for binding within the NMDAR channel pore, NMDAR subtypes with weaker Mg^{2+} block (i.e. GluN2C and GluN2D) are preferentially inhibited, whereas GluN2B and GluN2A-mediated currents are less sensitive to ketamine (Khlestova et al., 2016). If GluN2B and GluN2A NMDARs underlie residual NMDAR current in 30μM ketamine, availability of these channel subtypes may be helpful for preserving synaptic plasticity in the recovering brain (Khlestova et al., 2016).

It is difficult to directly compare the ketamine concentration used here with prior clinical observations, in part because of species-dependent differences of *in vivo* ketamine distribution and metabolism, and brain concentrations following intravenous infusions were not determined in the ICU studies. Furthermore, while both the racemic mixture and the S (+)-isomer of ketamine are in clinical use, the racemic ketamine mixture used in the present study is approximately half as potent as the S-ketamine isomer (Peltoniemi et al., 2016) used in published clinical work with SD. The present results imply that brain concentrations effective

at blocking SD clinically are higher than 30μM (for racemic ketamine, or ~15μM for S-ketamine), but more detailed studies are needed to resolve whether infusions used for clinical sedation far exceed this value. Non-sedative concentrations that effectively prevent deleterious consequences of SD could be clinically valuable.

Ketamine's efficacy was progressively enhanced during a series of repetitive SDs (Figure 2.2), or by prolonged (~3hr) ketamine pre-incubations (Supplementary Figure 2.1A). The time course of effects may be due in part to ketamine's use-dependent mechanism of action at the Mg^{2+} - site of NMDARs (Johnson et al., 2015) and/or drug diffusion into brain slices. Time-dependent effects of ketamine have been noted previously in *in vivo* recordings in pigs (Sanchez-Porras et al., 2014). In the present study, the progressive decrease in the DC shift duration of SD was particularly notable (Figure 2.2). NMDAR activation is prominent during the secondary phase of the "inverted-saddle" - shaped DC shift. During the late-phase of SD, glutamate release probability is substantially enhanced for ~ 1 minute, at a time when postsynaptic neurons remain persistently depolarized. These conditions favor relief of Mg^{2+} from its binding site within the NMDAR pore, and lead to massive cationic influx. As such, targeted application of NMDAR antagonists (i.e. AP5) during the late-phase, can abolish the secondary component of the DC shift and reduce extended Ca^{2+} loading (Aiba and Shuttleworth, 2012). Use-dependency of block with ketamine may be particularly useful for targeting excessive glutamate accumulation during SD in injured tissues.

Our GCaMP5G imaging of neuronal Ca^{2+} accumulation showed significant reductions in total Ca^{2+} loading after ketamine (Figure 2.3 & Supplementary Figure 2A), associated with reduced

DC shift durations. In addition, recovery of synaptic potentials after SD was significantly accelerated by ketamine exposures (Figure 2.4). The long-lasting suppression of evoked EPSPs in brain slice after SD (≥ 5 minutes) is largely a result of extracellular adenosine accumulation and activation of presynaptic adenosine-1-receptors (A-1R) and provides a measure of the metabolic burden imposed by SD (Lindquist and Shuttleworth, 2012, 2014). Taken together, these data show that a concentration of ketamine that does not block SD in nominally healthy tissues, decreases NMDAR- mediated Ca^{2+} influx during the late phase of the DC shift, reduces the metabolic burden of SD and enables faster recovery of EPSPs.

2.5.3 Protective effects of ketamine in vulnerable tissues

We used a novel brain slice model of metabolic insufficiency, in order to recapitulate the deleterious consequences that peri-infarct SDs have on viable, but vulnerable brain regions. By limiting aCSF superfusion to one side of the slice, metabolic capacity was sufficient for slices to remain viable for hours in the recording chamber. However, on this compromised baseline, an SD generated by focal KCl microinjection led to severely impaired 1) recovery of neuronal Ca^{2+} elevations, 2) recovery of synaptic potentials, 3) ability to generate a second SD, as well as signs of structural disruption (suggested from intrinsic optical signals) (Figures 2.5&6). This model of vulnerability to SD is fundamentally different from the oxygen-glucose deprivation (OGD) or hypoxia induced SD (HSD) paradigm that we and others have used to *generate* SD in brain slices (Somjen, 2001, Dietz et al., 2008). In the standard OGD or HSD models, severe oxygen and/or glucose reductions are used as the inciting stimulus for SD, as Na/K^+/ATPase failure produces progressive loss of membrane potential and extracellular K^+ accumulation. SD is usually triggered within ~10 minutes, and even if SD can be delayed or prevented by antagonists, cell damage invariably occurs if substrate removal is continued. The

OGD or HSD paradigms are therefore useful for understanding initiation of events in infarct cores, but are not as well suited for understanding how at-risk penumbral tissue suddenly succumbs to injury when it is invaded by an SD. The partial inhibition model here addresses this concern and is straightforward and reproducible. It is also noted that the recording configuration tested here (with slices superfused on a single side) is common for many neurophysiology studies.

Ketamine exposures (30μM) provided substantial protection against the deleterious consequences of SD under these conditions of metabolic compromise. As described above for nominally healthy tissues, SD was not prevented by this concentration of ketamine, but the total Ca^{2+} loading after SD was significantly reduced, and both optical signals and functional recovery after SD in vulnerable conditions were significantly improved (Figures 2.5&6).

2.5.4 Potential beneficial effects of targeting consequences (rather than initiation/propagation) of SD

We expect the degree of NMDAR block in our experiments to leave a significant portion of the NMDAR pool available for plasticity and Ca^{2+}-dependent synaptic signaling that is presumably beneficial for recovery and repair mechanisms required in the immediate aftermath of an injury (Shohami and Biegon, 2014). In addition to NMDAR availability, the fact that SDs still propagate may be directly beneficial effects to recovering brain. This is because SDs can travel long distances throughout the cortex, including to relatively healthy tissue that is remote from an injury site. While SDs can clearly cause damage when they propagate through metabolically compromised tissue, there is good evidence for protective effects of SD, when it is allowed to propagate through otherwise healthy brain regions (see Introduction). Whether

or not substantial benefit could be derived from targeting the consequences of SD *in vivo*, could be tested by assessing SDs at different locations from an injury site and relating to outcome. In this scenario long-term functional outcomes, rather than lesion volume alone would be valuable to assess the importance of potential beneficial effects of SD on cortical plasticity remote from the infarct core.

2.6 Conclusions

Results from the current study suggest that SDs that occur in the presence of ketamine could be shorter in duration and less metabolically demanding. By reducing intracellular Ca^{2+} influx during SD, ketamine may minimize the amount of energy needed for recovery (exemplified by accelerated recovery of evoked synaptic activity). These results raise the possibility that ketamine may be effective clinically, even at lower concentrations that do not prevent SD, but may shorten the duration of ECoG suppression and minimize lesion development in patients with acute brain injuries. Our study focused on ketamine but the main pre-clinical findings here could be generalized to other interventions that improve recovery of neurons after the passage of SD. This includes other use-dependent NMDAR antagonists such as memantine, which are clinically well tolerated and may lack some of the negative side effects of ketamine (Johnson et al., 2015). Alternative approaches that improve neurovascular coupling after SD propagates through vulnerable tissues (Dreier, 2011) would be expected to be complementary or additive with ketamine effects.

2.7 Acknowledgements

This study was supported by NIH grants NS051288, P20GM109089 and T32 HL007736. The authors are grateful to Russell Morton, Ph.D. and Donald Partridge, Ph.D. for helpful discussions and input throughout the course of the study, and for excellent pilot studies contributed by Kisa King.

2.8 Supplementary Figures

Supplementary Figure 2.1

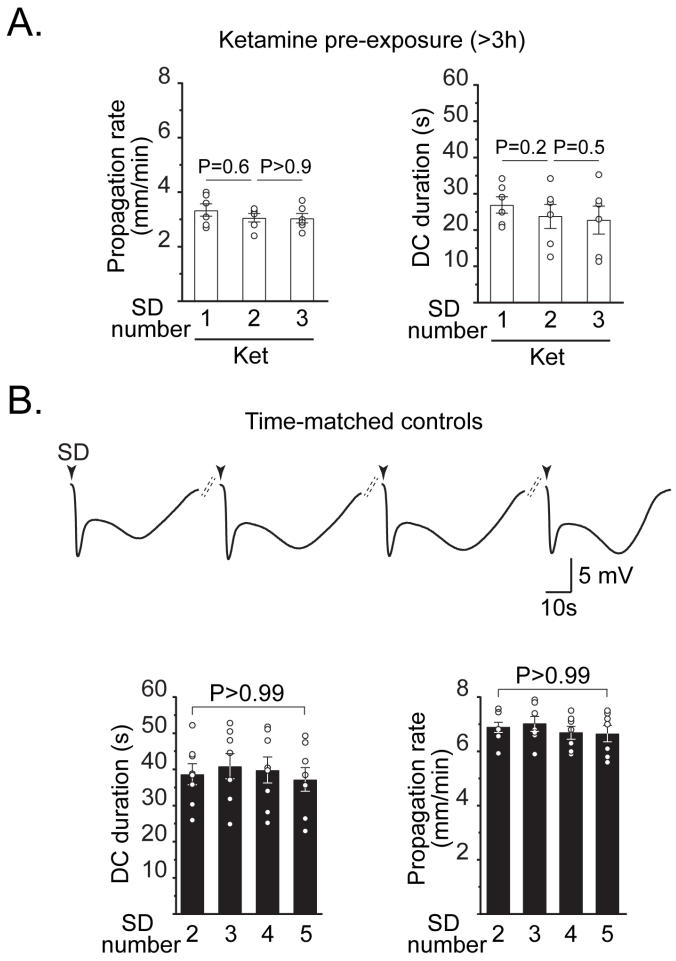

Supplementary Figure 2.1. A: Summary data from 6 preparations showing ketamine pre-exposure immediately reduced both SD propagation rate and DC shift duration and was not enhanced by successive SDs. **B:** DC potential recordings (*traces*) show that the DC shift duration is consistent during a sequence of SDs in a time-matched control slice not exposed to ketamine. *Black arrowheads* indicate DC shift onset, and *dashed lines* represent 15 minutes recovery between stimulations. Population data from 6 such experiments, confirm that SD propagation rate and DC shift duration are stable over consecutive SD stimulations.

Supplementary Figure 2.2

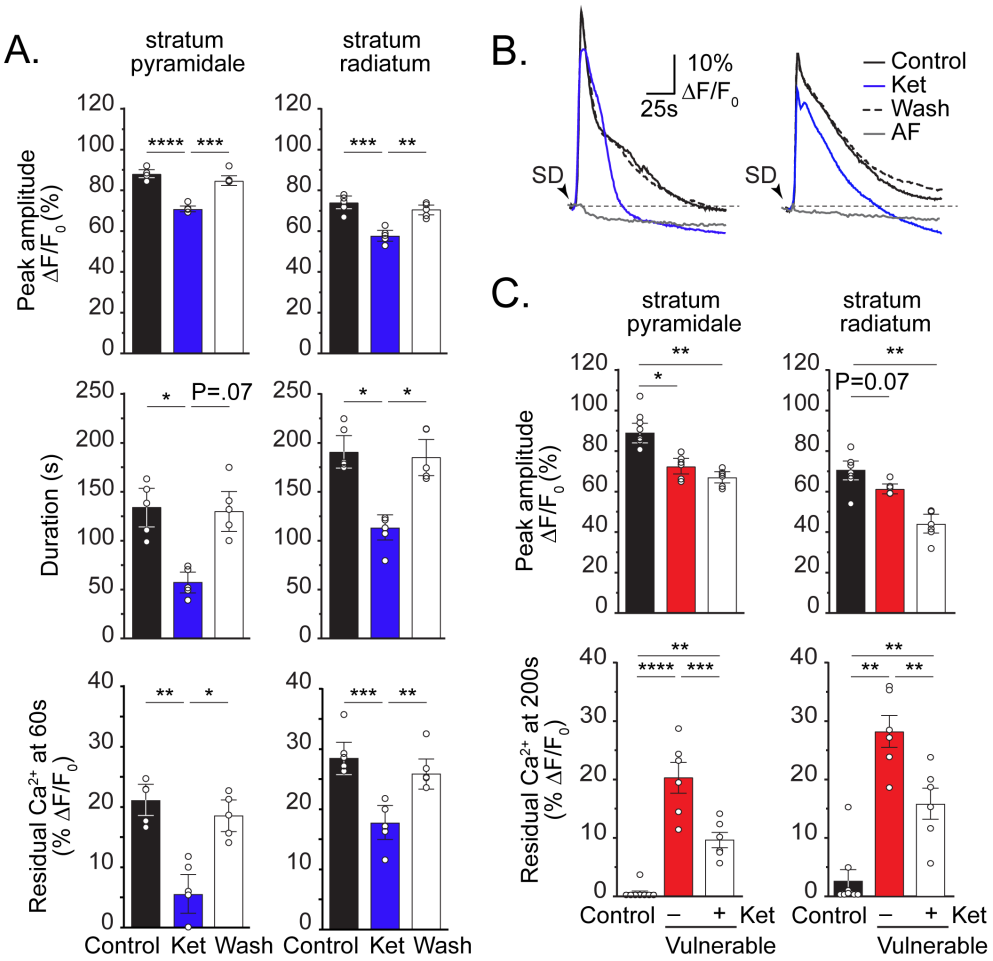

Supplementary Figure 2.2. **A:** Summary data of GCaMP5G imaging experiments shown in Figure 3 (n=5). Ketamine significantly and reversibly reduced the peak amplitude (top panel) of intracellular Ca^{2+} transients during repetitive SDs in cell body (pyramidale) and dendrite (radiatum) regions. Ketamine reduced the duration of transients (see Methods) resulting in decreased residual intracellular Ca^{2+} accumulation 60s after SD. Comparison of control SDs in pyramidale and radiatum (*black bars*) showed that peak Ca^{2+} was larger in cell bodies compared to dendrites (P=0.005). However, the duration of Ca^{2+} transients (middle panel) and residual intracellular fluorescence at 60s after SD were slightly increased in dendrites vs. cell bodies (P=0.06 and P=0.09 for duration and residual Ca^{2+}, respectively). **B:** Representative Ca^{2+} traces from stratum pyramidale and radiatum regions from the same slice as shown in Figure 3B without background and autofluorescence correction. *Gray traces* in each plot represent autofluorescence (AF) decreases in cell body and dendrite regions during SD in a brain slice not expressing GCaMP5G. *Black arrowheads* indicate SD onset **C:** Summary of GCaMP5G imaging from the same data set shown in Figure 5 (A-C). The peak amplitude of Ca^{2+} signals during SD in vulnerable slices tended to be reduced compared to control SDs, while residual intracellular Ca^{2+} fluorescence remained significantly elevated 200s after SD. Ketamine reduced residual Ca^{2+} accumulation 200s after SD in vulnerable slices. *P<.05, **P<0.01, ***P<0.001, ****P<0001.

3. Novel model of metabolic compromise increases brain slice vulnerability to deleterious consequences of spreading depolarization

Katelyn M. Reinhart & C. William Shuttleworth
Department of Neurosciences, University of New Mexico School of Medicine.

Corresponding Author:
C. W. Shuttleworth, Ph.D.
Department of Neurosciences, MSC08 4740
1 University of New Mexico
Albuquerque, NM 87131
(505) 272 5826
bshuttleworth@salud.unm.edu

Keywords:
Spreading depression; brain slice; excitotoxicity; metabolic compromise; NADH; glutamate; neuronal injury; excitatory postsynaptic potentials; PPR.

3.1 Introduction

Spreading depolarization (SD) is a slowly propagating wave (2- 4 mm min^{-1}) likely fueled by feedforward release of potassium and/or glutamate (Somjen, 2001) and characterized by near-complete depolarization of neuroglia (Leao, 1944; Somjen, 2001). These "brain tsunamis" have been detected in humans with acute brain injuries (Hartings, 2017, Dreier et al., 2017; Eriksen et al., 2019) including ischemic stroke (Dohmen et al., 2008, Woitzik, 2013). After stroke, SDs have been detected in ICU patients up to a week after the initial ictus and repetitive SDs are associated with poor clinical prognoses (Dohmen et al., 2008). This suggests that targeting SD may extend the therapeutic window for stroke as there are currently no treatment options beyond 24 hours after the initial insult (Powers, 2018).

SD can be initiated by ischemia or other stimuli that induce supply-demand mismatches in tissues surrounding the infarct core (e.g. penumbra) (von Bornstädt et al., 2015) that is comprised of metabolically vulnerable, but salvageable brain. Due to its massive energetic burden, greater even than seizures (Dreier, 2015), SD may be responsible for the recruitment of otherwise viable neurons into the necrotic infarct core. Here we describe a brain slice model of moderate metabolic impairment in order to study cellular mechanisms relating to injurious consequences of SD in penumbral tissues.

Brain slices are an important tool for studying neuronal mechanisms of SD injury (and neuroprotective drugs targeting SD), as profound blood flow responses to SD *in vivo* (Ayata and Lauritzen, 2015), provide further complexity to an already complicated physiology. To create a stroke-like environment *in vitro* most brain slice studies employ complete metabolic

substrate removal (i.e. hypoxia, oxygen and glucose deprivation (OGD)), conditions that initiate SD within ~10 minutes (Andrew, 1999). These models are important for evaluating cellular mechanisms of SD that occur at the onset of ischemia, during the initial development of the infarct core; however, they may be less applicable to metabolically vulnerable penumbral brain that is viable for hours or days following ictus, and only later succumbs to deleterious consequences of SD. This aligns with a recent consensus in the field that SD, and its consequences, occur along a continuum in relation to brain metabolic capacity (Hartings et al., 2017). Therefore, in addition to OGD studies, *in vitro* models examining SD consequences under a less severe degree of metabolic stress may be useful. Such studies could be relevant to mechanisms of injury that occur during SD in peri-infarct brain regions after stroke that contain functionally intact but metabolically vulnerable neurons (Nakamura et al., 2010; Strong et al., 2006).

To increase neuron vulnerability to the deleterious consequences of SD we altered the configuration of the brain slice recording chamber to reduce metabolic substrate availability. We recently employed this model (Reinhart, 2018) and here we sought to further characterize changes using electrophysiology, imaging, and histology techniques. We found a minor impact of substrate restriction on synaptic efficacy and metabolic parameters in this configuration indicating slices were viable but with reduced metabolic capacity. However, SD consequences were more deleterious as indicated by reduced pO_2 availability, increased NADH fluorescence, prolonged glutamate release, and impaired structural and functional recovery. These findings support the use of this model to study consequences of SD in brain slices resembling peri-infarct tissues that are otherwise viable in the absence of SD.

3.2 Materials and methods

3.2.1 Animals

All animal procedures were performed in accordance with protocols approved by the UNM Health Sciences Center Institutional Animal Care and Use Committee. Adult (1−4 months old) male and female mice (C57Bl/6) maintained in standard group housing were used for all experiments. Homozygous mouse strains were purchased from The Jackson Laboratory (Bar Harbor, ME, USA).

3.2.2. AAV injections

The fluorescent reporter iGluSnFR (Marvin et al., 2013) was delivered via intracortical injection of the adeno associated virus (AAV; pAAV1.hSyn. iGluSnFr.WPRE.SV40; Addgene, Cambridge, MA, USA) to enable imaging of extracellular glutamate on hippocampal neurons in the CA1 subregion of C57Bl/6 mice. Animals were anesthetized with isoflurane (4-5% induction, 1-2% maintenance) and head fixed into a stereotaxic frame (Kopf Instruments). After sanitization using Betadine and alcohol wipes, a scalp incision was made for burr hole preparation (0.295" drill diameter). A total volume of ~ 0.5 µl of iGluSnFR-containing AAV (6.52 x 10^{12} GC/mL) was infused bilaterally (1 injection per hemisphere) at a depth of 150 µm using coordinates AP: -1.75 mm and ML: ± 1.25 mm, relative to bregma. Slow infusion (~0.1µl min^{-1}) was achieved using a 5.0 µl gastight syringe (Hamilton Company Inc., Reno, NV, USA) connected via polyethylene tubing to a 33G diameter infusion cannula (C315I/SPC; Plastics One Inc., Roanoke, VA, USA). The scalp was sutured to close and topical lidocaine and antibiotic ointment were applied to the incision site. Mice recovered on a heating pad and 40% buprenorphine (0.1 mg kg^{-1}) saline solution was delivered (i.p.) for

postoperative pain. Animals were returned to their home cages with littermates and experiments were performed ~2-4 weeks post injection to enable adequate iGluSnFR expression (Marvin et al., 2018).

3.2.3 Brain slice preparation

Acute brain slices were prepared as previously described (Shuttleworth et al., 2003). Briefly, mice were deeply anaesthetized with 0.15mL (s.c.) ketamine-xylazine mixture (85 and 15 mg ml^{-1}, respectively) and decapitated. Brains were quickly removed into 150 mL ice-cold cutting solution (in mM): sucrose, 220; $NaHCO_3$, 26; KCl, 3; NaH_2PO_4, 1.5; $MgSO_4$, 6; glucose, 10; $CaCl_2$ 0.2; equilibrated with 95% O_2/5% CO_2 and supplemented with 0.2 ml ketamine (100 mg/ml, Putney Inc., Portland, ME) to minimize excitotoxicity during slice preparation as described previously (Shuttleworth et al., 2003). Coronal cortico-hippocampal slices (350 μm) were prepared using a Pelco 102 Vibratome (Ted Pella, Inc., Redding, CA), hemisected, and then transferred to 35°C artificial cerebrospinal fluid (aCSF; containing (in mM): NaCl, 126; $NaHCO_3$, 26; glucose, 10; KCl, 3; $CaCl_2$, 2, NaH_2PO_4, 1.5; $MgSO_4$, 1; equilibrated with 95% O_2/ 5% CO_2) for recovery. After 60 min recovery, holding aCSF was replaced with chilled (20°C) aCSF and slices equilibrated to room temperature until the start of recordings.

3.2.4 Generation of SD and brain slice metabolic compromise

Individual brain slices were transferred to a submersion recording chamber (RC-27L, Warner Instruments, Hamden, CT, USA) maintained at 32°C via an inline heater assembly (TC-344B, Warner Instruments) and continuously super-fused at 2.2 ml min^{-1} with oxygenated (95% O_2/95% CO_2) aCSF. SD was evoked by pressure microinjection (40ms, 30 psi; Picospritzer; Parker Hannifin, OH, USA) of KCl (1M) via a glass micropipette ~3 MΩ placed in

hippocampal CA1 stratum radiatum. In control conditions, slices were elevated ~0.5 mm above the coverslip floor using a nylon slice support (SS-3, Warner Instruments) enabling continuous flow of aCSF on both sides of the slice. To reduce metabolic capacity and increase vulnerability to SD, the slice support was inverted and aCSF flow under the slice was reduced. After placement of electrodes into the slice (See Electrophysiology methods) wash in of modified aCSF with elevated K^+ (8mM) commenced and slices were allowed 20 minutes for equilibration prior to SD initiation. This exchange with elevated K^+ aCSF was made to reflect similar pathological ionic disturbances observed in peri-infarct tissues in animals (Nedergaard and Hansen, 1993) and (Petzold, 2005) and brain injured patients (Rogers et al., 2016). In this configuration, SD did not initiate spontaneously in any preparation, but slices were rendered functionally and structurally impaired after SD, as described previously (Reinhart and Shuttleworth, 2018).

3.2.5 Electrophysiology

Extracellular analog recordings were amplified and digitized using Axon Instruments' MultiClamp 700A amplifier (CV-7A headstage) and Digidata 1332A for acquisition (1-10 kHz) by pCLAMP10.2 software (Molecular Devices, Sunnyvale, CA, USA). Glass recording microelectrodes were filled with aCSF (tip resistance ~3MΩ) and positioned ≥ 200 μm from the glass pipette containing KCl (See Generation of SD, above) at a depth of 50 –100 μm in CA1 stratum radiatum. Excitatory postsynaptic potentials (EPSPs) were evoked using a concentric bipolar electrode (CBAPC74, FHC, Bowdoin, NE, USA) driven by a current controller (A.M.P.I., Jerusalem, Israel) and positioned for stimulation of Schaffer Collateral inputs using a paired-pulse protocol (2 x 70 μs; interpulse interval of 50ms). After placement of electrodes, input-output curves were generated during the equilibration period (See

Generation of SD, above) and current pulses (25-150 μA) that evoked 40-60% of maximum EPSP amplitude responses were delivered at 0.1 Hz during recording sessions.

Postsynaptic potentials were resolved from gap-free recordings with a high-pass filter (1 Hz cut-off) and the duration of EPSP suppression after a single SD was measured from the time of the maximum negative potential of the DC shift to the time at which postsynaptic potentials first returned to $\geq$ 50% of baseline values. The paired-pulse ratio (PPR) of EPSP responses evoked with brief interpulse intervals (50ms) was calculated as the ratio of EPSP amplitudes ($amplitude_{EPSP2}$ / $amplitude_{EPSP1}$) and was used to assess changes in presynaptic release probability as a form of short-term synaptic plasticity (Lindquist and Shuttleworth, 2012).

3.2.6 Fluorescence imaging in brain slices

Neuronal extracellular glutamate fluorescence reported by iGluSnFR or endogenous nicotinamide adenine (phosphate) dinucleotide (NAD(P)H) autofluorescence were examined using a fiber optic/monochromator system (TILL Polychrome V, Till Photonics, GmBH, Graefelfing, Germany). After focusing onto the slice surface with 10X / 0.30W (for iGluSnFR) or 20X / 0.50W (for NAD(P)H) water-immersion objectives (UMPlanFL N, Olympus Corporation, Shinjuku, Tokyo, Japan), 480 nm or 360 nm wavelengths were used to excite iGluSnFR or NAD(P)H, respectively. An acquisition rate of 4Hz was used to monitor long-pass filtered (515 nm DCLP) iGluSnFR emission; and, in separate experiments, NAD(P)H signals were acquired at 1 Hz and emitted light was filtered using a 458 nm dichroic mirror (Semrock, Rochester, NY, USA). All fluorescence signals were captured using a cooled interline transfer CCD camera (Imago, Till Photonics) for image analysis in TILL Photonics

Imaging System Software (TILLvisION v.4.01), and GraphPad Prism 8.1.0 (GraphPad Software, San Diego, CA, USA) was used for statistical analyses.

Image analysis involved background subtraction and calculation of the change in pixel intensity relative to pre-SD values. Fluorescence data is thus expressed as $\Delta F/F_0$ (F_0 = 3 frames). For glutamate imaging experiments, brain slices inevitably had varying degrees of basal iGluSnFR expression in relation to the injection site, likely resulting from diffusion constraints of AAV-gene delivery. In order to evaluate glutamate accumulation across different preparations and metabolic conditions, fluorescence transients were normalized to the peak of the iGluSnFR signal during SD in specific regions of interest. Therefore, iGluSnFR fluorescence is expressed as the change from baseline as a percent of the peak amplitude during SD ($(\Delta F/F_0)/F_{max}$) x 100; where the value of 100 = peak amplitude at t = 0s). The integral of iGluSnFR transients from ≥ 5% of peak to 160s post-SD was used to evaluate total glutamate accumulation during SD. Nonlinear regression curves for glutamate transients were generated using GraphPad's algorithm for exponential one phase decay and ROUT's method of identifying outliers (Q = 1%) was used to exclude data points based on R^2 values. From best-fit curves, the time constant (tau) of decay from 5s to 120s ($t_5 - t_{120}$ seconds) after the peak glutamate response (t = 0 seconds) were determined.

3.2.7 Oxygen measurements

In some studies, the partial pressure of oxygen (pO2) was measured (~1.5 Hz) in CA1 stratum radiatum using an oxygen microsensor (50 μm diameter) connected to a PC-controlled fiber optic oxygen meter with temperature compensation (OXY MICRO, World Precision Instruments, Inc., Sarasota, FL, USA). Prior to experiments, a two-point calibration of O_2

probes was performed using water-saturated air and O_2-free water solution (sodium sulfite 1% w/v) and the local barometric pressure was used to convert sensor outputs into mmHg.

3.2.8 MAP2 Immunohistochemistry

Microtubule associated protein (MAP2) immunohistochemistry was used to evaluate dendrite disruption in non-resected brain slices (350μm) as described previously (Hoskison et al., 2007; Hoskison and Shuttleworth, 2006) with minor modifications. After electrophysiology and imaging sessions, brain slices were carefully removed from the recording chamber at 15 minutes following the DC shift of SD and fixed in freshly prepared 4% paraformaldehyde solution. Each section was rinsed (3 x 15 min) with phosphate buffered saline containing 0.1% Tween-20 (PBS-T) and permeabilized in PBS containing 0.4% Triton X-100 for 40 min with gentle rotation. Slices were then gently rotated for 120 min in a blocking solution of PBS-T containing 10% normal donkey serum (NDS) and 1% bovine serum albumin (BSA). After blocking, preparations were exposed to primary antibody (mouse monoclonal anti-MAP2 1:500 (M-1406; Sigma-Aldrich, St. Louis, MO) for a total of 48h (solution was exchanged at 24h and incubated again for 24h) and then extensively washed in PBS-T (1 x 60 min and 4 x 30 min). After an additional blocking step (120 min, 10% NDS, 1% BSA in PBS-T solution), samples were incubated for 180 min with Cy3 goat anti-mouse serum and rinsed with PBS-T (3 x 30 min) prior to overnight wash in PBS at 4°C. Final rinses in PBS (3 x 30 min) and PBS-T (2 x 30 min) were preformed prior to preparation mounting using Fluromount-G.

3.2.9 Confocal imaging and analysis

A Leica TCS SP8 inverted confocal microscope equipped with a Galvo-Z-stage and resonance scanner was used for acquisition of z-stacks (0.6μm steps) in preparations with adequate MAP-

2 antibody penetration at a depth up to ~20µm from the slice surface. A white light laser was tuned for excitation of Cy3 (590-643nm) at low power settings (<6%) and emission was detected with a Hybrid Spectral Detector (HyD) at a gain set below 20% of maximum. Each z-stack image acquired was deconvoluted using Huygens Deconvolution software (Scientific Volume Imaging, Hilversum, Netherlands) and maximum intensity projections of 3µm in depth beginning ~5µm below the slice surface was used for subsequent analysis using open-sourced Fiji software.

3.2.10 Drugs and solutions

Ketamine (100 mg/ml, racemic: R (-)/S (+)) used during brain slice preparation was prepared daily and purchased from Putney, Inc. (Portland, ME, USA). All other chemicals including antibodies, as well as salts and glucose for aCSF solutions were purchased from Sigma-Aldrich (St. Louis, MO, USA). The selective A_1 adenosine receptor antagonist, 8-cyclopentyl-1,3-dipropylxanthine (DPCPX), was prepared as a 10 mM stock in dimethyl sulfoxide (DMSO) and aliquots were stored at -20°C until daily use at a final concentration of 300 nM in aCSF. As mentioned in prior studies (Lindquist and Shuttleworth, 2012) extensive chamber washout and use of separate tubing was employed to minimize drug carryover effects of DPCPX between experiments.

3.2.11 Statistical analysis

Data are reported as mean ± SEM. Statistics were performed using GraphPad Prism and included: ROUT's method of identifying outliers, one- and two-way analysis of variance (ANOVA) with repeated measures for examining drug wash-in effects compared to baseline,

and unpaired t-tests. Statistical significance was determined by P values < 0.05, with Bonferroni correction during multiple comparisons.

3.3. Results

3.3.1 Brain slice metabolic impairment

Figure 3.1

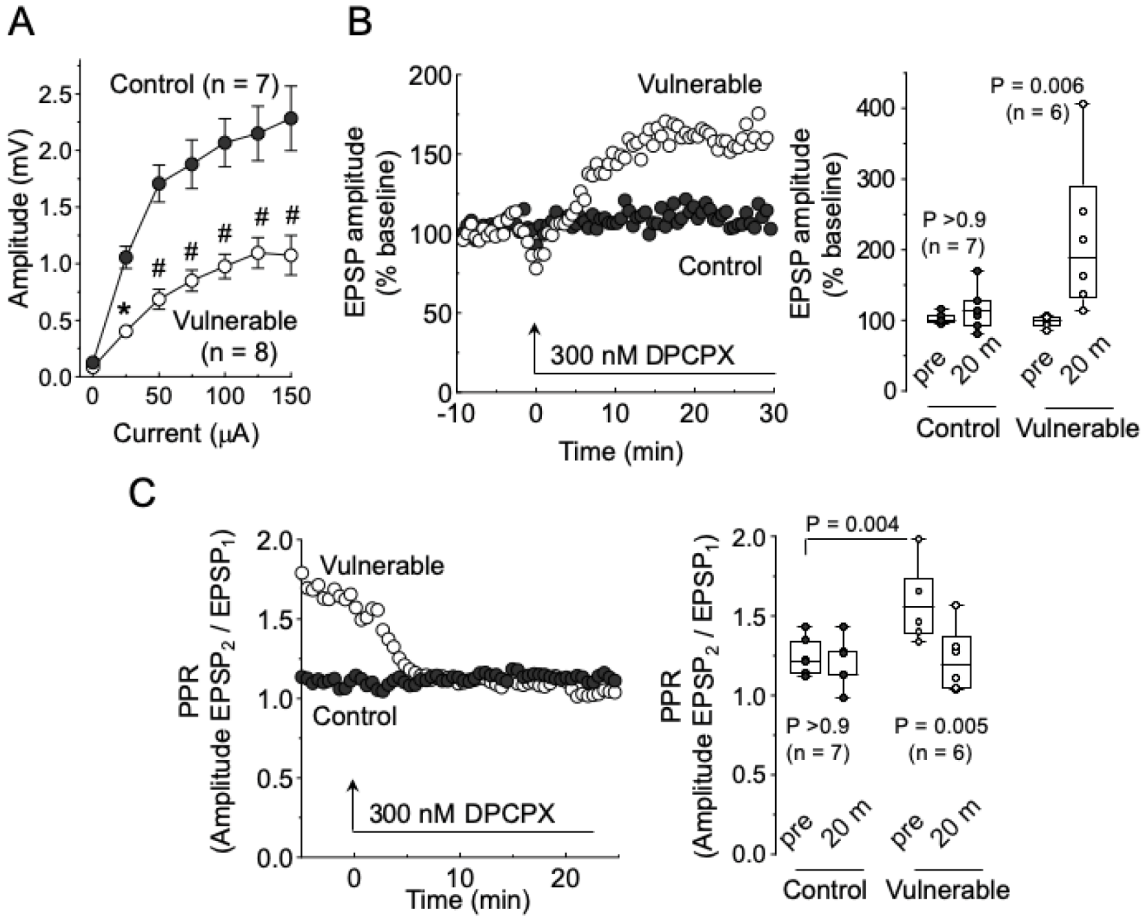

Figure 3.1. A1-mediated suppression of evoked synaptic transmission during metabolic compromise. A. Input-output of evoked postsynaptic response amplitude (raw values) generated at baseline in control (filled circles) and vulnerable (open circles) preparations. Responses were recorded in stratum radiatum of CA1 and showed decreases in all current steps in vulnerable slices. B. Left: representative EPSP amplitude changes (normalized to baseline) from a control and vulnerable slice during wash on of A1R antagonist DPCPX (beginning at time = 0 min.). Data from 6-7 slices (right) show that EPSP amplitude is significantly increased in vulnerable slices in the presence of DPCPX, while response amplitude remained consistent throughout the exposure period in control preparations. C. Paired-pulse ratio (PPR) of postsynaptic responses during DPCPX exposure in the same slices shown in (B) indicate that initial release

Figure 3.1A, shows a significant reduction in the amplitude of evoked postsynaptic potentials (EPSP) recorded in CA1 dendrites in metabolically impaired brain slices. Panels in Figure 3.1B show that wash-in of the A_1 adenosine receptor antagonist DPCPX increased EPSP amplitudes in vulnerable, but not control, brain slices. We further examined paired-pulse ratios (PPR), as an indirect measure of initial glutamate release probability. Figure 3.1C shows increased PPR in impaired preparations that was again normalized by the application of DPCPX (Figure 3.1C). Taken together, these data suggest that initial release probability is reduced at baseline in vulnerable brain slices and is mediated by A_1 receptor activation.

We next evaluated endogenous NAD(P)H fluorescence and tissue pO_2 in CA1 stratum radiatum after brain slice equilibration and prior to SD induction. Consistent with metabolic compromise, we observed a slight increase in NAD(P)H signal prior to SD in vulnerable slices (103.6 ± 3.5 counts) compared to controls (90.1 ± 4.4 counts, P = 0.04, n = 5,5 slices from 3 animals). While these findings suggest increases in NAD(P)H primed for mitochondrial oxidation, there was not a significant effect of baseline metabolic status on pO_2 values monitored at ~50 μm increments from the surface (0 μm) to center (~175 μm) of brain slices (range of pO_2 measured at slice depths of 0 – 175 μm: 165.1 ± 7.4 – 60.5 ± 11.5 mmHg in control (n=7) versus 166.5 ± 9.1 – 61.3 ± 8.1 mmHg in vulnerable (n=8), P = 0.34; also See Figure 3.2A). These data show that increased NAD(P)H autofluorescence does not correspond to significantly decreased pO_2 availability in vulnerable brain slices, under baseline conditions.

3.3.2 Metabolic vulnerability increases deleterious consequences of SD

In agreement with our prior findings (Reinhart and Shuttleworth, 2018) this model of mild metabolic impairment did not result in spontaneous SD initiation in any preparation. However,

Figure 3.2

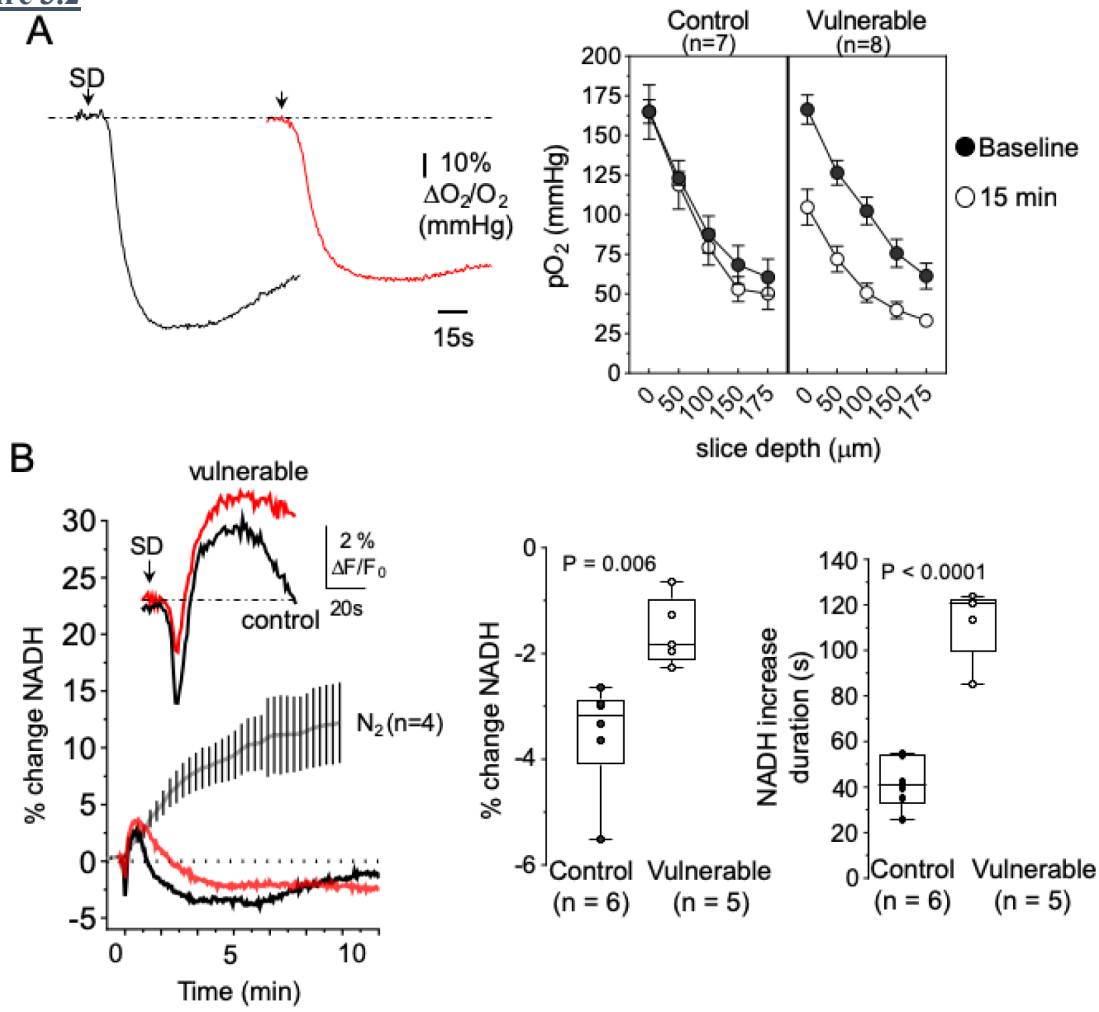

Figure 3.2. Indicators of metabolic stress are enhanced by SD. **A**. Continuous tissue pO_2 measurements during SD (expressed as percent of baseline ~1 min. prior to SD onset) in a control (left trace) and vulnerable (right trace) brain slice. Arrowheads point to baseline just prior to SD indicated by a drop in pO_2 during the DC shift. On the right shows pO_2 measurements at progressive increments from the slice surface (0∝m = surface to 175∝m or approximately the middle of the slice) slice depths from control and vulnerable slices. Measurements were taken before (filled circles) and after (open circles) SD. **B** Fluorescence NAD(P)H changes during SD in a single control (black) and vulnerable (red) brain slice. Data from 4 preparations during and after SD induced using via replacement of O_2 with N_2-supplemented aCSF (gray). Traces are aligned to onset of SD, indicated by sharp changes in NAD(P)H fluorescence. Inset traces from the same control and vulnerable slices show small dips and prolonged increases in fluorescence during SD (arrowhead) in vulnerable conditions (red trace). Pooled data quantifying the maximum amplitude of dips and the duration of fluorescence increases during SD from 5-6 preparations are shown on the right.

SD initiated by K^+ microinjection resulted in poor recovery of EPSPs and failure of slices to propagate a subsequent SD 15 minutes later. Traces in **Figure 3.2A** show continuous pO_2 measurements during SD. The initial drop in pO_2 during SD was similar in control and vulnerable brain slices (-46.1 ± 3.8 versus -41.7 ± 4.9 % change pO_2 in mmHg, for control and vulnerable slices, respectively; P = 0.46, n = 6,7). 15 minutes after SD tissue pO_2 gradients across all measured depths had recovered to baseline levels in control tissues (Figure 3.2A). However, vulnerable brain slices had significantly less available pO_2 at all depths during this same time point (Figure 3.2A).

Throughout the CA1 region NAD(P)H signals have a typical biphasic transient in response to neuronal depolarization (Foster et al., 2005; Hall et al., 2012; Shuttleworth, 2010) and during SD in adequately oxygenated brain slices (Foster et al., 2005; Lindquist and Shuttleworth, 2014). Figure 3.2B shows biphasic responses (traces) with larger oxidative transients indicated by the dip in NAD(P)H fluorescence in control compared to vulnerable slices. This dip was followed by a prolonged increase in NADH fluorescence and was reliably longer in duration after SD in vulnerable conditions (Figure 3.2B). After NADH increases, a long-lasting reduction below baseline was noted in all experiments and appeared to slowly return to baseline in control slices (see traces over extended time scale in Figure 3.2B). These changes were not further investigated in this study as they have the potential of arising as artifacts due to tissue optical changes during SD (Shuttleworth, 2011). However, it is possible that the impaired return to baseline in vulnerable slices is due to extensive oxygen utilization at this time point (Figure 3.2A). In a subset of experiments, brain slice hypoxia was induced by replacement of carboxygenated with 95% N_2 / 5% CO_2 supplemented aCSF. Figure 3.2B shows

substantial near-linear increases in the NADH signal during hypoxia that 1) indicate that elevated basal fluorescence in vulnerable slices did not blunt NADH signals during SD due to ceiling effects and 2) emphasize the differences between this model of metabolic vulnerability compared to complete substrate removal. Taken together these data indicate that brain slices have mild metabolic impairment at baseline that is augmented in the wake of SD.

Figure 3.3

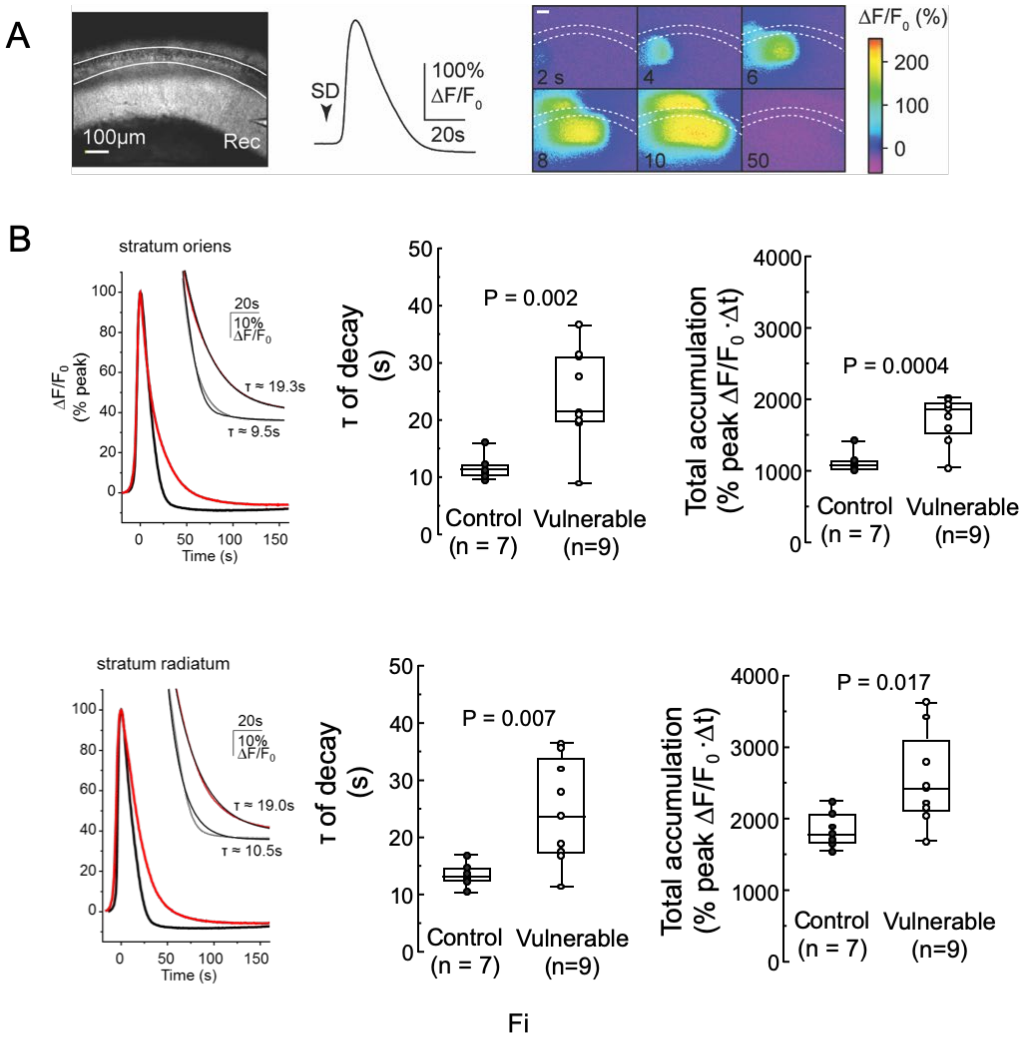

Fi

Figure 3.3. Prolonged glutamate accumulation during SD in vulnerable slices. **A.** Example of field of view in hippocampus and iGluSnFR fluorescence transient during SD in a control preparation. Images in the montage are taken during the passage of the SD wave front in the same slice. **B.** Fluorescence changes in the cell body layer (stratum oriens) and dendrite layer (radiatum) are extended during SD in vulnerable (red) compared to control (black) slices. Inset gray traces show best curve fit from nonlinear regression analyses. Time constant (τ) and total accumulation (area under the curve) calculations show reliable and extended glutamate accumulation in vulnerable slices during SD in both regions of interest.

3.3.3 Extracellular glutamate accumulation is prolonged in vulnerable brain slices

To examine the excitotoxic burden of SD in vulnerable brain slices we monitored extracellular glutamate accumulation during SD using iGluSnFR fluorescence imaging. **Figure 3.3A** shows a representative iGluSnFR transient and image montage during SD. In ROIs taken from CA1 stratum oriens (pyramidal cell bodies) and stratum radiatum (largely dendrites from pyramidal neurons) in Figure 3.3 B &C, demonstrate that glutamate transients are significantly prolonged across the hippocampus in vulnerable brain slices. The inset traces show examples of the curves generated via nonlinear regression used for determining decay constants (tau), where the R^2 goodness of fit parameter was used to determine data set outliers. Results from the entire data set reveal that the time course of glutamate recovery as well as total accumulation is impaired during SD in vulnerable slices.

3.3.5 Structural and functional recovery is impaired after SD in vulnerable slices

We have previously reported that EPSP recovery is significantly impaired after SD in vulnerable preparations (Reinhart and Shuttleworth, 2018). Prior work has shown that action of adenosine at presynaptic A1 receptors is a main contributor to the prolonged suppression of neuronal activity that outlasts action-potential blockade during the DC shift (Lindquist and Shuttleworth, 2012). We thus examined whether A1 receptor activation contributes to the lack of recovery of EPSPs in vulnerable preparations. Figure 3.4A confirms previous findings and demonstrate that in vulnerable conditions EPSPs only recovered to ~25% of baseline amplitudes after SD (**Figure 3.4A**). In these experiments, DPCPX incubation (500nM, ~10 min.) prior to SD improved recovery of responses and suggest that adenosine's actions at A1 receptors could mask, in part, the synaptic potential of neurons after SD. However, even

though neurons were able to respond to their presynaptic inputs, IOS read-outs of brain slice structural integrity were not improved by DPCPX (Figure 3.4C).

Figure 3.4

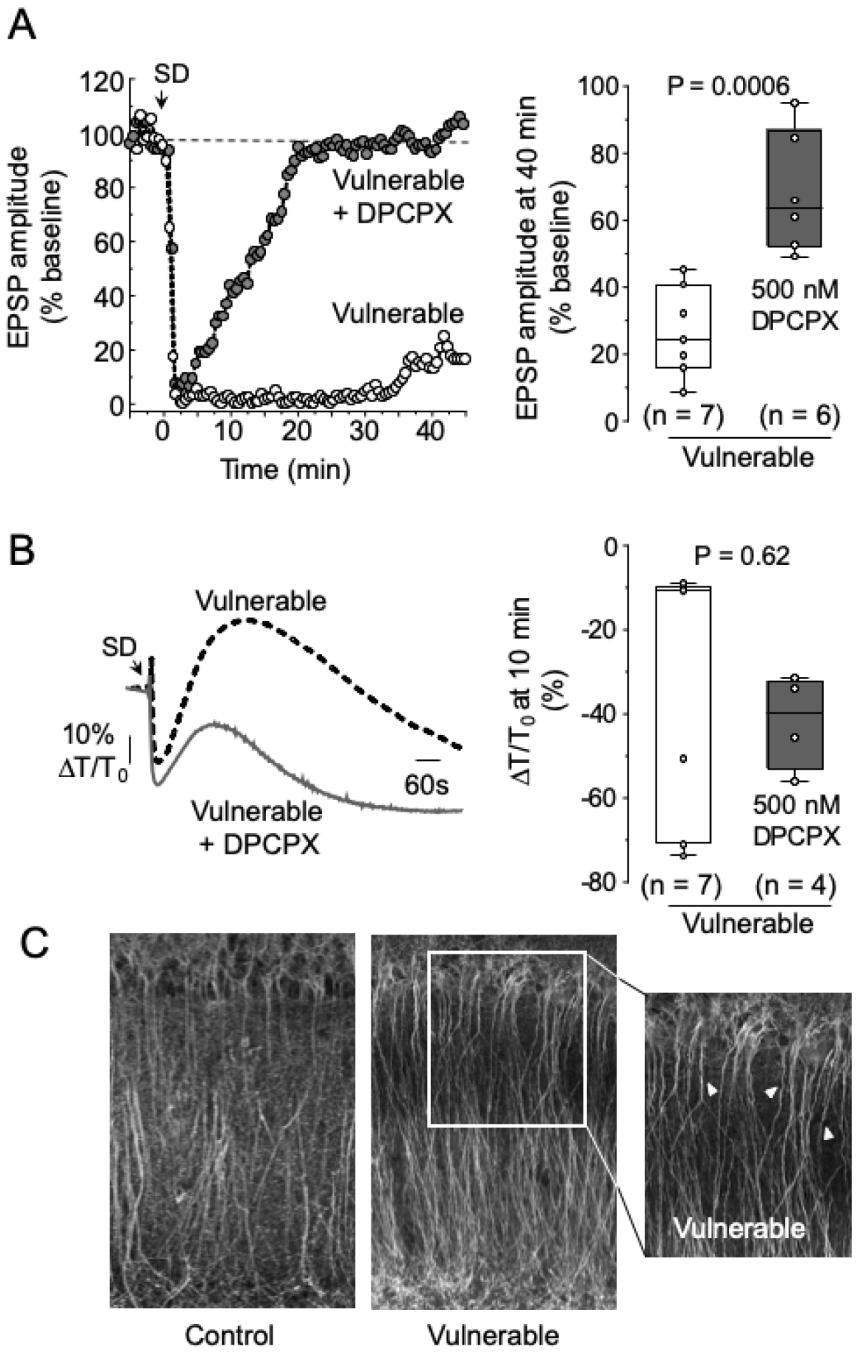

Figure 3.4. A1 receptor activation contributes to synaptic but not structural signs of neuronal impairment. **A.** EPSP amplitude during SD (arrow) in vulnerable with vehicle (open circles) or DPCPX treated (filled circles) preparations. Data from 6-7 preparations shown substantial recovery of postsynaptic responses after SD in vulnerable slices in the presence of DPCPX (300nM). **B** Changes in transmitted light during SD (arrow) in the same slices as (A) show that DPCPX does not prevent optical signs of slice damage, even 10 minutes post SD (right). **C.** representative images of MAP 2 immunoreactivity in control (left) and vulnerable (right) brain slices that were fixed at 10 min. after SD (DC shift onset). Arrowheads in inset box from vulnerable show point to tortuous dendrite processes

3.4 Discussion

3.4.1 General Findings

Here we further characterized a previously used brain slice model of metabolic impairment and assessed baseline changes in evoked synaptic transmission, slice oxygenation, and fluorescence metabolic read-outs before and after SD. Based on our findings, we propose the use of moderately compromised tissues in order to study mechanisms that contribute to the damaging consequences of SD. Such studies could promote our understanding of how vulnerable brain succumbs to SD-mediated injury and also elucidate potential targets for intervention at delayed time points after focal ischemia.

3.4.2 Metabolic compromise in brain slices

At baseline in control brain slices we observed almost no effect of the specific A1 receptor antagonist DPCPX on the amplitude and PPR of EPSPs (Figure 3.1). This suggests that basal adenosine production is minimal in these preparations. On the contrary, in vulnerable conditions, DPCPX wash-in significantly increased the amplitude (Figure 3.1B) of initially attenuated (Figure 3.1A) postsynaptic responses while normalizing elevated PPR to control levels. Though extracellular adenosine concentrations were not measured in these slices, results with DPCPX indicate that A_1 receptors are important mediators of depressed EPSPs and elevated PPR in vulnerable brain slices prior to SD stimulation. Since both pre- and postsynaptic processes for glutamate neurotransmission rely on substantial ATP production via oxidative phosphorylation (Hall et al., 2012), adenosine production may serve as protective feedback mechanism for limiting neuronal ATP expenditure when metabolic capacity is low. Activation of presynaptic A_1 receptors by adenosine can reduce energy expensive vesicular

release while postsynaptic actions of adenosine mediate neuronal hyperpolarization to reduce postsynaptic currents.

The reduction of synaptic activity may in part explain the similar rates of *basal* pO_2 consumption (or availability) measured in vulnerable compared to control preparations (Figure 3.2A). However, since the redox state of NAD^+/NAD(P)H influences tissue autofluorescence intensity – the reduced form (i.e. NAD(P)H) is fluorescent compared to the oxidized and non-fluorescent NAD^+ – increased NAD(P)H fluorescence in vulnerable brain slices may still implicate mitochondrial dysfunction and reduced oxygen availability for the final stages of oxidative phosphorylation in neurons.

3.4.3 Vulnerability to deleterious consequences of SD

Drastic differences between the two recording configurations was most apparent upon SD stimulation (Figures 3.2-3.4). Consistent with previous studies, we observed a precipitous drop in tissue pO_2 levels (Figure 3.2 traces) that coincided with the DC shift of SD. This likely is due to increased oxidative phosphorylation and O_2 consumption in response to sizeable ATP demands necessary for ion gradient reestablishment. The magnitude of the O_2 transients was not significantly larger in vulnerable slices compared to controls; however, 15 min. after SD O_2 measurements remained low in vulnerable preparations while controls had fully recovered. Further evidence of SD-induced metabolic stress is shown via prolonged fluorescence increases and buildup of NAD(P)H in vulnerable slices (Figure 3.2).

The increased burden of SD in compromised slices is also shown in studies employing iGluSnFR (Figure 3.3). During SD, massive amounts of glutamate accumulate extracellularly

likely due to extended depolarization and Ca^{2+}-mediated vesicular release and/or transporter reversal mechanisms that normally rely on electrochemical gradients for the clearance of glutamate. Disturbances in either of these processes could thus be in part responsible for extended glutamate transients measured in vulnerable metabolic conditions. Prolonged action at postsynaptic glutamate receptors (especially NMDA receptors) after the SD wave front can thus result in lengthy durations of intracellular neuronal Ca^{2+} loading; as observed previously using this brain slice model of compromise (Reinhart, 2018).

Basal elevations in NAD(P)H autofluorescence are positively correlated to adenosine accumulation in response to SD in thick hippocampal brain slices (>350 μm); tissues that are also metabolically strained due to steep reductions in O_2 delivery within the depths of the slice (Lindquist and Shuttleworth, 2014). Furthermore, adenosine A_1R activation after SD is largely responsible for the period (>5 min. in slice experiments) of synaptic depression that extends beyond action potential failure during the DC shift (Lindquist and Shuttleworth, 2012). The duration of A_1R mediated suppression of activity serves as a read-out of the metabolic demand of SD, where extended depression durations are a consequence of elevated adenosine–likely a result of augmented ATP consumption. Enhanced metabolic burden of SD in vulnerable slices is further supported by our results where DPCPX enabled virtually complete recovery of postsynaptic responses after SD in vulnerable slices (Figure 3.4). However, this did not change optical indicators of structural integrity disruption (i.e. dendritic beading, swelling and/or cell shrinkage, etc.) that have been previously evaluated in submerged brain slices using IOS imaging (Andrew, 1999)

3.5 Conclusions

For decades, researchers have been divided regarding mechanisms of SD that are induced in healthy brain compared to SD initiated in response to ischemia (or OGD *in vitro*); which has led to confusion regarding the relevance of SD in different conditions (e.g. migraine and ischemic stroke) (Hartings et al., 2017). While classical techniques of complete substrate removal are important for studying injury at the core of infarction or mechanisms of cell death during global cerebral ischemia (e.g. cardiac arrest, hypoglycemia, or altitude sickness) they may be less applicable to injury mechanisms in penumbral regions after stroke. Here we provide additional findings from a novel model of metabolic compromise that confers increased vulnerability to deleterious consequences of SD. This model could be used to examine mechanisms of injury during SD and/or therapeutic interventions.

4. Metabolic heterogeneity influences excitotoxic consequences of spreading depolarization in vivo

Katelyn M. Reinhart, Andrew P. Carlson, and C. William Shuttleworth
Department of Neurosciences, University of New Mexico School of Medicine.

Corresponding Author:
C. W. Shuttleworth, Ph.D.
Department of Neurosciences, MSC08 4740
1 University of New Mexico
Albuquerque, NM 87131
(505) 272 5826
bshuttleworth@salud.unm.edu

4.1. Abstract

Spreading depolarization (SD) has emerged as an important contributor to enlargement of acute brain injuries. We recently showed that the NMDA receptor antagonist ketamine was able to prevent deleterious consequences of SD in brain slices, under conditions of metabolic compromise. The current study aimed to extend these observations into an *in vivo* stroke model, to test whether gradients of metabolic capacity leads to demonstrable differences in glutamate and calcium accumulation following SD. In addition, we tested whether ketamine protects vulnerable tissue while allowing SD to propagate through surrounding undamaged tissue. Focal lesions were generated using a distal middle cerebral artery occlusion in mice, and clusters of SD were generated at 20 min intervals with a remote microinjection of KCl. SDs invading into peri-infarct regions had significantly different consequences, depending on distance from the infarct core. Close to the lesion, calcium and glutamate transients were extended, as compared with responses in better-perfused tissue more remote from the lesion. Extracellular potential shifts were also longer in regions proximal to lesions, and hyperemia following SDs were reduced. Consistent with *in vitro* studies, ketamine, at concentrations that did not abolish the propagation of SD, reduced severity of excitotoxic signaling in vulnerable peri-infarct regions without preventing spread of SD waves through more remote regions. These findings suggest that deleterious consequences of SD can be targeted *in vivo*, without preventing the spread of waves into tissue that may benefit from preconditioning or other potentially beneficial effects of SD.

4.2 Introduction

Spreading depolarization (SD) is a slowly propagating wave of near-complete neuroglia depolarization (~0 mV) that has been detected in intensive care unit (ICU) patients suffering from acute brain injuries including trauma (Eriksen et al., 2019; Hartings et al., 2011), subarachnoid hemorrhage (Dreier et al., 2006), and ischemic stroke (Dohmen et al., 2008). Repetitive SDs and/or SDs with prolonged depolarizations are particularly challenging to metabolically compromised brain and are associated with secondary lesion expansion and poor neurological outcomes (Dreier et al., 2017; Hartings et al., 2017, 2003). After stroke, SDs have been detected for days after ischemia onset (Dohmen et al., 2008; Nakamura et al., 2010; Woitzik et al., 2013) and during this time there are currently no clinically approved interventions (Powers, 2018). This suggests that therapeutics targeting SD mechanisms of injury may be neuroprotective after ischemic stroke.

A retrospective review of ICU medications showed that the NMDAR-antagonist ketamine can reduce SD frequency when used for sedation in brain injured patients (Hertle et al., 2012; Sakowitz et al., 2009). A recent prospective study demonstrated that ketamine infusion dose-dependently prevented SD over a range of clinically sedative doses after acute brain injury (Carlson et al., 2018). While these findings demonstrate SD can be prevented with ketamine, there is the theoretical possibility that SD propagating into non-ischemic brain regions can induce ischemic tolerance and/or preconditioning (Dreier, 2011; Pincherle et al., 2018, Shuttleworth et al., 2019). Therefore, doses of ketamine that block SD may also prevent any theoretical benefits of SD in tissues with adequate cerebral perfusion outside of the ischemic

penumbra (Hartings, 2017). Thus, it remains to be determined whether approaches that limit deleterious consequences without outright blocking SD may be clinically useful.

Extracellular recordings of SD reveal a large shift in the extracellular slow potential (DC shift) (Leao, 1947, Somjen, 2001). The duration of the DC shift is an indicator of underlying ionic loading that can be particularly deleterious to metabolically compromised neurons. Thus, prolonged or irrecoverable Ca^{2+} accumulation mediated by glutamate release and activation of NMDARs is prominent during the late phase of SD (Aiba, 2012). In brain slices, a concentration of ketamine that did not block SD reduced the duration of the late-phase of DC shifts (Reinhart, 2018). Additionally, ketamine attenuated intracellular neuronal Ca^{2+} loading during SD and improved functional recovery of evoked synaptic potentials in metabolically vulnerable slices (Reinhart, 2018). This indicates that ketamine, in the absence of vascular effects, can reduce the ionic burden of SD *in vitro* and mitigate neuronal injury without blocking SD. Whether ketamine can attenuate deleterious consequences in vulnerable neurons within the ischemic penumbra without preventing SD in more intact brain regions after *in vivo* stroke had not previously been examined. Here we studied SD clusters initiated *in vivo* after distal middle cerebral artery occlusion in mice and tested whether a ketamine in mice could reduce deleterious consequences without blocking SD outright.

4.3 Materials and Methods

4.3.1 Animals

All animal procedures were performed in accordance with protocols approved by the UNM Health Sciences Center Institutional Animal Care and Use Committee. Adult (10-20 weeks) male and female mice and maintained in standard group housing were used for all experiments. C57Bl/6 mice and homozygous breeding pairs for generation of neuronal GCaMP5G expressing mice were purchased from The Jackson Laboratory (Bar Harbor, ME). For Ca^{2+} imaging experiments, mice expressing the floxxed calcium indicator GCaMP5G under the CAG promoter (B6;129S6-*Polr2a*$^{tm1(CAG\text{-}GCaMP5g,\text{-}tdTomato)Tvrd}$/J; from (Gee et al., 2014)) were bred with mice expressing Cre Recombinase under the CamK2a promoter (B6.Cg-Tg(Camk2a-cre)T29-1Stl/J). Offspring had robust GCaMP5G expression throughout the hippocampus and cortex (Wang et al., 2013) and were thus utilized for experiments.

4.3.2. AAV injections

Neuronal expression of the fluorescent glutamate reporter iGluSnFR was achieved via intracortical injection of the adeno associated virus (AAV; pAAV1.hSyn. iGluSnFr.WPRE.SV40; Addgene, Cambridge, MA, USA)(Marvin et al., 2013) in C57Bl/6 mice. Animals were anesthetized with isoflurane (4-5% induction, 1-2% maintenance) and head fixed into a digital stereotaxic alignment system (Model 1900, David Kopf Instruments, Tujunga, CA, USA). After sanitization using Betadine and alcohol wipes, a scalp incision was made for burr hole preparation (0.295" diameter). In each burr hole, a total volume of ~0.5 µl of AAV (3.8×10^{13} GC ml^{-1}) was slowly delivered at ~0.1µl min^{-1} using a 5.0 µl Hamilton gastight syringe (Hamilton Company Inc., Reno, NV, USA) connected via polyethylene tubing to a 33G diameter infusion cannula (C315I/SPC; Plastics One Inc., Roanoke, VA, USA). After

infusions, the scalp was closed with silk sutures and topical lidocaine applied over the incision site. A 40% buprenorphine (0.1 mg kg^{-1}) saline solution was administered intraperitoneally (i.p.) for postoperative pain and animals recovered from surgery on a heating pad. Mice were returned to their home cages with littermates and experiments were performed ~2-4 weeks post injection to enable adequate iGluSnFR expression (Marvin et al., 2013).

4.3.3. Surgical preparation and distal middle cerebral artery occlusion

Mice were anesthetized with urethane (1.5 mg g^{-1} induction dose with ≤ 0.75 mg g^{-1} for maintenance, if needed), placed in a small animal stereotaxic frame assembly (David Kopf Instruments, Tujunga, CA, USA) and body temperatures were maintained at 37°C using a feedback-controlled heating pad system (Kent Scientific Corporation, Torrington, CT, USA). Urethane-anesthetized mice undergoing prolonged *in vivo* experiments have increased mortality rates when combined with airway obstruction by stereotaxic frames (Moldestad et al., 2009). We thus provided continuous O_2 supplementation via the stereotaxic frame gas inlet port throughout recording sessions as an alternative to additional invasive procedures (i.e. tracheotomy). An incision was made, and the exposed skull was kept moist with saline (0.9% NaCl) and mineral oil-soaked cotton to improve image quality (Chung et al., 2018). Burr holes were drilled (1 mm diameter) and the dura was carefully removed by microdissection for subsequent SD induction (initiated from bilateral burr holes in the frontal bone (ML: ± 1.0 mm, AP: + 3.0 mm, relative to bregma) and electrophysiological recordings. Burr holes above the motor cortex (AP: - 2.0 mm, ML: 1.0 and 2.0 mm) were used for simultaneous electrophysiological recordings from these two locations within the right hemisphere.

After burr hole preparation, focal stroke was induced by occluding the right distal middle cerebral artery (dMCAo) via cauterization, as described previously (KURAOKA et al., 2009; Lindquist and Shuttleworth, 2014). Briefly, an incision in the skin was made between the lateral part of the orbit and external auditory meatus and the temporalis muscle was removed. A small craniotomy (~2 mm) was drilled on the frontal bone just rostral to the zygomatic and squamosal bone union to allow transtemporal exposure of the MCA for coagulation (see Figure 4.1A). In sham-operated animals, the MCA was exposed but not cauterized. After occlusion or sham procedures, animals stabilized for 60 min prior to SD induction; during this time recording electrodes were placed in burr holes over the motor cortex (see Electrophysiology).

4.3.4 SD generation

It is likely that an initial SD occurred shortly after onset of occlusion in all animals but were not detected as this was prior to establishment of electrode recordings. After waiting approximately one hour for recovery from initial occlusion, SDs were initiated by microinjection of 1M KCl, to provide reproducible sets of SDs that propagated through regions of different metabolic capacity. KCl-evoked SDs were generated as previously described (Aiba et al., 2011) at a rostral location, distant from the MCA territory (see Surgical Preparation and **Figure 4.1A**). After visual confirmation of SD propagation (using imaging techniques, described below), any residual KCl was quickly removed (absorbed with cotton-tip applicator). The first induced SD was evoked 60 min. following dMCAo or sham surgeries and there were no significant differences in the onset time of KCl-induced SDs between groups (64.4 ± 2.0 min. versus 66.5 ± 3.1 min. for sham and dMCAo animals, respectively). We examined tissue consequences during repetitive SDs (a total of 3) separated by ~20-minute intervals (Figure 4.1B), as SDs that occur in clusters are particularly challenging for the injured brain. Under

these conditions of repetitive induction of SDs with focal KCl microinjection, Spontaneous SDs, were infrequently recorded, with clusters of KCl-induced SDs generated before spontaneous events were established (von Bornstädt et al., 2015). The experimental strategy employed here was designed similar to early work by Busch et al., that demonstrated step-wise lesion expansion with each SD evoked in 15 min. intervals after MCA occlusion (Busch, 1996).

4.3.5. Imaging

Laser speckle contrast imaging (LSCI) experiments were conducted in a subset of C57Bl/6 and GCaMP5G expressing mice (n = 4 male, 4 female for C57Bl/6 and n = 3 male, 3 female GCaMP5G mice). LSCI acquisition began shortly after dMCAo or sham surgeries (~5−10 minutes) and was used to monitor blood flow changes during SD, as previously described (Lindquist and Shuttleworth, 2014). Briefly, the intact exposed skull was illuminated by a 785 nm laser diode (Thorlabs, Newton, NJ, USA) and reflected backscattered light was longpass-filtered (720 nm) and focused with an SLR camera lens (55 mm; Nikon, Tokyo, Japan). Images were collected at ~ 6 Hz using a digital CCD camera (Stingray F-504B, Allied Vision Technologies, Stadtroda, Germany) and cerebral perfusion maps were calculated and displayed in real time by LabVIEW software modified from Bernard Choi, UCI (Yang et al., 2011). Offline calculations in Fiji (Schindelin et al., 2012) were used to normalize blood flow in ipsilateral regions of interest (ROIs) to corresponding ROIs on the contralateral hemisphere. ROIs were ~750µm in diameter (avoiding major blood vessels) and created in cortical areas close to ("proximal") and more distant from ("remote") the ischemic MCA territory (see schematic in Figure 4.1A). ROI coordinates were similar in sham and dMCAo groups for remote (ML: 1.4 ± 0.05 & AP: -1.3 ± 0.09 mm in sham versus ML: 1.5 ± 0.06 & AP: - 1.3 ± 0.08 mm in stroke, $P > 0.9$ for both ML and AP, relative to bregma, n = 7 animals/group) and

proximal locations (ML: 3.5 ± 0.04 & AP: -1.3 ± 0.08 mm in sham versus ML: 3.5 ± 0.06 & AP: -1.2 ± 0.07 mm in stroke, $P > 0.9$ for both ML and AP, relative to bregma, n = 7 animals/group).

For Ca^{2+} and glutamate imaging, a custom LED-based system was built to monitor wide-field fluorescence through the intact skull. LEDs and associated optical components were purchased from Thorlabs (Newton, NJ, USA). A 470 nm LED was collimated and mounted to a cage cube containing a 505 nm dichroic long pass (DCLP) beam splitter and incident light was orthogonal to the dorsal surface of the exposed skull. Fluorescent signals were long pass (505 nm DCLP) and bandpass filtered (510/40nm). Images (1280 x 960 pix, 1 x 1 binning) were collected at 4 Hz using a CCD camera controlled by Micro-Manager open source microscopy software (Edelstein et al., 2010). ROIs (500 μm diameter) on dMCAo or sham ipsilateral (right) hemispheres were normalized to corresponding contralateral ROIs and values were then transformed to reflect change in fluorescence from baseline ($\Delta F/F_0$; F_0: average intensity of 10 baseline frames prior to each SD). GCaMP5G and iGluSnFR signals during SD had contaminating signals ~30s after the peak and during the secondary phase of the transient (see **Supplementary Figure 4.2** for an example from an individual GCaMP5G sham experiment). These are likely artifacts due to blood flow changes and/or intrinsic optical signals arising from parenchyma tissue undergoing SD (see Discussion). In order to exclude these contributions from both GCaMP5G and iGluSnFR analyses and examine neuronal kinetics of recovery from SD, the peak amplitude of transients were aligned, and curves were fit using nonlinear regression algorithms (from the peak to 30s after peak). From these curves, recovery of fluorescence to 50% of mean baseline signals was calculated and reported as the half-life of

recovery (t_{50}). Due to variations in iGluSnFR signals with respect to the injection site, glutamate signals were normalized to the peak amplitude during individual SDs, to enable comparisons of the duration of transients. While this prevented quantitative analysis of peak amplitudes during SD, previous reports suggest that the absolute magnitude of glutamate accumulation during SD does not correlate with DC shift duration and/or lesion progression after ischemia in animals (Hinzman et al., 2015; Iijima et al., 1998). In contrast, the duration of depolarization does correlate with the duration of glutamate increases (Hinzman et al., 2015) and suggests that the time course of recovery is likely a better indicator of potential neuronal damage during SD versus the amplitude of the glutamate response.

4.3.6 Electrophysiology

Glass micropipettes containing Ag/Cl wires were filled with artificial cerebral spinal fluid (aCSF; containing (in mM): NaCl, 126; $NaHCO_3$, 26; glucose, 10; KCl, 3; $CaCl_2$, 2, NaH_2PO_4, 1.5; $MgSO_4$, 1) or normal saline (0.9% NaCl) and carefully placed in the two burr holes over the motor cortex (see surgical preparation, above) at a depth of ~500μm for continuous recording of DC and electrocorticographic (ECoG) potentials. Recordings were referenced to a Ag/Cl ground wire placed under the skin through a small incision in the neck. Signals were amplified using an Axoclamp-2B amplifier (Molecular Devices, Sunnyvale, CA, USA) and 1X or 100X (for ECoG signals) gain outputs were A/D- converted and displayed using a PowerLab 8/35 digitizer and LabChart 7 software, respectively (AD Instruments, Dunedin, New Zealand). A lowpass filter (0.5 Hz) was used for DC recordings and DC potential shift durations were calculated from onset (drop below baseline voltage) to 80% recovery. ECoG signals were bandpass filtered (0.5 – 45 Hz) and depression was evaluated according to established clinical guidelines in LabChart 7 software, with minor modifications (Dreier et al.,

2017b; Hartings et al., 2003, 2017) and performed by an individual who was blinded to the experimental group. Briefly, a standard integral (20s tau of decay) was calculated from the total ECoG power and depression durations were evaluated as the initial decrease in the integral to the time of first recovery.

4.3.7. Drugs

Urethane was purchased from Sigma-Aldrich (Merck KGaA, Darmstadt, Germany) and dissolved daily in normal saline (0.9% NaCl). Ketamine (100 mg/ml, racemic: R (-)/S (+), Putney, Inc., Portland, ME), was diluted in saline and administered (i.p.) at a dose of 5 $mgkg^{-1}$. This dose was chosen based on pilot experiments (data not shown) and did not block SD initiation. Ketamine or saline vehicle control was administered (i.p.) 30−45 minutes after dMCAo or sham surgery based on recent reports showing maximum plasma concentrations of ketamine are achieved within ~30 minutes after injection (i.p.) (Toki et al., 2018) and closely resemble CSF concentrations (Khlestova et al., 2016; Toki et al., 2018). All other chemicals were obtained from Sigma-Aldrich (St. Louis, MO, USA).

4.3.8 Statistical analysis

Data are reported as mean ± SEM. Statistical analyses (one-way analysis of variance (ANOVA), unpaired t-tests, nonlinear regressions) were calculated using GraphPad Prism (version 8.1.0, San Diego, CA, USA) and Statistical significance was determined by *P* values < 0.05, with Bonferroni correction during multiple comparisons.

4.4 Results

4.4.1 Regional heterogeneity of cerebral perfusion responses to SD after dMCAo

After stroke, brain tissue surrounding the infarcted region is often viable but at risk for succumbing to SD-mediated injury. To better understand mechanisms that lead to injury progression in vulnerable tissue during SD we performed dMCAo in mice. In this model, transtemporal access of a distal branch of the MCA allowed for occlusion under direct visualization (representative image of MCA shown in Figure 4.1A) and resulted in perfusion gradients across cortical areas supplied by the MCA watershed; including a necrotic core, penumbra, and intact/undamaged brain regions (KURAOKA et al., 2009). Images created using LSCI are shown in Figure 4.1C and show blood flow maps normalized to the contralateral hemisphere at approximately 50 – 60 minutes post sham and dMCAo surgeries. Group data in Figure 4.1C show cerebral perfusion deficits after dMCAo are moderately exacerbated in regions of interest (ROIs) proximal to the infarction compared to more remote ROIs and confirms regional differences in metabolic capacity across the cortex (Figure 4.1A). In ROIs even closer to the site of MCA infarction, but still within the imaging field on the surface of the cortex, relative perfusion deficits tended to be further reduced (~32 ± 1.6% decrease from the contralateral hemisphere) compared to remote and proximal ROIs (~19 ± 3.2% and ~27 ± 2.0% for remote and proximal, respectively and also shown in Figure 4.1C). This was a significant decrease in cerebral perfusion compared to remote ($P<0.01$, $n=7$), but not proximal, ROI locations ($P=0.11$, $n=7$).

Figure 4.1

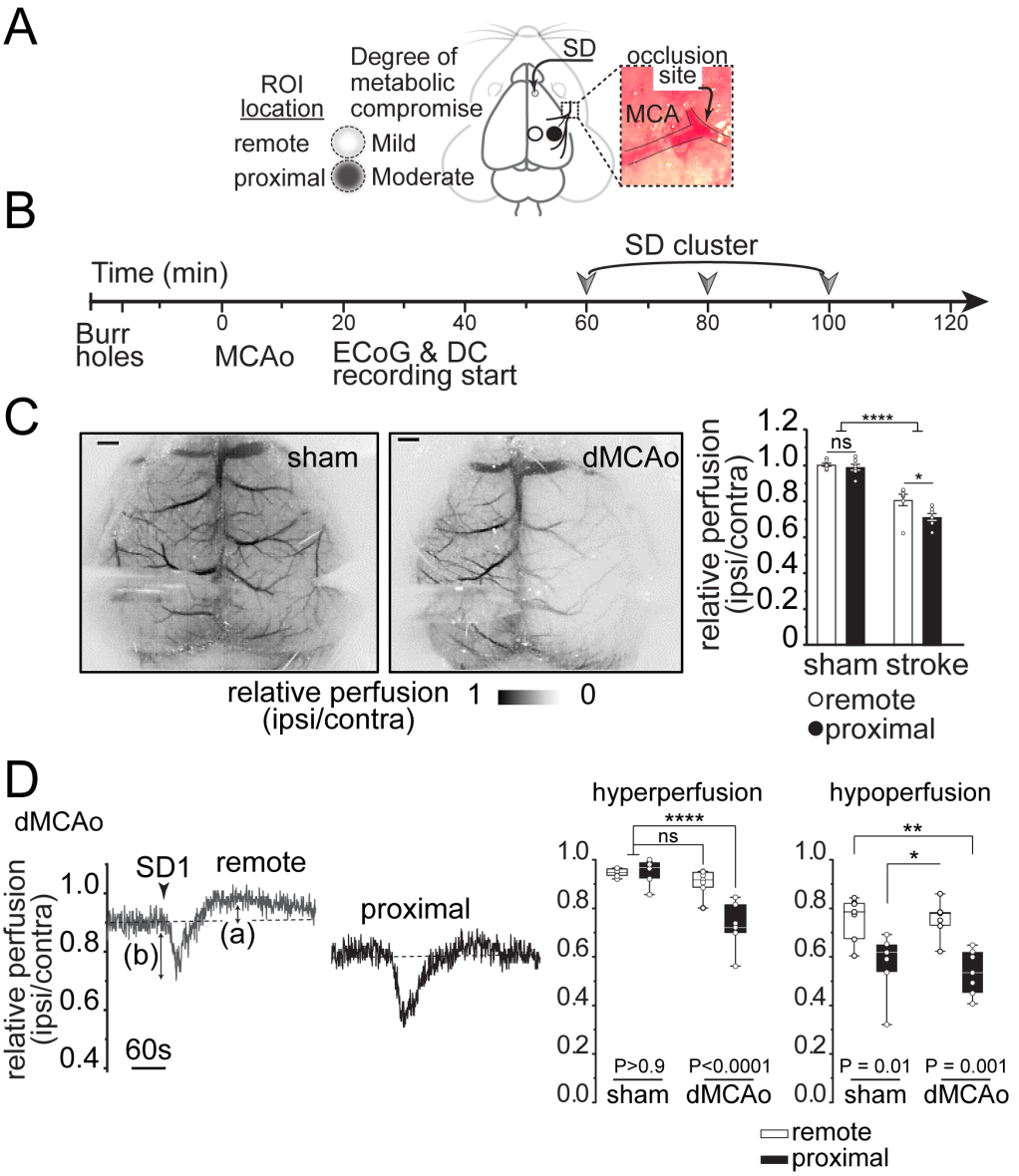

Figure 4.1. Regional heterogeneity of cerebral perfusion during SD after dMCAo. **A.** Diagram of ROIs used during imaging studies with respect to SD initiation site and MCA occlusion with proximal regions being more metabolically compromised compared to slightly more remote locations. The image on the right shows a distal MCA branch indicating the site of occlusion (arrow) used throughout this study. **B.** Experimental design for study. Prior to dMCAo or sham surgeries burr holes were prepared, and electrophysiological recordings began after placement of recording electrodes. SDs were stimulated at ~20-min intervals. **C**. Average projection of LSCI images acquired ~50 minutes after sham or stroke surgeries showing decreases in blood flow in the ipsilateral hemisphere as MCA occlusion (scale bar = 1mm). Group data at this same time point (n = 7 animals/group) show perfusion from ROIs (shown in A) normalized to corresponding regions on the contralateral hemisphere. **D.** Traces show representative perfusion responses during the first SD initiated at 60 min. after dMCAo (arrowhead indicates onset of CBF response) in remote and proximal ROIs from a single experiment. Data from the same animals shown in C, illustrates that relative hyperperfusion (indicated by (a) in traces on the left) in response to SD was blunted only in proximal ROIs after dMCAo. Hypoperfusion (b) are more pronounced in proximal regions in both sham and dMCAo.

To evaluate whether modest perfusion deficits in proximal ROIs made these cortical regions vulnerable to injury during SDs, we generated repetitive SDs at ~20 min intervals. Focal microinjection of KCl into a rostral burr hole distant from the immediate MCA territory was used to initiate SDs (see Methods; Figure 4.1A). In line with previous work (Ayata and Lauritzen, 2015), relative perfusion changes during the first evoked SD (initiated 60 min. post-surgery) were predominately characterized by profound hypoperfusion with minimal hyperperfusion in proximal ROIs, compared to more biphasic transients in less ischemic (remote) ROIs in dMCAo mice (Figure 4.1D**)**. Results in Figure 4.1D show that SD-induced hyperperfusion responses during the first SD were reliably blunted only in proximal locations in dMCAo animals. More remote regions after stroke were initially no different than respective remote ROIs in sham animals (Figure 4.1D), however hyperemic responses were less prominent during repetitive SD events (Figure S4.1).

The magnitude of hypoperfusion responses to SD was larger in proximal locations than in remote areas from both sham and dMCAo animals, indicating a smaller impact of ischemia on this parameter (Figure 4.1D). However, only dMCAo animals showed less pronounced perfusion responses during repetitive SDs in proximal ROIs (Figure S 4.1). This could be due to lesion expansion or other mechanisms that inhibit SD propagation in these regions. In sham animals, successive SDs (Figure S4.1) were initiated on an already oligemic background (resulting from the first SD stimulation, as reviewed by (Ayata and Lauritzen, 2015) and thus hypoperfusion transients may be underestimated under this imaging paradigm (i.e. macro-scale, intact skull with no thinning). This suggests that CBF measurements of hypoperfusion during SD may be less diagnostic for determining the metabolic capacity of underlying tissue

as it could reflect either ischemic injury progression or normal vascular responses during SD clusters. Collectively, these data show that brain tissues proximal to the MCA occlusion are

Figure 4.2

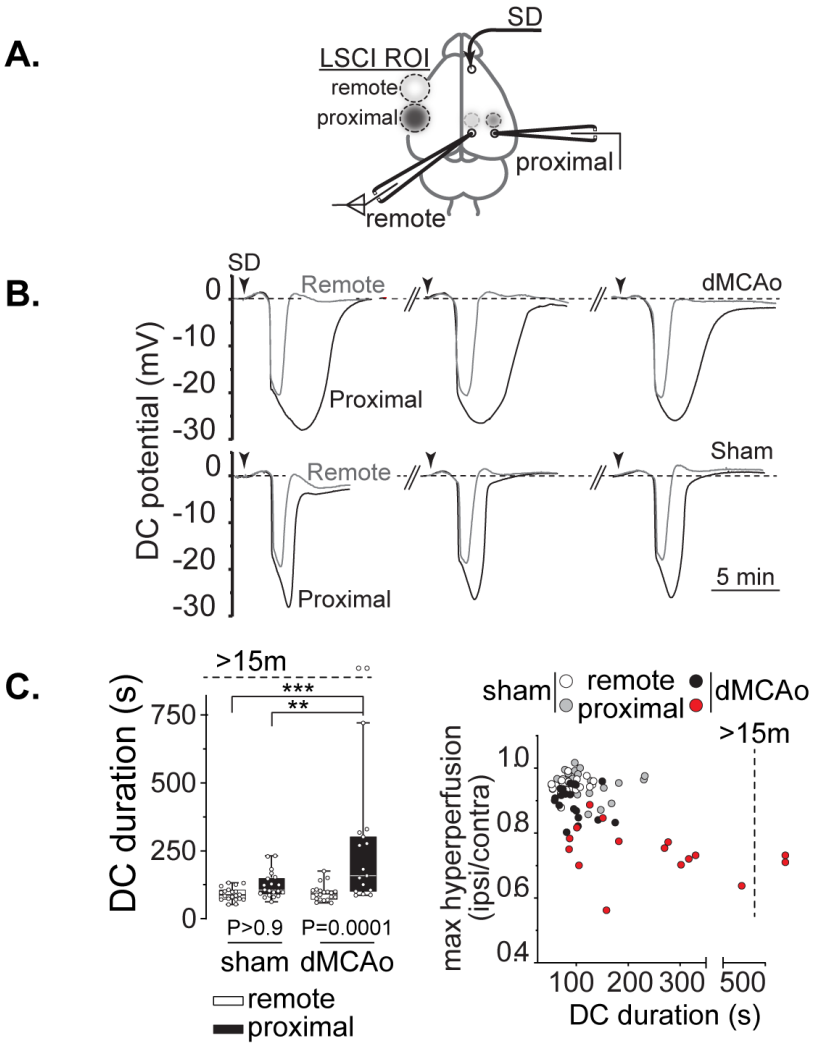

Figure 4.2. Prolonged DC shift durations in proximal brain regions after dMCAO. A. Recording schematic in relation to LSCI ROIs (show in Figure 4.1). Traces on the right show DC potential shifts during repetitive SDs (arrowheads) separated by ~20 minutes (double lines) in remote (gray) and proximal (black) recording locations after dMCAo and sham procedures. B. Data from 7 animals (shown in Figure 4.1) demonstrate that DC shift durations were prolonged in proximal locations after dMCAo. During repetitive SDs, DC shifts that did not recover to 80% of baseline prior to the next SD are symbols plotted (above dashed line) and were not included during analysis (n = 2 SDs in 2 dMCAo animals). C DC shift duration versus the maximum hyperemic response (recorded in the same animal) shows that DC shifts in proximal locations were also characterized by decreased hyperperfusion during SD. Symbols plotted to the right of the dashed line show that SDs with DC shifts that did not recover to baseline prior to the next stimulation also had reduced hyperemia during SD.

less able to mount hyperemic responses after SD and reflects vulnerability to further injury in these regions (Feuerstein et al., 2014).

DC shift durations are prolonged in penumbral regions

SDs characterized by prolonged durations of depolarization can be indicative of underlying tissue metabolic failure (Dreier et al., 2017a). We therefore monitored DC shift durations during repetitive SDs using electrodes placed near remote and proximal LSCI ROIs (diagram in **Figure 4.2A**). Representative DC shifts during SD in dMCAo and sham mice in Figure 4.2A and group data in Figure 4.2B show DC shift durations are significantly longer only in proximal recording locations after dMCAo. In 2 mice from the dMCAo group, the DC potential did not recover to baseline prior to the next SD stimulation in proximal tissues (Figure 4.2A, points above 15 minutes) and DC shifts were less distinguishable in recordings during subsequent SDs. In total ~80% of all SD attempts successfully propagated (confirmed via LSCI and/or DC recordings) into proximal tissues (17 confirmed SDs / 21 stimulations) compared to 100% in respective remote ROIs (21 confirmed SDs / 21 stimulations; n=7 mice) from dMCAo animals. In sham experiments 100% of stimulations evoked SD that was detected in both recording locations (21/21 for both remote and proximal; n=7 mice). Comparisons of hyperemia responses (shown in Figure 4.1) during SD and respective DC shift durations in these same animals are plotted in Figure 4.2B and demonstrate that prolonged depolarizations are accompanied by reduced tissue ability to increase blood flow (i.e. supply demand mismatch).

4.4.3 Extracellular glutamate recovery is delayed in proximal brain regions after dMCAo

Figure 4.3

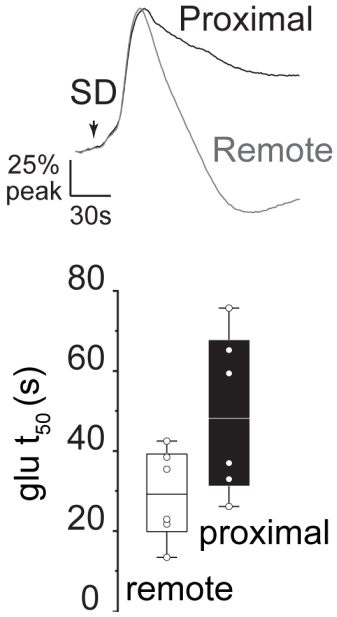

Figure 4.3. Proximal dMCAo brain regions have slower recovery from extracellular glutamate increases during SD. Traces show representative iGluSnFR fluorescence signals during the first SD after dMCAo. Data from 6 animals show that the time course of extracellular glutamate recovery was delayed in more ischemic ROIs.

Employing glutamate-sensitive microelectrode arrays, it was recently reported that extracellular glutamate increases are tightly time-locked with spontaneously occurring SDs after MCAo, and also that the duration of glutamate elevations positively correlates with DC shift durations (Hinzman et al., 2015). We thus evaluated the influence of dMCAo metabolic gradients on the extent of extracellular glutamate accumulation during SD in our experiments. **Figure 4.3** shows representative traces and group data of fluorescence signals during SD and indicate that neurons in proximal zones experience prolonged exposure to extracellular glutamate. These data indicate that regions in proximal areas after dMCAo are vulnerable to glutamate-mediated excitotoxicity during the DC shift of SD.

4.4.4. Ketamine reduces neuronal Ca^{2+} and DC shift durations after dMCAo

In brain slice models of metabolic compromise SD induces irrecoverable neuronal Ca^{2+} loading that can be reduced by NMDAR antagonists (Aiba and Shuttleworth, 2012) including ketamine (Reinhart and Shuttleworth, 2018) to improve neuronal recovery. We thus monitored cortical neuron Ca^{2+} accumulation during SD through the intact skull of GCaMP5G-expressing mice (**Figure 4.4)**. Ca^{2+} signal half-lives from best-fit curves show a marked delay of Ca^{2+}

recovery during SD in proximal ROIs in dMCAo animals (Figure 4.4B). In these experiments, SD intervals were not different between groups, however in vehicle-treated dMCAo mice, ~83% of SD initiation attempts (15/18) resulted in Ca^{2+} transients observed in proximal ROIs compared to 100% (18/18) success within remote regions. Traces in Figure 4.4C from one of these experiments show irrecoverable Ca^{2+} signals during the first SD that become significantly lost during subsequent SDs. Additionally, remote ROIs show step-wise increases in the duration of neuronal Ca^{2+} that resemble more proximal areas by the final SD in the cluster. In ketamine treated animals, SD-induced Ca^{2+} signals were confirmed in both remote and proximal ROIs during all SD attempts (18/18). Results in Figure 4.4B show the time course of recovery was accelerated in penumbral regions in the presence of ketamine compared to delayed recoveries in proximal locations in vehicle-treated mice. However, the Ca^{2+} load was still elevated compared to proximal regions in non-ischemic animals (Figure 4.4B). Traces in Figure 4.4C show that Ca^{2+} dysregulation is still observed in proximal locations after ketamine-treatment likely due to the immense challenge that SD clusters pose to vulnerable brain. Additionally, ketamine prevented the progression of irrecoverable Ca^{2+} accumulation in remote regions during SD. DC recordings during SD showed that ketamine treatment could

Figure 4.4

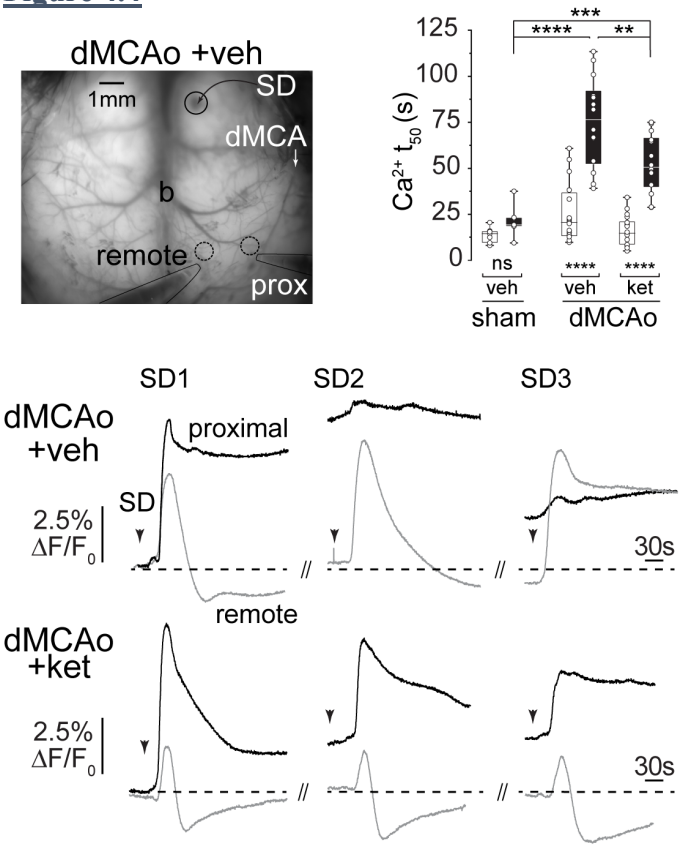

Figure 4.4. Ketamine reduces intracellular neuronal Ca2+ load during SD. A. Average projection 10 frames during image acquisition ~50 minutes after dMCAo in a vehicle-treated animal indicating the location of recording electrodes, Ca2+ ROIs, and SD initiation site relative to bregma (b) and dMCA. B. Ca2+ signal half-life during repetitive SDs in sham (n=3 animals) and dMCAo mice treated with vehicle (n=6) and 5mgkg-1 ketamine (n=6). C. Top: Ca2+ traces during repetitive SDs (arrowhead) in the presence of vehicle showing prolonged elevations in neuronal Ca2+ during the first SD in proximal locations (black) and failure of subsequent SDs to propagate in the same location. In this animal, neurons in remote (gray) brain regions had progressively worse recovery of SD-induced Ca2+ elevations during repetitive events. Traces below during SD in the presence of ketamine showed delayed progression of irrecoverable Ca2+ transients in proximal ROIs with and no change in remote locations during repetitive SDs. Fluorescence changes are normalized to levels prior to SD1.

reduce the duration of depolarization in proximal locations (**Figure 4.5**) during repetitive SDs. Comparisons of Ca^{2+} recovery half-life to the duration of DC shifts showed that ketamine could reduce damaging consequences of neuronal Ca^{2+} loading in part by reducing the DC shift duration after dMCAo.

4.5 Discussion

4.5.1General Findings

In this study we examined mechanisms of neuronal injury that occur during repetitive SDs in the ischemic brain and tested whether the clinically-approved NMDAR antagonist ketamine could reduce these damaging consequences. Using LSCI to monitor CBF, we identified brain regions with reduced perfusion and poor neurovascular responses to SD which are implicated

in tissue deterioration and expansion of injury after stroke. In vulnerable brain regions (proximal to the infarction), we observed prolonged DC shift durations and impaired recovery of extracellular glutamate and intracellular neuronal Ca^{2+} accumulation during SD. A dose of ketamine that did not block SD reduced the duration of DC shifts and was accompanied by improved neuronal recovery of intracellular Ca^{2+} loading during SD. Collectively, these results indicate that excitotoxic mechanisms can be targeted to reduce deleterious consequences of SD *in vivo* after stroke.

4.5.2 Experimental design

We induced focal ischemia in mice by occluding the MCA, as this approach is thought to resemble the most common type of insult experienced in stroke patients (Alessandra et al., 2014). MCA occlusion has the advantage over global ischemia or bilateral common carotid artery (CCA) intraluminal filament approaches as it promotes the development of collateral flow and thus readily-discernable regions of metabolic differences (i.e. necrotic core, salvageable penumbra, and healthy tissue) (KURAOKA et al., 2009) and (Xi et al., 2004). We chose to occlude a distal branch of the MCA (dMCAo) as other methods, including intraluminal approaches, occlude the MCA at more proximal locations which can also interrupt perfusion along bifurcations within the Circle of Willis as the suture ascends the internal carotid artery (ICA) (Alessandra et al, 2014). As such, although the intraluminal MCAo is less invasive during stroke induction, it results in larger ischemic lesions beyond the MCA territory that includes neuronal death in subcortical structures including the caudate and hippocampus. These larger stroke models are useful for examining functional deficits as there are no obvious functional impairments elicited by the surgical dMCAo model in mice (KURAOKA et al., 2009, Xi et al., 2004).

We took advantage of the resultant metabolic heterogeneity of the focal dMCAo stroke model to examine SD mechanisms that contribute to neuronal injury and lesion expansion. This was also useful for examining the effect of ketamine as prior work has demonstrated that NMDAR antagonists are less effective in tissues that are closer to the infarction due to pathological elevations in extracellular K^+ in these regions (Petzold et al., 2005). Since the delayed phase of injury progression occurs in the hours to days after stroke onset (Hartings et al., 2003), we initiated a cluster of 3 SDs using local application of K^+ in order to image excitotoxic mechanisms during SD over a shorter time-scale. This experimental design is according to similar protocols employed in earlier work by Busch et al. that provided a causal role of SD in stepwise injury expansion monitored via diffusion-weighted MRI (Busch et al., 1996).

4.5.3 SD-induced cerebral perfusion responses reflect regional heterogeneity in brain metabolic capacity

Using LSCI to monitor CBF throughout the entire cortex, we confirmed regional differences in perfusion (prior to SD stimulations) in dMCAo animals (Figure 4.1). Due to technical limitations (i.e. repositioning of animals for imaging and electrophysiology after surgery) we did not collect baseline perfusion maps prior to dMCAo or sham surgeries. Therefore, residual blood flow compared to baseline levels was not used to determine stroke core and penumbra areas based on previous literature. Instead, ROIs were normalized to their respective locations in the intact contralateral hemisphere during analyses and cortical areas with mild (remote) and moderate (proximal) levels of perfusion deficits were identified. ROIs placed as close as possible to the site of surgical occlusion and still within the imaging field showed a slight but not significant decrement in perfusion compared to proximal ROIs (i.e. ~32% vs. ~27%). This

could indicate that more severe perfusion deficits exist outside of our field of view and represent the true infarct core.

After identifying remote and proximal ROIs with reduced vascular supply, we examined CBF responses to SD in sham and dMCAo animals (Figure 4.1). In the naïve otherwise healthy cortex in mice, intact neurovascular coupling in response to a single SD is most often characterized by profound initial hypoperfusion which is followed by transient hyperperfusion and long-lasting oligemia (as shown Figure S4.1. traces during the first SD in a sham animal). On this oligemic background, we saw that subsequent SDs did not exacerbate blood flow decreases, and hemodynamic responses to SD were predominately hyperemic, as previously described (Ayata and Lauritzen, 2015). Though dMCAo did not drastically alter the magnitude of hypoperfusion, we did observe a marked reduction in the degree of hyperperfusion responses to SD in proximal ROIs closer to the infarct (Figure 4.1D) that was consistent during repetitive SDs (Figure S4.1). Initially, hyperperfusion responses in remote ROIs after dMCAo were similar to sham experiments (Figure 4.1D). However, there was progressive loss of SD-induced hyperperfusion in these regions during repetitive SDs, that was not observed in control animals (Figure S4.1). This transition of SD hemodynamics relates to tissue metabolic capacity and has been observed after ischemia in animals (Feuerstein et al., 2014; Shin et al., 2005; Sukhotinsky et al., 2008; Strong et al., 2006) and in humans after malignant middle cerebral artery infarction (Woitzik et al., 2013) and may be attributed to pathological mechanisms preventing hyperemia (Dreier, 2011; Dreier et al., 1997), and/or the inability of maximally dilated vessels to increase local CBF (Feuerstein et al., 2014).

Our findings further emphasize the continuum of consequences of SD in the injured brain (Ayata and Lauritzen, 2015; Dreier, 2011). In combination with poor vascular supply, impaired neurovascular coupling during SD (especially in more proximal areas), likely signifies that a brain region is compromised (Ayata and Lauritzen, 2015) and at risk for tissue deterioration during SD (Feuerstein et al., 2014). We therefore sought to examine cellular mechanisms that contribute to deleterious neuronal consequences of SD and test whether ketamine could interfere with these injury processes.

4.5.4 DC shift duration

The breakdown of electrochemical gradients during the DC shift of SD (Somjen, 2001) is estimated to be the largest disruption of homeostasis in living neural tissue and is thus energetically costly, even in non-injured brain (Dreier and Reiffurth, 2015). After MCAo in rats, spontaneous and repeated SDs with prolonged DC shifts correlate with histological neuronal damage (Mies, 1993). Injurious consequences of SD are also implicated in brain trauma patients where poor neurological outcomes are associated with prolonged DC shift durations (Hartings et al., 2011).

In our experiments, we saw a range of DC shift durations (Figure 4.2) after dMCAo in proximal locations that became significantly prolonged with repetitive SDs. However, there were many DC shifts that had similar durations to sham controls and remote recording locations. Across studies there seems to be no concrete time period of depolarization required for injury but prolonged DC shifts and accompanying low perfusion appear to be main contributors (Dreier et al., 2018). In support of these findings, we observed that SDs in

proximal dMCAo regions have longer DC shift durations and reduced hyperemia, and further suggest these regions are vulnerable to injury (Figure 4.1 & 4.2).

4.5.5. Glutamate

Brain slice studies have demonstrated that substantial glutamate release and NMDAR-mediated Ca^{2+} influx into fully depolarized neurons during the late-phase of the DC shift are important mediators of deleterious SD consequences (Aiba and Shuttleworth, 2012; Dietz et al., 2008). To examine neuronal mechanisms of injury during SD, we used viral delivery of the glutamate sensitive reporter iGluSnFR that is expressed on the extracellular surface of neurons (Marvin et al., 2013). In a recent report, glutamate transients following K^+- induction of SD were monitored with two-photon imaging of iGluSnFR in the healthy cortex and demonstrated relatively rapid recovery of extracellular signals returning to baseline levels within ~20 seconds (Enger et al., 2015). In nominally healthy brain slices, we have observed similar recovery time courses of glutamate during SD (data not shown). Here, we examined iGluSnFR transients during SD initiated from a less ischemic brain region after dMCAo and saw that SD-mediated glutamate increases were prolonged (> 30 seconds, based on t_{50} calculations). While the use of different imaging modalities prevents direct comparison to published findings (Enger et al., 2015; Iijima et al., 1998), it is likely that neuronal compromise contributes to enhanced glutamate accumulation that occurs only in synchrony with SD after dMCAo (Fabricius et al., 1993; ijima et al., 1998). This is also supported by glutamate microelectrode array findings where glutamate durations, but not absolute magnitudes of increases, correlated to prolonged DC shift durations during SD (Hinzman et al., 2015).

Our data confirms these findings and provides further evidence that damaging consequences of SD are in part mediated by extended exposure of penumbral neurons to the excitotoxic effects of glutamate (Figure 4.3). In addition to contributing to regenerative presynaptic glutamate release (Zhou et al., 2013) and ionic disruption during SD (Somjen, 2001), clearance of extracellular glutamate is metabolically costly; consuming ~1 ATP per molecule of glutamate (Danbolt, 2001). These results suggest that gradients of glutamate accumulation during SD can exist simultaneously across different brain regions after focal ischemia and further support the notion of a continuum of SD consequences with respect to tissue metabolic capacity (Hartings et al., 2017).

4.5.6 Calcium

Extracellular glutamate concentrations (>10 μM) (Hinzman et al., 2015; Iijima et al., 1998) and near-complete depolarization of neurons (Somjen, 2001) are sufficient to activate all receptor subtypes of NMDARs (EC_{50}: ~0.5- 2μM) (Nakanishi et al., 1992). It is thus likely that prolonged glutamate signals observed during SD in metabolically compromised brain regions results in excitotoxic intracellular Ca^{2+} accumulation. Using GCaMP5G-expressing mice, we observed relatively uniform basal Ca^{2+} fluorescence in the parenchyma through the intact skull (Figure 4.4).

During SD, profound perfusion artifacts likely contribute to the intensity of Ca^{2+}-bound GCaMP5G fluorescence as both oxy- and deoxyhemoglobin (HBO_2 and HBR, respectively) have absorption at the GCaMP wavelength (470nm, used here) (Ma et al., 2016). Prior to SD in the healthy cortex, molar extinction coefficients of HBO_2 and HBR are relatively comparable and thus similarly absorb excitation light. During SD in the naïve brain,

hypoperfusion and vasoconstriction will cause a decrease in both HBO_2 and HBR (likely at the SD-wave front) while subsequent hyperemia will increase delivery of HBO_2. During the prolonged phase of oligemia, CBF can be decreased by ~60% (Shin et al., 2005) and coincides with increases in oxygen metabolism and hemoglobin desaturation (Yuzawa et al., 2011). Corresponding to this phase, we observed a substantial increase in Ca^{2+} fluorescence intensity after the first SD in sham animals (Supplementary Figure 4.2) and is likely due to less absorption of both HBO_2 and HBR compared to pre-SD levels. Thus, in order to compare GCaMP5G dynamics during SD, we used the initial time course of fluorescence recovery from peak (aligned to 0s) to 30s as an indicator of the capacity of neurons to recover from intracellular Ca^{2+} accumulation during SD (Figure 4.4).

We observed slower recovery of Ca^{2+} in proximal regions after SD that failed to return to baseline in 3/6 mice during imaging. When SD-induced Ca^{2+} transients failed to recover, SDs did not propagate into the same ROI during subsequent stimulations. Traces in Figure 4.4C show that failure of SD to propagate into proximal locations was coincident with progressively delayed time courses of Ca^{2+} recovery in remote ROIs and could indicate expansion of the injury into these brain areas.

4.5.7 Ketamine

Based on prior animal studies and recent findings in humans, we tested whether ketamine could reduce neuronal Ca^{2+} load in metabolically vulnerable brain regions without preventing SD in remote regions. In rodents, intraperitoneal injection of up to 30 $mgkg^{-1}$ are considered subanesthetic ketamine doses and are used in many animal models examining ketamine's rapid anti-depressive effects (Zanos et al., 2016; Zanos and Gould, 2018). Additionally, the potency

of ketamine blockade of NMDARs depends not only on receptor subunit composition but also ketamine stereospecificity (Glasgow et al., 2017; Khlestova et al., 2016). Both stereoisomers of ketamine S (+) and R (−) are clinically used however the S (+) isomer is ~ 2-times more potent at NMDARs (Peltoniemi et al., 2016). Here we used a 5 $mgkg^{-1}$ dose of racemic ketamine which is thus expected to correspond to subanesthetic doses in humans (~0.5 mg/kg; (Khlestova et al., 2016)).

Ketamine (5 $mgkg^{-1}$) reduced intracellular Ca^{2+} loading in neurons and the duration of depolarization during SD (Figures 4.4&4.5). Here, we detected DC shifts and/or Ca^{2+} transients in all animals undergoing repetitive SD challenge (in sham and ketamine-treated dMCAo groups) and thus suggests that underlying tissue is viable as it can sustain subsequent SDs (Koroleva and Bures, 1996). Since SDs that occur in clusters are particularly challenging for compromised tissues, ketamine did not completely prevent the development of irrecoverable Ca^{2+} transients during SD in more ischemic regions. However, ketamine exposure did delay the progression of injury into remote regions (Figure 4.4). These data are consistent with our prior findings using ketamine in metabolically vulnerable brain slices challenged by SD (initiated by K^+); where neuronal Ca^{2+} influx was attenuated by ketamine (30μM) without preventing SD propagation (Reinhart and Shuttleworth, 2018). In those studies, ketamine improved recovery of evoked neurotransmission and brain slices were capable of propagating subsequent SD waves and is indicative of viable neurons (Koroleva and Bures, 1996).

4.5.8 Conclusions and Implications

In this study, we saw increased vulnerability of neurons to excitotoxic injury during SD *in vivo* that was based on proximity to the infarction. In these proximal regions, insufficient blood supply and prolonged DC shift durations can contribute to neuronal injury during SD. We additionally found that accumulation of extracellular glutamate and intracellular neuronal Ca^{2+} are enhanced in vulnerable brain regions and serve as potential cellular targets for limiting excitotoxicity during SD. This is supported by our findings that ketamine could reduce the duration of DC shifts and neuronal Ca^{2+} loading during SD.

Doses of ketamine and other NMDAR antagonists required to suppress SD are greater than those needed to prevent NMDAR activation under normal physiological conditions (Pietrobon and Moskowitz, 2014). NMDAR activation is likely important for brain recovery after injury, and blockade of downstream cell survival mechanisms is thought to contribute to the unsuccessful clinical trials of NMDAR-antagonists in acute ischemic stroke patients (Wu and Tymianski, 2018). Additionally, NMDAR antagonists are less effective at preventing SD after brain injury likely due to pathological increases in extracellular K^+ concentrations (Petzold et al., 2005). Together, the high doses of ketamine capable of blocking SD in the injured brain might do so at the expense of important NMDAR-dependent repair processes. While work is needed to determine whether SD itself contributes to cellular repair and/or other processes (i.e. preconditioning) in remote tissues in the aftermath of stroke, these findings support the clinical use of ketamine to reduce SD-mediated injury after ischemic stroke.

4.6 Supplementary Figures

Figure 4.5

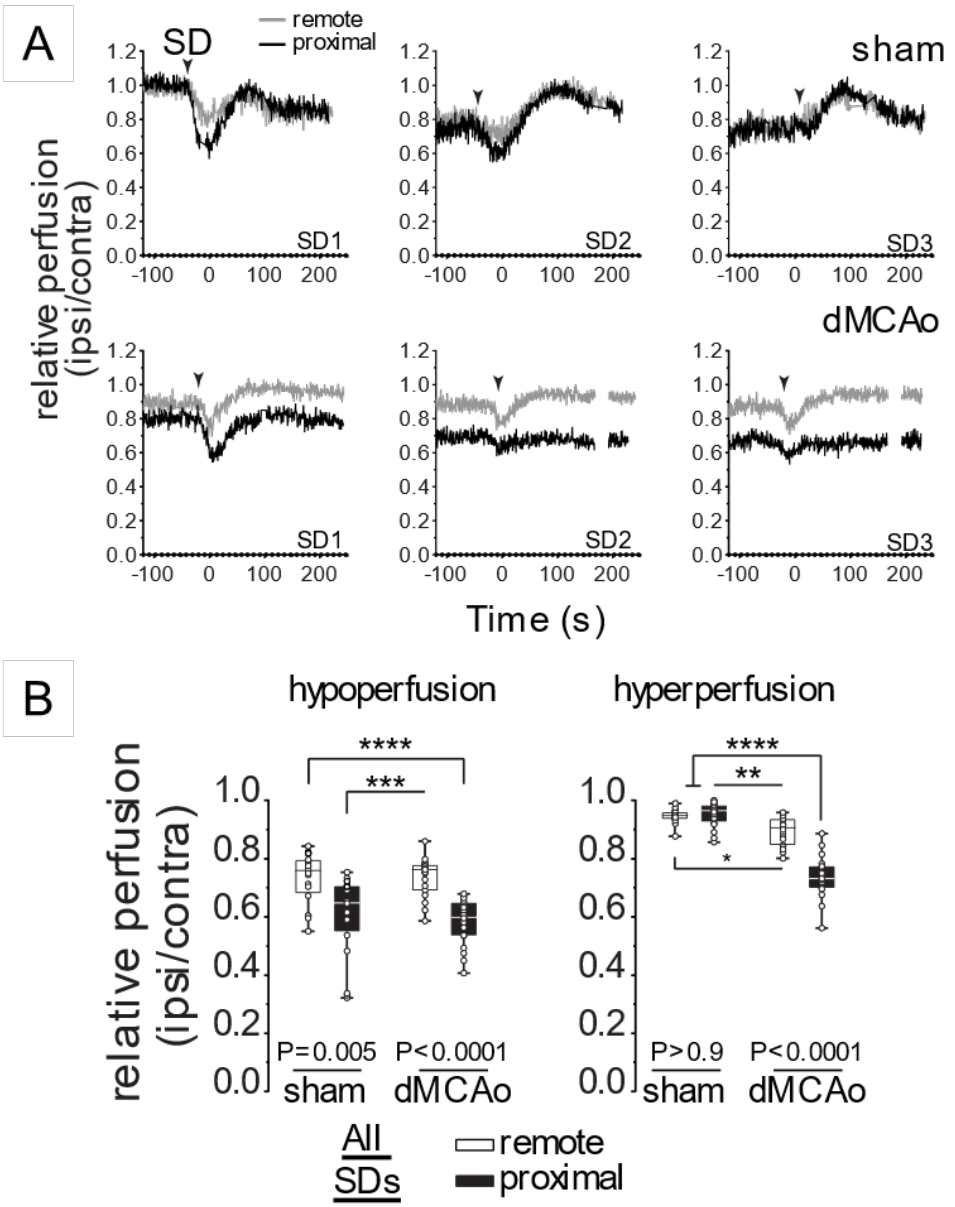

Supplementary Figure 4.1. A. Cerebral perfusion responses during repetitive SDs. Traces from LSCI experiments showing representative perfusion responses during repetitive SDs (arrowheads) in sham and dMCAo animals. **B.** Group data from all animals (n=7, shown in Figure 4.1) demonstrates that hyperperfusion in proximal locations was consistently less than corresponding remote regions within the same animal as well as sham controls.

Figure 4.6

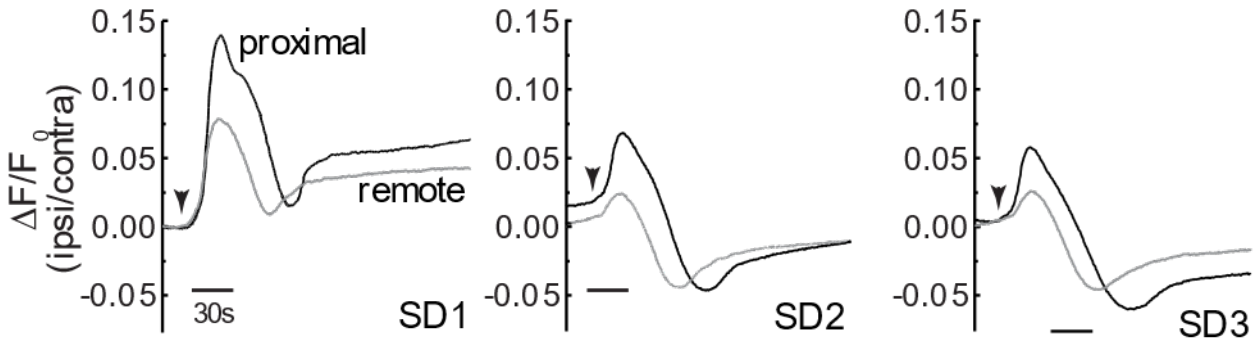

Supplementary Figure 4.2. Intracellular neuronal Ca^{2+} transients during repetitive SDs following sham surgery. GCaMP5G signals during SD show artifacts that may arise from perfusion-related changes during SD clusters as shown in S4.1.

.

5. DISCUSSION

5.1 Summary

Initial studies in this dissertation project were designed in brain slices using fluorescent glutamate and Ca^{2+} reporters in order to exclude complex vascular responses to SD (as seen in Chapter 4 experiments) and evaluate consequences specific to neurons. Early during the pursuit of this work, it became clear that current models for examining SD consequences in metabolically impaired tissues were limited and relied on mostly complete substrate removal (hypoxia or OGD). A novel brain slice model of metabolic compromise that conferred neuronal vulnerability to SD was thus initially employed in Chapter 2 and subsequently characterized in Chapter 3. In these studies, extracellular glutamate (Chapter 3) and intracellular neuronal Ca^{2+} (Chapter 2) accumulation in response to SD were both prolonged by metabolic compromise and associated with poor recovery of synaptic responses—revealing an opportunity for therapeutic intervention. Brain slice studies with ketamine (Chapter 2) provided proof of concept data that mediators of injury can be reduced (i.e. Ca^{2+} loading via NMDAR opening) to improve neuronal recovery without preventing SD outright.

Prolonged accumulation of glutamate and Ca^{2+} during SD was confirmed in Chapter 4 studies that translated brain slice findings to *in vivo* experiments after dMCAo. Findings that glutamate and neuronal Ca^{2+} levels are enhanced during SD in peri-infarct tissue are consistent with the role of these mediators in lesion expansion. Chapter 4 studies also demonstrated the protective nature of ketamine where reduced DC shift durations and NMDAR-mediated Ca^{2+} loading made neurons less vulnerable to SD consequences. Importantly even though mechanisms and interventions were first characterized in brain slices, they remained prominent in the presence

of massive cerebrovascular responses to SD; responses that involve elevations in virtually all vasoactive substances– including NO, adenosine, K^+ (Ayata and Lauritzen, 2015). Also important is the efficacy of ketamine on SD consequences in penumbral tissue– regions where NMDAR antagonists have been previously shown to have little effect on SD (determined as the ability of blockade) due to pathological elevations in interstitial K^+ concentration (Petzold et al., 2005). While information regarding the best effective dose for reducing SD consequences were not examined in this dissertation (largely due to substantial species-dependent differences in effective ketamine doses, discussed in Chapter 2), this work provides evidence that ketamine or even related (e.g. memantine (Emnett et al., 2013)) medications may be repurposed to limit deleterious consequences of SD after stroke (see Appendix A for initial brain slice studies with memantine). The figure below summarizes mechanisms involved in deleterious consequences of SD that will be considered throughout the discussion of this dissertation work (Figure 5.1).

Figure 5.1

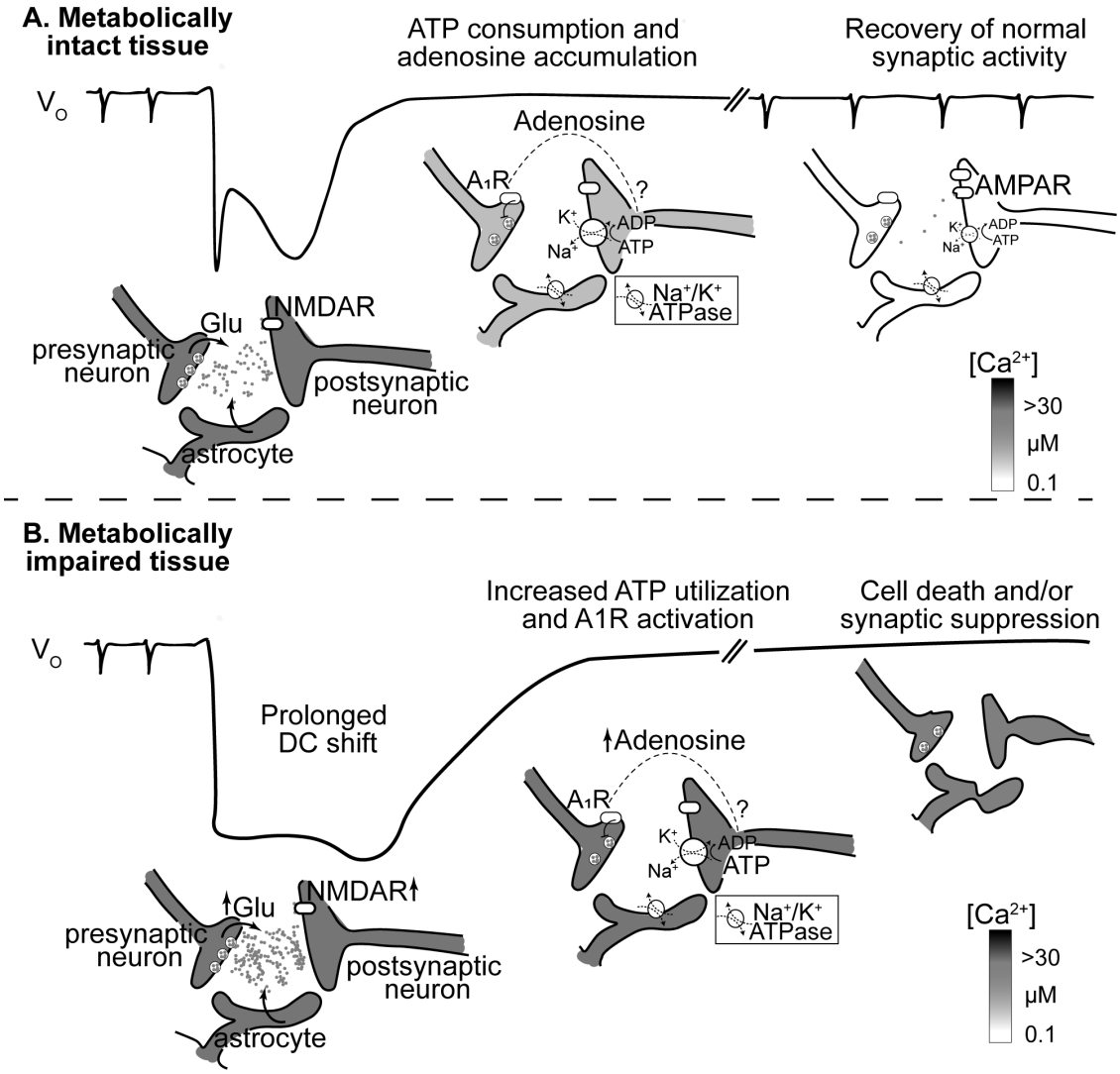

Proposed mechanisms of enhanced glutamate-mediated excitotoxicity during SD in vulnerable neurons. Traces of extracellular voltage (V_O; not to scale) begin with small synaptic potentials prior to the massive depolarization during SD (DC shift). Below each trace are simplified cellular events in neuronal processes considered to influence SD consequeces and tissue outcomes. In metabolically intact tissues (top), SD coincides with abrupt loss of neuronal activity and substantial glutamate accumulation. Intracellular neuronal calcium levels are also pronounced, in part due to activation of NMDARs. The extent of calcium accumulation is illustrated by the grayscale bar (on right). Recovery from this profound burden diminishes tissue ATP and the metabolite adenosine mediates long-lasting A_1R mediated suppression of activity. **A.** In healthy (metabolically intact) tissues neuronal glutamate and intracellular calcium loading returns to basal levels in the wake of SD and is followed by recovery of synaptic potentials (due to adenosine clearance). **B**. When tissues are viable but metabolically impaired (i.e. vulnerable) synaptic activity may be present (although potentially altered); after SD, however, there is poor recovery of neuronal responses. The duration of extracellular glutamate increases in vulnerable tissues are prolonged during SD, possibly due to both synaptic and alternative sources of neurotransmitter release. Prolonged glutamate exposure and DC shifts during SD in vulnerable neurons likely contribute to extended NMDAR activation and neuronal calcium loading consequences. This could lead to increased ATP utilization and adenosine acuumulation. Cell death and/or A_1R-mediated synaptic suppression may underlie poor recovery of synaptic potentials after SD in these conditions.

5.2 Brain slice model of metabolic compromise

5.2.1 SD consequences and the relationship to tissue metabolic capacity

Brain slice techniques are important in basic neuroscience, as experiments can be well-controlled and enable separation of neuronal from confounding *in vivo* vascular responses. However, *in vitro* tools present a challenge for stroke researchers as the complexities of brain ischemia are hard to achieve outside of the intact animal. Current *in vitro* techniques for examining neuronal injury after ischemia are thus largely limited to OGD or hypoxia models that induce injury and thus complete substrate removal. While these methods are important for understanding tissue and cellular responses to energy depletion, findings from such studies may only be directly applicable to the core of the injury that is established shortly after infarction (Dirnagl et al., 1999) As such, complete deprivation models may offer little information about injury development in vulnerable tissues surrounding an infarct core—i.e. in tissues that are viable until the additional burdensome hit of SD.

Pharmacological studies indicate that no single ion channel or receptor can be targeted to reliably prevent SD during OGD in brain slices or *in vivo* following CBF arrest (and if there was, perhaps this would be the key for immortality). In support of this idea, early studies in this dissertation found no effect of ketamine (up to 100μM, data not shown), and the related less-potent antagonist memantine (up to 300μM), in delaying or preventing SD induced by OGD in brain slices (discussed in more detail in Appendix A) Prior to this work, similar findings were observed *in vivo* where ketamine had no effect on blocking terminal depolarization in rats exposed to anoxia (via inhalation of N_2) or asphyxiation (Amemori and Bures, 1990; Hernández-Cáceres et al., 1987; Marrannes et al., 1988b). This is further supported by the failure of more potent antagonists than ketamine (e.g. MK801) or competitive

NMDAR antagonists (e.g. APV) in preventing SD initiated by OGD (Jarvis et al., 2001; Obeidat et al., 1999) or circulatory arrest in rats (Lauritzen and Hansen, 1992). These studies collectively indicate that extensive ion loading and the absence of metabolic substrates during SD are sufficient to kill neurons in the ischemic core– even when NMDARs are inhibited (Hartings et al., 2017).

The above studies emphasize the overt inability of NMDAR antagonists to prevent SD (or neuronal injury) in situations of complete metabolism arrest. However, in light of our understanding that SD is not always detrimental to tissue, perhaps our models for examining SD simply need adjustment in order to better test both interventions and mechanisms in a variety of metabolic conditions. The development of the brain slice model of SD vulnerability (Chapters 2 & 3) in this dissertation thus adds another step along our progress in understanding consequences that fall along the 'continuum' of SD. This continuum can be inspected *in vivo*, especially after a focal occlusion (as employed in Chapter 4 studies) that greatly augments regional heterogeneity in cerebral perfusion and tissue metabolic requirements. *In vitro* studies, on the other hand, have largely been limited to the two extremes along the continuum–SD in nominally healthy conditions (generated via K^+ or electrical stimuli) or SD in severely compromised brain (induced by hypoxia/OGD).

From this dissertation work and the description of a new model of compromise, we are now able to reliably assess mechanisms by which otherwise viable neurons succumb to the excitotoxic consequences initiated by SD. Moderate metabolic compromise was used to increase neuronal vulnerability to deleterious consequences of SD without complete substrate removal (Chapters 2 & 3). This was achieved using modified artificial cerebral spinal fluid (aCSF) containing elevated K^+ (8mM) and by reducing super-fusion of aCSF (i.e. oxygen and glucose delivery) to one only side of the preparation. This reduction was achieved via a slight modification in the recording chamber configuration, as described in Chapter 3 and shown in **Figure 5.2.**

Figure 5.2

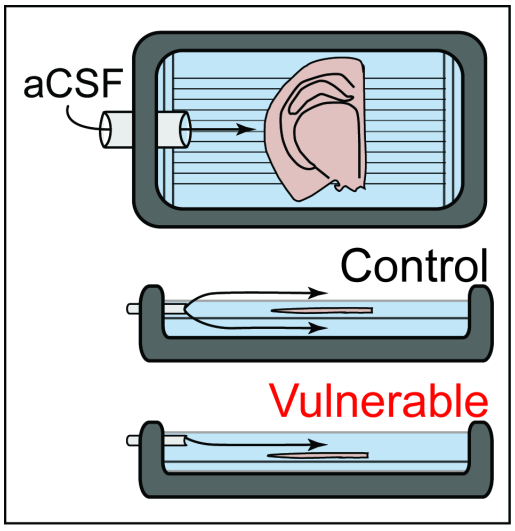

Figure 5.1. Brain slice model of metabolic compromise. Schematic showing artificial cerebral spinal fluid (aCSF) in the recording chamber. In control conditions, oxygenated aCSF is super-fused above and below the preparation that is lifted above the coverslip surface of the chamber using a slice support. Inversion of the slice support reduces aCSF supply below the brain slice rendering prepartions vulnerable to SD consequences.

As opposed to OGD, SD did not spontaneously develop in these conditions and thus SD was initiated using focal K^+ microinjection. This type of focal SD induction, on top of mild metabolic compromise and moderate extracellular K^+ increases, is likely related to SDs generated in response to fluctuations in tissue pO_2, depolarization and K^+ efflux, or other stimuli that create supply-demand-mismatches in penumbral zones after stroke (von Bornstädt et al., 2015).

5.2.2 *In vitro* models of moderate metabolic impairment

Additional techniques exist for limiting brain slice substrate, without total deprivation; although the impact of compromise is sparsely evaluated in the context of SD (except see Canals et al., 2008; Lindquist and Shuttleworth, 2014). In submerged slices, the rate of aCSF super-fusion can drastically alter tissue oxygenation levels which in turn influences evoked and spontaneous network activity, short-term plasticity, and other processes that rely on oxidative metabolism (Ivanov et al., 2011; Frengulli, 2017). However, perfusion rates of aCSF not only increase delivery of substrates but also influence normal clearance of metabolites and neurotransmitters which makes results more difficult to interpret and compare to control slices. Brain slices of varying thicknesses have also been utilized to mimic ischemic environments *in vitro* (Newman et al., 1990; Lindquist and Shuttleworth, 2014). The lack of capillary support makes brain slices completely reliant on aCSF delivery of oxygen and glucose substrates; as such, pO_2 measurements at the well-perfused slice surface are often drastically higher than pO_2 levels buried in the depths of the tissue (Chapter 3, Figure 3.2) and in Hall et al., 2012; Lindquist and Shuttleworth, 2014) . This steep gradient is even more pronounced in thicker brain slices and additional evidence of diminished metabolism is suggested by elevated lactate concentrations, increased basal NAD(P)H, and impaired oxidative transients following synaptic stimulation (Lindquist and Shuttleworth 2014; Ivanov et al., 2011). Other models, still, have employed gliotoxins (Canals et al., 2008) or chemical anoxia (ouabain, (Rosen, 1993; Dietz et al, 2008)) that also induce SD and subsequent neuronal injury (Obeidat and Andrew, 1998), but do not require complete metabolic restriction.

While chemical toxicity can provide useful information about the involvement of certain cell types and receptors theoretically involved in ischemia/SD-induced injury, the vulnerable

model (developed in this dissertation) has an advantage of not requiring poisoning of the tissue and related off-target effects. While thicker brain slices are indeed impaired and likely resemble vulnerable tissues after ischemia, proper comparisons to healthy (control) slices must be corrected for tissue size which could augment perceived contributions of metabolic byproducts (e.g., lactate, adenosine, etc.) (Lindquist and Shuttleworth, 2014) in addition to influencing the accumulation of neuroactive substances, differences in slice volume could also affect fluorescence signals (i.e. glutamate, $Ca^{2+,}$ NAD(P)H) and SD-induced IOS read-outs of slice integrity that were used heavily throughout this dissertation The experimental model of tissue vulnerability to SD (Figure 5.2) requires further characterization studies; however, aCSF perfusion and slice thickness were held constant (~2 mL min^{-1}, 350µm) and thus potentially circumvented the above limitations of alternative experimental conditions.

5.2.3 Relationship between complete substrate removal and brain death

Classical OGD or hypoxia models of ischemia create a gradual run-down of ATP concentrations causing impairment of Na^+/K^+ ATPases and other ATP-dependent pumps or channels. In hippocampal slices exposed to hypoxia, a brief phase of hyperpolarization (Czeh et al., 1993) is followed by the failure of action potential-dependent presynaptic neurotransmitter release (Hershkowitz et al., 1993; Pietrobon and Moskowitz, 2014). However, spontaneous (largely TTX-insensitive) synaptic potentials (excitatory and inhibitory) are not prevented by hypoxia and actually may increase very early on (within seconds) along the progression of ATP depletion in hippocampal (Hershkowitz et al., 1993; Pietrobon and Moskowitz, 2014) and neocortical slices (Fleidervish et al., 2001). These swift disturbances in neurotransmission during hypoxia (prior to SD onset) could underlie the rapid and reversible alterations of cortical activity during global ischemia experiments *in vivo* (see

Introduction). Perhaps this sequence of perturbed integration of presynaptic inputs with postsynaptic responses (Fleidervish et al., 2001; Revah et al., 2016) underlies the loss of consciousness seen in Red Wing experiments (Rossen et al., 1943) (or perhaps in patients with orthostatic hypotension, for example) that was coincident with cortical EEG slowing and occurred within ~20s after the critical drop in cerebral perfusion (Lennox et al., 1938). The decline of postsynaptic evoked activity could be an attempt to preserve ATP, as active synapses are high consumers of energy, and thus neuronal hyperpolarization would attenuate postsynaptic currents and thus truncate ATP consumption (Dreier and Reiffurth, 2015; Revah et al., 2016). This is supported by recent work (mentioned in Introduction) showing extracellular glutamate levels decrease by ~60% at the onset of ischemia prior to terminal SD near the core of infarcted tissue after MCAO (Hinzman et al., 2015). While potentially protective in the early stages, if substrate removal is sustained neurons and their mitochondria will continue to depolarize and extracellular K^+ will progressively increase. Once the net current flow across the cell membrane turns inward, SD erupts and the electrochemical gradient collapses (Table 1.1., in Introduction) (Dreier, 2011).

Along the progression of persistent ischemia (as in experiments performed by Leão) SD develops shortly after (~2-5 min.) the decline of evoked cortical activity— which now becomes irrecoverable in the absence of reperfusion (LEAO, 1947). As mentioned previously, in these metabolically desolate environments no single channel or receptor can be targeted to completely prevent SD and the subsequent neuronal injury in either *in vitro* or *in vivo* experiments. This pathophysiological sequence was also confirmed in severely brain injured patients where, upon withdrawal of life-sustaining treatment, cortical activity deteriorated

(Norton et al., 2017) and according to recent findings, was followed (~13 – 14.5 min. later) by terminal SD (Dreier et al., 2018). It is important to note this order of events as they diverge from tissues that are viable *until* the additional hit of SD, described in more detail below.

5.2.4 Vulnerable slices are similar to outer penumbral regions after stroke

Some characteristics of tissue heterogeneity after focal ischemia were described by Lindsay Simon and colleagues in the late 1970s and early 1980s (Astrup et al., 2018; Branston et al., 1977; Hartings et al., 2017). In general, the ischemic core of the infarct (i.e. the initiation site of the first terminal SD) is characterized by electrical silence and very low residual perfusion (<5-10ml/100g/min); the inner penumbra has slightly improved residual flow due to collateral circulation (>5-10 and <15-23ml/100g/min) and is structurally intact though remains functionally inactive. The outer penumbra is oligemic (>15-23 and <35ml/100g/min), but neurons show only moderate signs of distress (Canals et al., 2008) while electrical activity is largely intact. In the course of hours to even days after stroke onset, SDs can initiate in either inner or outer penumbral regions (Hartings et al., 2017) and hot spots for SD induction may be more likely in the outer penumbral due to intact neuronal activity and mismatched vascular coupling (von Bornstädt et al., 2015). This may be especially augmented owing to pathological elevations in extracellular K^+ levels that transform steeply across the different flow thresholds, described above (Branston et al., 1982). The extracellular ionic environment (namely K^+ increases) have been shown to reduce the ability of NMDAR-antagonist blockade of SD leading to dominant assumption in the field that the most vulnerable brain regions will benefit the least from drugs targeting NMDARs (Petzold et al., 2005). This is particularly important for studies in this dissertation and thus will be discussed in upcoming sections for both brain slice and *in vivo* stroke experiments.

Based on these broad definitions (and work in Chapter 3, described below), the brain slice model of metabolic compromise developed during experiments in this dissertation is proposed to be a model of outer penumbral tissues after ischemic stroke. It is noteworthy that the recording configuration used here to model tissue at-risk (i.e. slice resting at the level of the glass coverslip) is commonly employed by slice electrophysiologists, albeit with minor changes in superfusion rate and/or slice thickness.

5.2.5 Cellular changes prior to SD

Chapter 3 in this dissertation focused on characterizing differences between vulnerable and nominally healthy brain slices (i.e. slices perfused on both surfaces) and the most significant effect was found on synaptic responses (described in more detail below). Signs of metabolic stress did not prevent extended EPSP recordings (up to 60 min) or synaptic plasticity (i.e. long-term potentiation) in vulnerable slices, thus confirming the presence of intact hippocampal circuitry (data not shown). This again contrasts to complete neuronal suppression observed shortly after OGD/hypoxia introduction.

Postsynaptic responses in vulnerable preparations were consistently decreased compared to controls (Chapter 3, Figure 3.1) in part due to a reduction in initial release probability of glutamate from schaffer collateral inputs (i.e. increased PPR). These changes could be attributed to an increase in A_1R activation (as shown in experiments using the selective antagonist DPCPX), which strongly suggests a rise in extracellular adenosine in vulnerable slices. Increases in adenosine in vulnerable slices could reflect changes in energy metabolism and mitochondrial bioenergetics in neuronal and nonneuronal cells (Boison et al., 2013).

In the healthy brain, extracellular adenosine levels are typically in the sub micromolar range (Frenguelli, 2017) and thus A_1R activation is relatively low, resulting in lower paired-pulse ratios and larger evoked synaptic responses, as shown in adequately perfused brain slices (Figure 3.1). Minor decreases in intracellular ATP concentrations can cause not only significant increases in adenosine levels (Boison et al., 2013) but also promote the opening of ATP-sensitive potassium (K_{ATP}) channels (Heurteaux et al., 1995); processes that both contribute to reduced neuronal excitability. Reduced synaptic efficacy and increased PPR could thus reflect mild metabolic stress and declining intracellular ATP concentrations in vulnerable brain slices.

In addition to presynaptic dampening of neuronal activity, adenosine can activate postsynaptic A_1Rs which can provoke downstream opening of inwardly rectifying K^+ channels (Boison et al., 2013) and result in membrane hyperpolarization. This would further reduce synaptic efficacy when ATP concentrations are diminished. Interestingly, adenosine itself can modulate (K_{ATP}) channels by inducing their internalization in metabolically stressed hippocampal CA1 neurons (Hu et al., 2003). Perhaps this provides insight with regards to mechanisms involved in hypoxia/ischemia-induced early hyperpolarization (K_{ATP} activation) versus subsequent action potential failure prior to the development of SD—i.e. perhaps adenosine's actions outweigh other mechanisms to overall illicit presynaptic inhibition and K_{ATP} internalization.

Together, actions of adenosine may be theoretically protective (or compensatory) and minimize metabolically costly neuronal activities (i.e. vesicular release and postsynaptic depolarization) in times of energy crisis (Boison et al., 2013). This concept of protection and/or

compensation will be further discussed in later sections regarding evolutionary responses of SD but may help explain why tissue pO_2 levels were unchanged in vulnerable slices at baseline. The changes observed in vulnerable slices seem to be intermediate between nominally healthy and severely compromised tissues (hypoxia/OGD). Therefore, findings from Chapter 3 further support the use of this model as a tool for studying consequences along the SD continuum.

5.2.6 Vulnerability to SD injury

A main concern for ICU patients and clinicians in the aftermath of stroke is progressive infarct expansion into previously viable brain tissue. This deterioration is usually only detected at infrequent snapshots in time (i.e. during neurological exams or brain imaging) and thus pinpointing the underlying pathophysiology related to SD remains very challenging today. This is especially difficult in the most severe cases of acute brain injury, where substantial sedation and attendant ICU complications are additional obstacles to patient stability and adequate assessment of brain physiology. While scalp-EEG has been employed in the ICU brain injury setting, current technical limitations prevent the identification of SD via these methods. As such, substantial efforts were made by COSBID investigators to record from subdural ECoG strips placed during neurosurgical procedures in patients after acute brain injury. In 2008, the first study in ischemic stroke patients was published showing SD can occur in patients up to a week after occlusion onset (Dohmen et al., 2008). In that report the authors highlighted an instance where functional brain activity was suddenly and irreversibly suppressed immediately after SD propagated through series of channels located within the ECoG recording strip. This emphasizes that brain tissue in the outer penumbra can be viable until faced with an insurmountable energy crisis produced by an SD.

In the present dissertation study, neurons in metabolically compromised brain slices were specifically vulnerable to the massive energetic demands imposed by SD, and these observations support the hypothesis that the additional hit of SD, on the backdrop of metabolic compromise (and not compromise alone), elicits acute neuronal impairment (Obeidat and Andrew, 1998). This was shown in Chapters 2 & 3 where synaptic potentials were intact, though reduced in amplitude (discussed above), prior to SD and were only lost or impaired after SD. Interestingly, pre-exposure to the A_1R antagonist DPCPX could almost fully restore postsynaptic responses in vulnerable slices (Chapter 3, Figure 3.1 and described below) which raises important questions as to the true viability of silent neurons in the wake of SD. While again further studies are needed, these experiments support prior findings (Lindquist and Shuttleworth, 2012, 2014) that extracellular adenosine is partially responsible for the prolonged synaptic depression after SD in vulnerable conditions. However, the indication that neurons can respond to stimuli contrasts with optical read-outs of slice heath (i.e. intrinsic optical signals, IOS) that were unaffected during DPCPX exposures (Chapter 3, Figure 3.4).

Intrinsic optical signals (IOS) have been well-characterized in the hippocampus of brain slices following OGD/hypoxia (Andrew et al., 1999; Jarvis et al., 2001) where substantial decreases in transmitted light through stratum radiatum dendrites (like those seen in Chapters 2 & 3 experiments, Figures 2.6 and 3.4) accompany acute signs of neuronal damage including dendritic beading. SD-induced dendritic beading can be observed *in vivo* where recovery can be rapid (<3 min.) in tissues with adequate CBF; however, when perfusion responses no longer meet the energetic demand of SD (i.e. in metabolically compromised brain), beading is irreversible (Risher et al., 2010). Experiments in vulnerable brain slices also demonstrated

profound decreases in light transmittance in stratum radiatum after passage of the SD wave front; changes that appear consistent with IOS signs of neuronal injury after SD (Andrew et al., 1999).

In that previous work, Obeidat and colleagues noted that when slices did not undergo SD (i.e. OGD was stopped prior to SD onset), that dendrites (visualized histologically or via bulk fluorescent dye loading) were smoothly contoured, as opposed to SD slices that had beaded processes that were more difficult to resolve. Interestingly, morphological changes in neurons were mentioned in early results by Grenell (described in Introduction) where he denotes the presence of pathological changes and increased "tortuosity" of neuronal processes in brains from seemingly different causes of death in animals (GRENELL, 1946; HOFF et al., 1945). Perhaps tortuosity is simply another word used to describe dendritic beading—which also deforms dendritic processes, making them more difficult to resolve. Additional work in brain slices has shown that acute pyramidal cell injury (resulting from NMDA exposure) is associated with dendritic beading and the relocation of microtubule-associated protein (MAP2) immunoreactivity from CA1 processes to somata compartments (Hoskison et al., 2007; Hoskison and Shuttleworth, 2006). Based on these descriptions, MAP2 immunohistochemistry was used to examine pyramidal cell changes after SD in vulnerable slices (Figure 3.4) at the same time-point that IOS changes were quantified (Figures 2.6 and 3.4).

At this time point (~10 min. post SD), vulnerable slices had variability in the extent of both MAP2 redistribution and obvious structural deformations; though pyramidal cell processes after SD did look more "tortuous" according to descriptions by (GRENELL, 1946; HOFF et

al., 1945). In retrospect, images immediately following toxic NMDA exposure also have a more tortuous appearance in (Hoskison et al., 2007); however, striking changes in MAP2 fluorescence were evident much later (> 20 min.) following NMDA in these experiments. It is thus possible that diminished MAP2 in processes (and corresponding somata increases) had not fully developed by this chosen time after SD in vulnerable slices. Additionally, since aCSF superfusion is predominately reduced below the slice (in the vulnerable configuration), there could be gradients of neuronal injury with respect to the extent of compromise throughout the thickness of the tissue. This is also supported by pO_2 measurements in Chapter 3 as well as previously described data by (Lindquist and Shuttleworth, 2014). In those results, gradients in pO_2 availability diminished along the depth of the slice and disruptions in oxidative metabolism (i.e. NAD(P)H transients) was also observed during SD (initiated by K^+). In metabolically vulnerable preparations pO_2 availability was also markedly attenuated at all depths after SD (Chapter 3), and thus additional studies would be useful to quantify MAP2 (or other markers of neuronal integrity) throughout the full thickness of the tissue. Due to challenges with antibody penetration throughout the full thickness of the slice (350μm), an in-depth characterization of MAP2 changes was not attempted in these dissertation experiments. However, overall findings elude to the presence of deep structural changes within vulnerable brain slices (and perhaps even well-perfused preparations) that alter light scattering properties of tissue after SD to contribute to IOS.

As mentioned earlier, antagonizing adenosine's inhibitory action at A_1Rs (with DPCPX) enabled detection of EPSP responses (collected at a slice depth of ~50-100 μm) after SD in vulnerable brain slices (Figure 3.4) but did not correct IOS decreases in these same slices

(Figure 3.4). This suggests that DPCPX is not protective against the possible morphological changes associated with neuronal deterioration that are perhaps ongoing at the most compromised depths of the slice (>100 μm). Furthermore, DPCPX has been shown to accelerate SD onset and decrease protective effects of adenosine in brain slices exposed to gliotoxins (Canals et al., 2008a), suggesting that lengthier electrophysiological recordings or other markers of slice health are needed to further evaluate DPCPX treated slices. Findings from Chapter 3 in vulnerable slices (i.e. DPCPX effects on EPSPs but not IOS after SD) may also indicate that some neurons succumb to injury while others are functionally intact, although suppressed by adenosine, after SD. If true, a potentially mixed population of viable and dead neurons could exist within a volume of compromised tissue.

Along these lines, early animal studies that employed histology (GRENELL, 1946) or electrophysiology (Sugar and Gerard, 1938) independently reported that certain cell types or brain regions are more sensitive (i.e. pyramidal cells, Purkinje cells, and higher cortical centers) to oxygen deprivation compared to others (life-supporting brainstem centers). This could be due to the propensity of different brain regions and cell types to participate in SD initiation and or propagation. In a review by Somjen it was noted that some neurons "refused" to participate in depolarization during SD even though recordings also confirmed the presence of mass depolarization in the extracellular slow potential (Somjen, 2001). More recent whole-cell recordings also demonstrated that neurons in higher gray matter centers are more inclined to propagating SD versus lower gray matter centers of the brainstem (Andrew et al., 2016). In this study it was noted that cytoarchitectural differences and do not seem to account for threshold differences and that perhaps the milieu of excitatory amino acid transporters or

Na^+/K^+ ATPases and their interaction may play an important role. A new publication by Andrew and colleagues is further evidence that a mixed population of neurons can exist even within the necrotic core after MCAo in mice (Petrin et al., 2019). In this study, structurally intact pyramidal cells were found within the lesion core after infarction (12 hr.); and although appropriate presynaptic inputs were absent, these neurons retained the ability to respond in the presence of external stimuli. While these ideas may further complicate our understanding of lesions in human brain, there is much to be learned from the heterogenous neurons that either survive or succumb to SD during focal ischemia. Per the discussion above, the vulnerable brain slice model could be an additional tool for understanding the complexity of SD mechanisms as they relate to tissue metabolic status.

5.3 Experimental design to evaluate injury mechanisms during SD after in vivo stroke

Distal locations along the middle cerebral artery (MCA) are a relatively common site of occlusion in human ischemic stroke. As such, there are many rodent stroke models that target the MCA by different avenues including intraluminal suture, embolic, endothelin-1, photochemical (i.e. photothrombosis), and craniotomy (as used in this dissertation) occlusion models. While preclinical stroke models have ranging advantages in their resemble to the human condition; various disadvantages make them suitable for different types of studies (e.g. infarct size determination, behavioral deficits, studies on thrombolytic agents) (Kleinschnitz et al., 2015). The craniotomy / dMCAo model (Chapter 4) is more invasive and requires fine surgical skills than other techniques, however it is highly reproducible (Kuraoka et al., 2009) with low mortality rates, likely due to the direct visualization of the MCA and its occlusion (Kleinschnitz et al., 2015). Functional deficits and infarct sizes are smaller in dMCAo models

compared to proximal MCAO and intraluminal approaches that also interrupt other large cerebral vessels (i.e. internal carotid artery) and concomitant damage to subcortical structures (KURAOKA et al., 2009). However, the main rationale behind employing dMCAo in this dissertation work was due to the development of metabolic heterogeneity (i.e. presence of healthy, penumbral, and necrotic tissue) with respect tissue to distance from the occlusion site (KURAOKA et al., 2009). This characteristic was important for examining 1) excitotoxic mechanisms during SD in relation to the infarct and 2) for testing ketamine's efficacy in tissues with varying metabolism— especially in the peri-infarct region where NMDAR antagonists are believed less protective.

As mentioned previously (Introduction), studies by Hartings, et al. in 2003 revealed that infarct expansion occurs alongside the second or delayed phase of increased SD frequency (Hartings et al., 2003). In order to employ fluorescent-based imaging modalities to examine SD mechanisms involved in the recruitment of penumbral tissue into the ischemic core, experiments were designed in alignment with previous work by Busch and colleagues in 1996 (Busch et al., 1996). That foundational study provided the first link between SD and infarct expansion *in vivo* by showing that recurrent SD induction (using exogenous K^+ application in a non-infarcted region) caused stepwise injury expansion in animals. As such, experiments in Chapter 4 examined exogenously evoked SDs initiated at ~20 min. intervals after 60 min. recovery from dMCAo or sham surgeries. It is important to emphasize that SDs generated experimentally in this work are different from "spontaneously" occurring SDs that have been reported in mouse stroke models. In the current study, sets of KCl-induced SDs originate a long distance from the recording sites, and this allows clear evaluation of the ***consequences*** of

SDs, as they propagate through tissues of different metabolic capacity. This is quite different from examining conditions that *influence the initiation* of SDs in peri-infarct regions, which is likely due to other factors as previous described (see Ayta and Lauritzen, 2015).

5.3.1 Impaired vascular responses and prolonged DC shifts indicate tissue vulnerability to SD

Leão was again the first to describe perfusion responses during SD as he denoted dramatic changes in pial vessel diameters and blood flow changes (Leao, 1944). Over the course of decades of research, vascular responses to SD have been characterized across different species and in relationship to various metabolic brain states, reviewed in depth by (Ayata and Lauritzen, 2015). In this dissertation work, laser speckle contrast imaging (LSCI) was used to monitor perfusion responses elicited by SD and responses were compared to previous literature for the identification of brain regions that had reduced capacity to recover from SD (Chapter 4). Imaging techniques used here (and during subsequent *in vivo* experiments) were designed to monitor both hemispheres which enabled simultaneous monitoring of SD in remote and proximal brain locations while providing internal normalization to the contralateral hemisphere.

Experiments confirmed prior reports (Feuerstein et al., 2014) that metabolically impaired brain tissue (i.e. proximal) has diminished capacity to mount hyperemic responses during SD (Figure 4.1). Furthermore, DC shift durations were greatly extended in peri-infarct regions (Figure 4.2). Combined with prolonged DC shift durations, experiments using LSCI demonstrated that prolonged electrochemical breakdown during the DC shift was not matched with adequate vasodilatory/hyperperfusion responses thus indicating increased vulnerability to SD-injury in these regions (Dreier et al., 2018a).

5.3.2 Wide-field fluorescence imaging in vivo

Based on the above pilot experiments, studies were next designed to evaluate contributions of glutamate (iGluSnFR) and Ca^{2+} (GCaMP5G-expressing mice) provoked by SD and used a custom-built wide field fluorescence imaging set up (discussed in Chapter 4). Fluorescence was monitored through the intact skull and was minimally invasive (skin removal and burr holes for SD induction and electrophysiology were created) compared to open skull craniotomies that have been used for glutamate-sensitive electrode arrays (Hinzman et al., 2015) or two-photon imaging of glutamate (Enger, 2015) and Ca^{2+} during SD (Murphy et al., 2008) .

In vivo, use of different wavelengths (250nm – 1000nm) can carry diverse information regarding concentrations of oxy- and deoxyhemoglobin (HbO_2 and HbR, respectively) and thus have been employed to study physiological parameters in the cortex (Ma et al., 2016). These intrinsic optical changes have been used in studies of SD revealing unique information about propagation patterns (Santos et al., 2014) and hemodynamic responses (Schöll et al., 2016) in the gyrencephalic brain of pigs. However, this can also create obstacles for determining fluorophore contributions during SD. The fluorophores employed in this dissertation work (i.e. iGluSnFR and GCaMP5G) were excited using a 470 nm LED and emitted fluorescence was collected in the green spectrum (510-550 nm). At 470 nm, both HbO_2 and HbR have relatively high tissue molar extinction coefficients (Ma et al., 2016) and thus absorb iGluSnFR or GCaMP5G excitation light. The impact of hemoglobin concentrations are further pronounced after SD and is even more complicated in the context of stroke due to heterogenous residual CBF in the ipsilateral cortex. In order to best eliminate these

confounding perfusion artifacts, multispectral LED assembly could be employed to excite tissue fluorophores (470 nm) and successive illumination of HbO_2 and HbR at wavelengths that reveal a) total hemoglobin (i.e. at the isosbestic point 530nm; where absorption qualities are roughly equivalent) and b) predominately HbO_2 contributions (~650-700nm). Post-hoc analyses could then be used separate hemodynamic responses from fluorescent reporter emission during SD (as in (Bouchard et al., 2009)).

To reduce the contributions of these artifacts during *in vivo* analyses in Chapter 4, only the initial recovery from Ca^{2+} or glutamate accumulation during SD were examined, and curves were fit to estimate the half-life of signals as a surrogate for measuring the duration of responses that would be underestimated due to remaining confounds, per the discussion above. In future studies, multispectral fluorescence imaging would be important, but do not change the overall findings from *in vivo* studies conducted in Chapter 4 of this dissertation work. Additionally, findings in brain slices from Chapters 2 & 3 corroborate *in vivo* experiments, and further emphasize the value of brain slice studies to separate cellular mechanisms.

5.4 Excitotoxic consequences of SD

Experiments conducted throughout this dissertation tested the hypothesis that extended glutamate and NMDAR-mediated Ca^{2+} accumulation mediate neuronal dysfunction in compromised but viable tissue. During the late phase of the DC shift, prolonged extracellular glutamate release combined with neuronal depolarization promote Mg^{2+} release from within the NMDAR pore which increases membrane permeability to cations including Ca^{2+} (Aiba and Shuttleworth, 2012). Furthermore, when individual neurons were chemically compromised

(via patch pipette sodium azide) activation of NMDARs during late-SD led to irrecoverable Ca^{2+} loading and dendritic signs of damage (Aiba and Shuttleworth, 2012); effects that were prevented by competitive blockade of NMDARs (using APV). This dissertation sought to extend these findings beyond single cells to both slice and intact animal experimental designs. Additionally, studies tested the non-competitive NMDAR antagonist ketamine, as competitive NMDARs have failed in previous clinical stroke trials, have undesirable side-effect, and also interrupt essential NMDAR-dependent cellular processes (discussed previously).

5.4.1 Fluorescent sensors used in this study

Studies were initially designed in mouse brain slices using fluorescent reporters of extracellular glutamate and intracellular Ca^{2+} to evaluated consequences of SD that were specific to neurons. These sensors had not been utilized in prior studies within Dr. Shuttleworth's lab, and thus *in vitro* studies in brain slices also provided feasibility for subsequent *in vivo* experiments.

Chapters 3 & 4 examined glutamate dynamics during SD using the recently developed intensity-based glutamate sensitive fluorescent reporter iGluSnFR (Marvin et al., 2013) delivered ~2 weeks prior to experiments via AAV injection into the hippocampus or cortex for brain slice or *in vivo* recording sessions, respectively. iGluSnFR is controlled under the synapsin promoter for expression in neurons with additional constructs that guides protein trafficking to the plasma membrane (Marvin et al., 2013). Upon binding of extracellular glutamate, a conformational change enables detection of fluorescence and thus provides a more direct indication (compared to microdialysis or glutamate-sensitive electrodes) that glutamate is in direct contact with neuronal membranes. Additionally, microdialysis and amphoteric techniques do not have single cell resolution which makes fluorescence imaging of iGluSnFR

a useful new tool for monitoring glutamate levels, not only during SD but in other neuroscience fields as well.

An overall limitation of the iGluSnFR variant used in this dissertation work, is that it cannot resolve fast or sparse glutamate release likely due to its relatively high affinity (~5μM, for glutamate) and slow off kinetics when expressed on neuronal surfaces (Helassa et al., 2018; Marvin et al., 2018). While this limitation did not play a major role in this dissertation work (due to massive and prolonged glutamate release during SD) it does prevent accurate calculations of glutamate concentrations as the indicator was most likely saturated during SD. These challenges may be overcome with new iGluSnFR variants that have higher or lower affinities due to slower or faster off-rates, respectively. The faster off-rate variants were designed for more accurate quantification of quantal glutamate release and thus higher dissociation constants (K_d 30-600 μM; (Helassa et al., 2018; Marvin et al., 2018) increase fluorescent range.

Experiments in Chapter 2 & 4 also utilized mice expressing the Ca^{2+}- sensitive fluorescent reporter GCaMP5G expressed in a Cre-dependent fashion under the CaMKIIa promoter (Gee et al., 2014). This enabled robust expression of GCaMP5G in hippocampal and cortical neurons without requiring bulk loading of fluorescent dyes and/or dialyzing neurons. Similar to limitations described for iGluSnFR, advancements in fluorescent Ca^{2+} reporters (with higher or lower affinities) could provide more information with regards to intracellular Ca^{2+} loading during SD in neurons (or in other cell types using different promoters). Additionally, future brain slices utilizing dual-band dichroic mirrors for fluorescence imaging of both glutamate

and Ca^{2+} (red and green, which are now available for glutamate detection via iGluSnFR variants (Marvin et al., 2018)) as well as transgenic mice designed with red-shifted Ca^{2+}-reporters (Dana et al., 2016)) would be interesting for the simultaneous detection of both excitotoxic mediators during SD.

5.4.2 Glutamate accumulation during SD

iGluSnFR for two-photon monitoring of glutamate dynamics during SD were recently reported *in vivo* (Enger et al., 2015), however studies in this dissertation are the first to utilize iGluSnFR to examine SD in brain slices and *in vivo* after focal ischemia. Vulnerable brain slices (Chapter 3) and peri-infarct cortex after dMCAo (Chapter 4) both exhibited prolonged glutamate fluorescence increases during SD. This advocates for lengthy presence of ligand within direct proximity to both pre- and post-synaptic glutamate receptors in neurons that are most vulnerable to excitotoxic SD consequences. Long-lasting glutamate increases could help explain why DC shifts and the ionic burden of SD are more pronounced during metabolic compromise. Furthermore, SD-induced glutamate increases were irrecoverable in both brain slices exposed to OGD (Appendix C) and during terminal SD *in vivo* (i.e. during euthanasia at the end of experimentation in Chapter 4, not shown). Notably, irreparable glutamate elevations were never observed during SD in vulnerable slices or in peri-infarct regions with recoverable DC shifts.

As formerly mentioned (Introduction), synaptic glutamate can significantly contribute to extracellular transmitter levels during SD, as proposed in earlier studies that employed Zn^{2+}-indicators. Preliminary studies in this dissertation work examined vesicular glutamate release using FluoZin3 and data showed strikingly similar kinetics as iGluSnFR transients when both

were evaluated during SD in healthy brain slices (not shown). These comparisons are preliminary due to limitations of both iGluSnFR and Zn^{2+} imaging techniques and thus future work is needed to examine sources of glutamate accompanying SD in healthy slices impart insight into mechanisms that go awry in compromising environments. While sources of glutamate formerly identified using OGD experimental models (described in Introduction) could be comparable to those here, it is possible that these mechanisms may play important roles (or can actually be targeted) in vulnerable brain tissue. This statement is supported by preliminary experiments in this dissertation work showing that glutamate accumulation during SD is vastly different in vulnerable compared to OGD conditions (Appendix C).

Newer iGluSnFR constructs (discussed above) could also be used to examine more dynamic fluctuations in glutamate (or its downstream read-outs) that sometimes overlap or occur shortly after the DC shift, for example. This is suggested due to recent unpublished data that, during the decay of glutamate transients during SD, small increases in iGluSnFR fluorescence called "glutamate plumes" can be detected (A previous brain slice study that employed glutamate sensitive electrodes (Zhou et al., 2013) also showed glutamate transients during SD that, in some instances, were contaminated with "plume-like" fluctuations during this same decay phase, although this was not discussed. Plumes are perhaps further confirmation that presynaptic release is enhanced during the late phase of the DC shift or theoretically responsible for the rapid voltage fluctuations that can be occasionally observed shortly after DC shift recovery, also noted but not specifically examined by (Aiba and Shuttleworth, 2012). If these plumes contribute to glutamate-mediated consequences of SD, experiments could be designed to evaluate the frequency of these events during SD in vulnerable brain slices or in

peri-infarct regions *in vivo* after dMCAo. Additionally, monitoring of Zn^{2+} could provide insight as to whether vesicular machinery is involved in plume induction.

In addition to eliciting depolarization, glutamate is a central mediator of astrocyte-dependent vasodilation in response to neuronal activity (i.e. neurovascular coupling) including during normal physiological responses. Glutamate-mediated neuronal depolarization, along with many other cellular and vascular factors (reviewed in (Ayata and Lauritzen, 2015)), should thus necessitate profound dilation during SD. However, hyperemic responses to SD were only observed in the cortex of non-injured animals or in remote regions after dMCAo (Chapter 4 and described above); supporting literature in the field that SD in metabolically impaired tissues is accompanied by impaired vasodilation and/or inverse-neurovascular coupling mechanisms (Dreier, 2011; Feuerstein et al., 2014).

This dissertation work extends our understanding of glutamate dysfunction that occurs after passage of the SD wave front in vulnerable tissue that is at-risk for neuronal injury. Compared to the irrecoverable increases observed during SD in environments of complete substrate deprivation (OGD or the infarct core), excitotoxic transmitter increases in vulnerable brain can recover back to baseline levels. These findings provide rationale behind reexamining the pharmacology of such SDs in a new light—perhaps revisiting interventions that were abandoned due to lack of efficacy in OGD/hypoxia *in vitro* models. For *in vivo* studies, evidence that glutamate increases are time-locked with SD may be important for controlling the time course of drug administration; specifically, interventions could be delivered when damage is most likely to occur (i.e. during or after passage of the SD wave front).

5.4.3 Calcium and NMDARs

Experiments in brain slices (Chapter 2) confirmed prior reports (Aiba and Shuttleworth, 2012; Dietz et al., 2008) that dendrites are particularly vulnerable to SD, as indicated by prolonged accumulation of intracellular Ca^{2+} in dense dendritic regions of stratum radiatum even in healthy brain slices. Ca^{2+} loading was further exacerbated during SD in vulnerable brain slices in both somata and dendrites and corresponded to poor functional recovery of synaptic responses. Prolonged Ca^{2+} durations (calculated from nonlinear regression half-lives) were also observed during SD in proximal locations after dMCAo and were associated with extended DC shifts; supporting evidence that metabolically impaired regions are faced with amplified energetic requirements during SD. This work provides more information regarding mechanisms that promote neuronal injury during SD and likely subsidize stepwise injury expansion—as suggested by the progressive impairment of intracellular Ca^{2+} buffering mechanisms that infiltrated remote regions during sets of SD in stroke animals. In these areas, neuronal Ca^{2+} responses were extended with each subsequent SD, and regions of irrecoverable Ca^{2+} loading could not propagate subsequent events. Based on brain slice studies, this could implicate either neuronal demise or adenosine-mediated suppression (Lindquist and Shuttleworth, 2012)—both of which oppose SD initiation and/or propagation (Koroleva and Bures, 1996; Canals et al., 2008). These findings provide evidence that extended glutamate observed during SD is likely sufficient to activate all NMDAR-subtypes (described below) enabling Ca^{2+} influx into metabolically vulnerable neurons. as glut likely sufficient to activate all NMDARs.

Unlike non-NMDA receptors, NMDARs are obligatory hetrotetramers based on various combinations of GluN1, GluN2A-D, and GluN3A-B; although requiring GluN1 and GluN2 subunits as prerequisites. Open channel conductance occurs upon neuronal depolarization and release of Mg^{2+} from within the pore in the presence of glycine or D-serine (interaction with GluN1) and L-glutamate (binding to GluN2 subunits) (Burnashev et al., 1992). The transmembrane domain of the NMDAR is responsible for the functional differences from other ionotropic glutamate receptors and confers this channel with voltage-sensing capacity, Mg^{2+} blockade, and substantial permeability to the Ca^{2+} cation (Karakas and Furukawa, 2014). While permeable to Ca^{2+}, NMDARs are nonselective cation channels and the majority NMDAR-mediated currents are actually carried by the influx of Na^{+}. NMDARs are involved in a variety of neuronal processes that include pro-survival and cell death mechanisms and are even located on presynaptic membranes where they participate in neuronal signaling and plasticity mechanisms (Bouvier et al., 2015). In addition to largely postsynaptic roles of NMDARs during SD, discussed previously, recent work has implicated presynaptic NMDARs in regenerative glutamate release during SD (Zhou et al., 2013). Theoretically, this could mean that blockade of presynaptic NMDARs (e.g. with ketamine) could further decrease vesicular release of glutamate but also may opposingly elevate release via disinhibition of GABAergic interneurons. Therefore, depending on presynaptic NMDAR (as well as subunit subtypes) expression levels, ketamine efficacy could have varying effects on SD in different brain structures. However, the disinhibitory effect of NMDAR antagonists may play a lesser role during SD, as suggested by studies performed in (Aiba and Shuttleworth, 2014).

The mixing of subunit compositions further confers varying degrees of cation permeability and relative strength of Mg^{2+} -blockade from within the pore of different NMDAR subtypes (Retchless et al., 2012). Influences of NMDAR combinations and localization could therefore confer variability in NMDAR roles and responses. For example, recent studies show that activation of GluN2A-containing subtypes localized at the synapse can be essential for the induction of pro-survival cascades important for neuronal survival and perhaps recovery and repair mechanisms after stroke injuries, reviewed in (Lai et al., 2014; Wu and Tymianski, 2018). As opposed to GluN2A subtypes, GluN2B-containing NMDARs have gained renewed interest for future stroke treatments due to their conductance properties and extrasynaptic location on neurons (Tu et al., 2010; Wu and Tymianski, 2018). Since it is largely believed that glutamate released after focal ischemia occurs only during the acute period (min-hrs after stroke onset) it is thought that targeting excitotoxic GluN2B-containing NMDARs would need to be early on. However, in knowing that SDs can occur for days after the initial ictus—and are major sources of glutamate—this could extend the utility of these drugs beyond the acute phase. This is proposed with the caveats that SD is unpredictable (even when recording from subdural electrodes) and glutamate levels are massive (>10μM) even in healthy brain. Therefore, it would be important to elucidate if certain NMDAR subtypes contribute more to the damaging Ca^{2+} accumulation observed in vulnerable neurons undergoing SD, as corresponding glutamate increases are likely sufficient to activate all NMDAR subtypes (EC_{50}: ~2μM (Nakanishi et al., 1992)).

5.5 Ketamine reduces excitotoxic consequences of SD

Studies prior to this dissertation work elucidated the role of NMDARs in not only SD initiation and propagation (Somjen, 2001) but also in Ca^{2+} loading and neuronal demise following SD in vulnerable neurons, discussed in Introduction and (Aiba and Shuttleworth, 2012). While decades of work suggest that blocking SD can reduce infarct sizes, the most reliable way for preventing SD is via high doses of NMDAR antagonists; blockers with a long and unsuccessful history in ischemic stroke trials. Highlighting overall failures of pharmacological neuroprotective efforts is the fact that not a single intervention has been approved for the treatment of ischemic stroke since tPA in 1996. When these trials are examined under the scrutiny of SD researchers, failures are perhaps attributed to the timing of drug administration—restricted to the acute period after stroke onset and not during the delayed phase of SD-mediated lesion growth. Additionally, the inability of NMDAR antagonists to block SD in more severe cases of injury (i.e. OGD/hypoxia or in peri-infarct tissues) has also led some to believe that glutamate and NMDAR antagonists are not involved in injury produced by SD. Complicating matters worse, is evidence that SD itself, in addition to pro-survival roles of tonic NMDAR activation, may provide benefits for repair after injury.

The multifactorial and theoretical issues presented above, generate many challenges for prospective clinical studies and thus suggest that targeting deleterious consequences of SD might be a useful approach to ischemic stroke treatment. Due to their unique properties, functions, and involvement in pathophysiology, many drugs have been developed and tested in humans targeting NMDARs (Gladstone et al., 2002). While none of these compounds are currently approved in ischemic stroke patients, the NMDAR antagonist ketamine has shown promise for reducing SD incidence (Carlson et al., 2018; Hertle et al., 2012; Sakowitz et al.,

2009; Schiefecker et al., 2015). Therefore, studies in this dissertation focused on testing ketamine in the context of reducing consequences of SD that can be deleterious to vulnerable brain.

As discussed previously, ketamine had no effect on SD initiated in response to OGD exposures in brain slices or *in vivo* after global ischemia. However, in reorganizing our thinking about the SD (Hartings et al., 2017) pharmacological interventions found to not prevent cell death *in vivo* after CBF arrest or *in vitro* after OGD/hypoxia may still provide protection against SD-mediated injury in vulnerable brain. While most work with ketamine in the past has focused on blockade of SD (Gorelova et al., 1987; Marrannes et al., 1988b), the literature provided hints that ketamine could reduce the metabolic demand of SD by limiting DC shift durations—observed in the healthy brain *in vivo* and in brain slices (Gorelova et al., 1987; Krüger et al., 1999). Findings in humans support these preclinical results by confirming that the NMDAR antagonist ketamine is capable of dose-dependently suppressing SD in brain injured patients (Carlson et al., 2018; Hertle et al., 2012; Sakowitz et al., 2009; Schiefecker et al., 2015).

Based on the discussion above, experiments were designed to test the hypothesis that ketamine lessens deleterious consequences of SD in neuro— measured using optical (IOS, Ca^{2+}) and functional (DC shifts, EPSPs) indicators of SD demand and neuronal recovery (Chapter 2). Chapter 4 of this dissertation focused on translating findings from brain slices to *in vivo* experiments in mice after dMCAo. In these studies, it was of particular interest to test ketamine's efficacy on NMDAR-mediated consequences in peri-infarct tissues where diminished perfusion and related elevations in extracellular K^+ (Branston et al., 1977) reduce

the potency of NMDAR block of SD ((Petzold et al., 2005). This assumption indicates that ketamine would only block SD in healthy brain where it is not damaging (and may even be protective), and furthermore confer no protection to regions most vulnerable to SD-induced injury. It was thus important in this dissertation to provide the first direct comparison of effects of ketamine on SD consequences in locations both remote and proximal to the lesion core after dMCAo.

In order to rigorously test drug effects of ketamine on consequences that occur after passage of the SD wave front (while also enabling SD in healthy brain), ketamine was used at concentrations (or doses) that did not prevent SD in healthy brain tissues (Chapters 2 & 4). In brain slice studies, 30 μM ketamine reliably did not block SD in adequately superfused, nominally healthy brain slices with physiological levels of extracellular K^+ (3mM). In alignment with prior reports (Petzold et al., 2005), we saw that the ability of ketamine in inhibiting SD was diminished in aCSF with elevated basal K^+ (8mM) (Chapter 2). In these slice experiments ketamine reduced DC shift durations, accelerated EPSP recovery, and was associated with reduced intracellular Ca^{2+} accumulation during SD (in GCaMP5G expressing mice). This suggests that decreased neuronal Ca^{2+} loading during the DC shift reduces the demand of SD. The reduced duration of A1-mediated suppression of neuronal activity is likely due to less adenosine production (and thus ATP hydrolysis) during repolarization from ionic disturbances, although this was not directly tested. Further examinations of MAP2 or other markers for neuronal integrity would also be useful, as described previously.

In vulnerable preparations, Ca^{2+} loading during SD was also decreased by ketamine, even in elevated K^+ -supplemented aCSF. Evoked synaptic potentials were also improved after SD in ketamine treated slices, perhaps a result of reduced ATP requirements that would normally be utilized for Ca^{2+} sequestration and extrusion processes. Residual adenosine may partially explain the incomplete recovery of EPSPs (as described previously) in these experiments. Interestingly, though vulnerable EPSPs appeared to recover quicker in the presence of DPCPX (Figure 3.4) versus ketamine (Chapter 2), ketamine prevented transmitted light signals associated with slice dysfunction, while DPCPX had no effect on this read-out. This suggests a possible disconnect between recovery of cortical activity and neuron health, in some situations.

Overall, slice studies showed that NMDAR-mediated excitotoxicity and signs of neuronal dysfunction after SD were minimized by ketamine, even in metabolically compromising environments. This same concentration of ketamine did not prevent SD in healthy preparations and subsequent *in vivo* experiments therefore employed non-blocking doses of ketamine and evaluated damaging consequences of SD in both remote (nominally healthy) and peri-infarct tissues after focal ischemia.

Early studies in the late 1980s found that high doses of ketamine (>40 $mgkg^{-1}$) *in vivo* were capable of blocking SD induced in the healthy cortex (Gorelova et al., 1987; Marrannes et al., 1988a). Recent *in vivo* work has also demonstrated that high dose infusion of the more potent S-ketamine (4mg/kg/h) can prevent SD induced by K^+ stimulation in the non-injured cortex of pigs (Schöll et al., 2016). Based on these reports and experiments showing that peak

concentrations are achieved in the brain within 30 min. of i.p. injection in mice (Toki et al., 2018) pilot studies here identified a dose of racemic ketamine (5 $mgkg^{-1}$ dose, i.p.) that reliably did not prevent recurrent SD induction when administered 30 min. after dMCAo (Chapter 4). Consistent with findings in brain slices, ketamine improved the recovery of intracellular Ca^{2+} loading in neurons located closer to the stroke injury as well as the duration of depolarization; processes that delayed SD-induced progression of neuronal Ca^{2+} dysfunction into the remote cortex. These studies confirmed the relevance of brain slice studies in excitotoxic mechanisms during SD in penumbral brain regions *in vivo* after dMCAo.

5.5.1 Mechanisms of ketamine

The ability of ketamine to reduce NMDAR-mediated currents is influenced its stereospecificity (*R* versus *S*) and by NMDAR receptor subunit compositions with IC_{50}s ranging from ~1 to ~5 μM for racemic ketamine (Khlestova et al., 2016). Ketamine also has a use-dependent mechanism of action as it's binding site overlaps with Mg^{2+} within the channel pore. Therefore, ketamine competes with Mg^{2+} for access within the pore and thus requires glutamate and concomitant membrane depolarization (i.e. Mg^{2+} release) for activity-dependent blockade of NMDARs (Johnson et al., 2015) Due to differences in the relative strength of Mg^{2+} binding, and thus open channel probability of specific NMDAR subtypes, ketamine blockade varies depending on NMDAR subunit compositions (i.e. is most effective block at GluN2C-containing NMDARs) (Khlestova et al., 2016).

While this dissertation focused predominantly on NMDAR sources of Ca^{2+} influx into neurons, this does not imply that additional sources of intracellular Ca^{2+} cannot also contribute to cytosolic increases during SD. These can include plasma membrane and mitochondrial

Na^+/Ca^{2+} exchangers (NCX) and mitochondrial calcium uniporters (MCU) shown to reverse during ischemia (Lai et al., 2014); perhaps due to electrochemical gradient breakdown during the DC shift of SD. Recent evidence also suggests that even when NMDAR-mediated currents are blocked using MK801, metabotropic NMDAR activity initiates the formation of complexes that can then recruit other nonconical ion channels and processes to ignite intracellular Ca^{2+} dysregulation (during OGD in cell cultures) (Weilinger et al., 2016). Interestingly, some studies indicate that delayed cytosolic Ca^{2+} elevations (discussed during the ischemic cascade in Introduction) can contribute to delayed cell death in cell cultures, though are considered "fully trigged" at the initial onset of ischemia. Future work in vulnerable brain slices could help resolve mechanisms of intracellular Ca^{2+} to confirm that dysfunction is temporally restricted to SD. Findings could thus help guide interventions that target deleterious consequences of SD *in vivo*; perhaps using combinations of low concentrations of ketamine or other neuroprotective agents.

5.6. Summary of studies

Collectively, this dissertation work provides evidence that extended glutamate accumulation and NMDAR-mediated Ca^{2+} influx promote deleterious consequences of SD in vulnerable tissues both *in vitro* and *in vivo* after dMCAo. Additionally, low dose ketamine attenuated deleterious consequences in both experimental models by reducing DC shift durations and NMDAR-mediated Ca^{2+} loading in neurons. Importantly this work provides the first evidence that NMDAR antagonist can be effective at reducing deleterious consequences of SD even in conditions with elevated K^+ concentrations including peri-infarct tissues. This supports future

work with NMDAR blockers and SD as it remains unknown whether they can confer protection to the compromised brain where SD is difficult to prevent.

Chapters 2 & 3 in this dissertation examined the degree of glutamate and neuronal Ca^{2+} accumulation during SD in metabolically vulnerable brain slices and found that these excitotoxic mechanisms were intermediate between SD in healthy and OGD conditions. These data further substantiate the SD continuum shift in our thinking about SD consequences, and suggest that incomplete metabolic compromise may be a useful tool for future studies examining mechanisms of SD. In addition, experiments demonstrated the feasibility of protecting neurons from deleterious consequences of SD using concentrations of ketamine that do not prevent SD in either vulnerable or healthy brain slices. These findings were then applied *in vivo* to examine excitotoxic mechanisms that occur during SD in penumbral brain regions after dMCAo (Chapter 4).

Overall findings indicate that drugs targeting NMDAR Ca^{2+} influx or other mechanisms of cytosolic Ca^{2+} elevations during SD may be useful therapeutic approaches in brain injured patients. Findings that non-blocking doses of ketamine can reduce excitotoxicity during SD in metabolically compromised brain are especially important while the role of SD in brain recovery after injury remain unknown. Based on experiments in the body of this dissertation, future work is required in order to answer whether SD can be beneficial to the recovering brain. In the meantime, trials could be designed to examine dose-dependent effects of ketamine on SD characteristics (DC shifts, ECoG recovery) as well as infarct sizes and long-term functional

outcomes—in hopes of solidifying the causal role of SD in lesion progression and poor clinical prognoses.

5.7 Future studies and beneficial outcomes of SD

5.7.1 Recovery and repair after injury

An emerging fundamental property of the brain is its capacity to undergo remodeling throughout life, even after brain injury (Rumpel, 2018). The construction and elimination of synapses and plasticity processes are also important after brain injury, especially in distant regions outside of the lesion core that are theoretically responsible for cortical remapping of the ipsilateral cortex after stroke (Murphy and Corbett, 2009). The reconfiguration of brain circuitry is important for regaining functionality after stroke and this "recovery phase" may be ongoing in the days to months after injury (Rumpel, 2018). Recent preclinical studies have shown that activity-dependent incorporation of AMPA- type receptors into synapses can modulate functional recovery days after stroke injury and can also be enhanced using small molecule therapeutics (Abe et al., 2018; Chambers and Rumpel, 2017). These dynamic changes that occur after stroke (even in the absence of intervention) underlies the importance of understanding intrinsic mechanisms that improve or prevent cortical remapping processes. During the recovery phase there are additional changes in gene expression, release of growth factors, and the regrowth of neuronal processes (Rumpel, 2018). Mounting evidence shows that SD can also initiate these (among many other) cellular responses. Preliminary work in this dissertation in brain slices (Appendix B) demonstrated that a single SD could elicit (in ~30 min.) a significant increase in mRNA expression of the neurotropic factor BDNF lasting at least 60 min post SD and is in accordance with prior studies of SD preconditioning (described in Introduction). These are the first data to show acute increases in plasticity-related genes in

the hippocampus of mouse brain slices. In these studies, moderate levels of protection from deleterious SD consequences was observed when slices were subjected to a subsequent SD in metabolically compromising conditions (i.e. vulnerable brain slice model) at the time of maximal BDNF increases (45-60 min). This was confirmed using optical read-outs of slice health (IOS). Additional pilot experiments (Appendix B) also showed that ketamine did not interfere with SD-induced BDNF increases (measured 45 min. after SD) and, when combined with preconditioning measures, enabled full recovery of postsynaptic potentials after SD in vulnerable metabolic conditions. These data provide the first evidence in brain slices that a) preconditioning with SD (or tolerance induced by SD) increases BDNF levels which may confer protection against the energetic demands of SD in "at-risk" tissues.

5.7.2 Role of SD-mediated adenosine accumulation and potential for protection

Providing more substrates to tissues could be an alternative approach for supporting neurons that are at risk for injury during SD. D-ribose and adenine (RibAde) has been shown to increase ATP levels in brain slices (Frenguelli, 2017). This theoretically should supplement ATP levels that are depleted upon breakdown of electrochemical gradients during the DC shift. However, in hydrolyzing more ATP this would likely also elevate extracellular adenosine levels after SD. Although prolonged A_1-receptor mediated suppression and corresponding ECoG suppression in humans may indicate injury, suppression of neuronal activity may be important for preventing the likelihood of subsequent SDs (Canals et al., 2008a), activating K_{ATP} channels or other tolerance mechanisms involved with adenosine and/or A_1R activation (as discussed in introduction). Preliminary experiments conducted during this dissertation work (data not shown) supplemented brain slices with RibAde prior to SD in vulnerable recording conditions. This supplementation attenuated decreases in transmitted light and improved

functional recovery (EPSPs) after SD in vulnerable brain slices. Importantly, the duration of A_1-mediated synaptic depression after SD was significantly longer than healthy control brain slices, and future work is needed to confirm extracellular adenosine increases as well as the role of A_1Rs in tolerance mechanisms.

If SD is important for adaptation/tolerance during subsequent ischemia, there are many other questions that arise. If SD is beneficial then why doesn't the initial SD (that occurs within minutes of experimental occlusion) protect against further tissue deterioration? Furthermore, SDs can spontaneously erupt for days in many malignant stroke patients (Dohmen et al., 2008; Woitzik et al., 2013). Do these SDs initiate endogenous protection mechanisms in remote brain regions (i.e. a form of postconditioning)? Do the damaging effects of SD in vulnerable brain regions outweigh any benefits of SD in healthier brain tissues? Along the lines of dual roles for NMDARs in promoting cell survival or mediating cell death cascades, perhaps SD causes injury to metabolically compromised brain regions but are essential for recovery and repair after stroke. Are these processes downstream of SD? Although these questions are beyond the scope of this dissertation work, they highlight how much is unknown regarding SD and stroke outcomes and may provide some hesitation with regards to interventions that block SD. It is thus essential to determine if SD is important for brain recovery and repair after stroke or other acute brain injuries. This would not only help guide clinical decision-making in whether SD should be blocked in the ICU but could also inform rehabilitation practices in the aftermath of an injury.

5.8 Conclusions

The main objective of this dissertation was to evaluate the influence of metabolic status on excitotoxic consequences of SD. Experiments tested the central hypothesis that prolonged glutamate release during SD in metabolically vulnerable tissue underlies excitotoxic NMDAR-

Figure 5.3

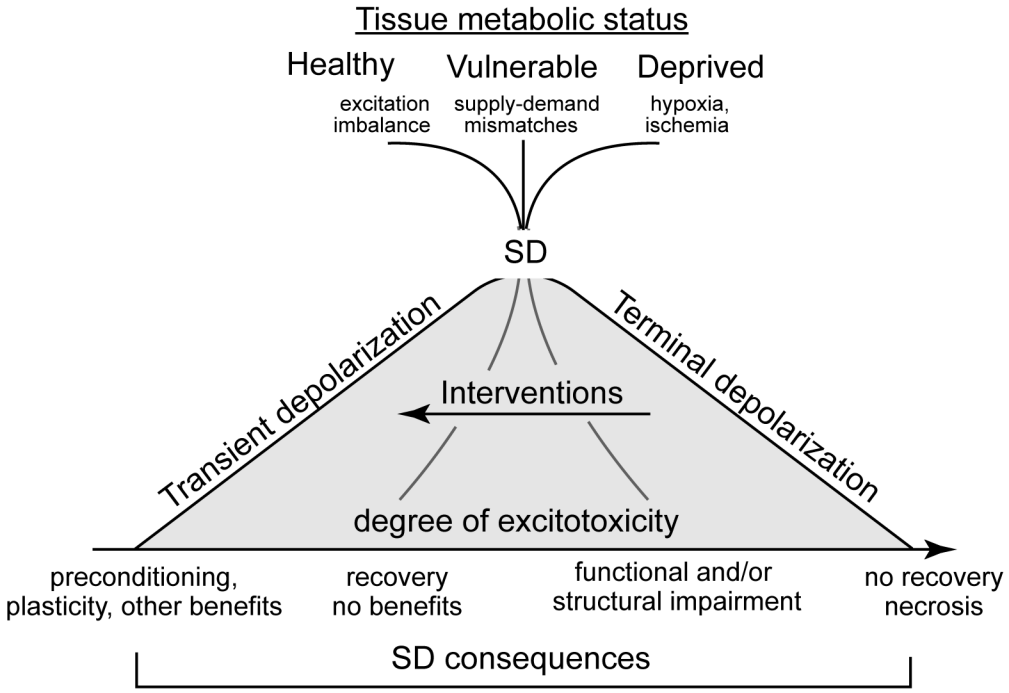

Figure 5.3. Continuum of SD consequences. Proposed model of brain metabolic capacity in relation to outcome after passage of SD. Depending on the environmental stimulus, SD can be ignited in healthy and injured brain. Additionally, metabolic status influences the degree of deleterious SD consequences (i.e. glutamate and NMDAR-mediated calcium accumulation) in neurons. In healthy brain, the depolarization during SD is transient (left) and the degree of resulting excitotoxicity is minimal. This could initiate mechanisms involved in important and/or beneficial cellular processes. After stroke or injury (right), SD ignites from the core of the infarct and no recovery is observed (unless reperfusion occurs shortly after). SD elicits massive excitotoxic consequences resulting in neuronal demise in metabolically deprived brain-- that likely cannot be prevented pharmacologically. In between these extremes, vulnerable brain (penumbra) is impaired but viable until eventually succumbing to the massive demands of SD. Initiated in response to supply-demand mismatches in neurovascular coupling, SD in vulnerable brain is characterized by extended glutamate-mediated consequences. Initially, SD may not cause neuronal injury; however with repeated 'hits' vulnerable neurons become increasingly susceptible to deleterious SD consequences. If true, interventions designed to target SD induced excitotoxicity may be beneficial for preventing injury expansion at discrete periods when the brain is most vulnerable--that is during SD. Theoretically, interventions that do not completely block SD (but reduce excitotoxicity) may be important for preserving potential beneficial outcomes; however, further work is needed to confirm these effects.

mediated neuronal injury. The ability of the NMDAR antagonist ketamine to reduce excitotoxic consequences, as a potential candidate for clinical utility, was also examined. **Figure 5.3** illustrates a proposed model of SD consequences based on this dissertation work in the context of the SD continuum (Hartings et al., 2017). Findings from these studies, here, extend our knowledge about cellular mechanisms involved with tissue demise and thus serve as a theoretical starting point for targeting these processes pharmacologically in brain injured patients.

Studies were first conducted in well-controlled brain slices using a novel model of energy substrate restriction that increased neuronal susceptibility to the additional 'hit' of SD. From these findings, it is now known that extended (extracellular) glutamate and (intracellular) NMDAR-mediated Ca^{2+} accumulation are associated with poor neuronal recovery from SD. Additionally, these data help identify mechanisms that may in-part explain neuroprotective effects of ketamine observed in the injured brain—i.e. the attenuation of neuronal Ca^{2+} loading after passage of the wave front. Chapter 4 transitioned findings from brain slices to test SD mechanisms and interventions *in vivo* after focal ischemia. The degree of SD-induced excitotoxic consequences. Similar to brain slice results, ketamine improved intracellular neuronal Ca^{2+} accumulation during SD and associated with reduced DC shift durations. Collectively, this work extends our knowledge of cellular mechanisms that confer vulnerability to SD-mediated injury and provide further evidence that ketamine (or other interventions that target excitotoxic SD consequences) may be useful for improving tissue recovery after ischemic stroke or other acute brain injuries.

Studies that examined therapeutic interventions in this dissertation project were largely focused on the NMDAR antagonist ketamine, as it is clinically used in the ICU setting and has shown efficacy at reducing SD frequency in brain injured patients (Carlson et al., 2018; Hertle et al., 2012). Prior to the work presented here, it was largely assumed that the only way to prevent damaging effects of SD was to completely block its initiation and/or propagation. In most cases, this requires a substantial degree of NMDAR inhibition and thus high ketamine doses in animals (Amemori and Bures, 1990; Hernández-Cáceres et al., 1987; Marrannes et al., 1988). In addition to challenges of preventing SD in peri-infarct brain (Petzold et al., 2005), the outright inhibition of SD may occlude any theoretical benefits of propagation in undamaged brain regions after stroke (Hartings et al., 2017, Dreier, 2011). Based on our knowledge that neurons are particularly vulnerable to injury when NMDARs are activated during the late phase of the DC shift (Aiba, 2012), studies examined if ketamine could be employed to reduce glutamate-mediated consequences (i.e. Ca^{2+} loading via NMDARs) of SD. Findings from this dissertation work suggest that ketamine may be used during discrete periods of increased SD frequency and clinical worsening to limit detrimental consequences of SD.

6. APPENDICIES

Appendix A: Effect of memantine on spreading depolarization consequences in brain slices

Katelyn M. Reinhart[1], Alanna Humphrey, & C. William Shuttleworth[1]
[1]Department of Neurosciences, University of New Mexico School of Medicine.

Corresponding Author:
C. W. Shuttleworth, Ph.D.
Department of Neurosciences, MSC08 4740
1 University of New Mexico
Albuquerque, NM 87131
(505) 272 5826
bshuttleworth@salud.unm.edu

Abstract

Spreading depolarization (SD) is thought to be a key mediator of secondary lesion progression after acute brain injuries, including ischemic stroke. Characterized by a large negative shift in the extracellular direct current (DC) potential, the duration of this "DC shift" is associated with poor clinical prognoses after brain trauma. The late-phase of the DC shift is particularly challenging for compromised tissues and is characterized by persistent glutamate release and *N*-Methyl-D- aspartate receptor (NMDAR) activation. Interventions that reduce the frequency and/or duration of the late phase of SD are thus promising therapeutic approaches for reducing secondary lesion progression after ischemic stroke. The NMDAR antagonist memantine can decrease the number of SDs *in vivo,* but the effect of memantine on the late phase of SD is unknown. We utilized electrophysiological and optical recordings to monitor neuronal consequences associated with the late-phase of SD in acutely prepared brain slices from C57Bl/6 and GCaMP5G-expressing mice. SDs were initiated by oxygen glucose deprivation (OGD) or by localized microinjection of K^+ in the hippocampus of preparations, and the effect of memantine (10-300μM) on SD onset (after OGD), DC shift duration, neuronal Ca^{2+} loading, and recovery of postsynaptic responses was examined. We found that even high concentrations (up to 300μM) of memantine did not prevent SD in any experiments and low concentrations (10μM) did not alter any SD properties. During repetitive SDs (K^+ induced at 15 min intervals), 100μM memantine accelerated the recovery of synaptic activity which was related to reduced propagation rates and durations of DC shifts. However, this concentration had no effect on SD onset following OGD exposure—conditions that model the core of the ischemic infarct deprived of metabolic substrates. In slices with less severe metabolic impairment the extent

of neuronal Ca^{2+} loading consequences of SD were attenuated by memantine. These data indicate that memantine can limit NMDAR-mediated neuronal Ca^{2+} loading during SD that is deleterious in metabolically impaired tissues. Memantine may therefore be a therapeutic option for protecting salvageable penumbral brain areas that are extremely vulnerable to SD-mediated injury in the days following ischemic stroke.

Keywords:
Spreading depression; excitotoxicity; NMDA receptor; brain slice; calcium; neuronal injury; metabolic compromise; oxygen glucose deprivation, OGD

A.1 Introduction

Spreading depolarization (SD) is a propagating wave of near-complete neuronal and glial depolarization (Somjen, 2001) that occurs in migraine with aura traumatic brain injury, stroke, and other acute brain injuries (Hartings, 2017). Initiated by stimuli that cause depolarization of a volume of excitable tissue (Tang, 2017) SD travels slowly at 2-4 mm min^{-1} and is characterized by a large negative shift in the extracellular direct current (DC) potential and "spreading depression" of spontaneous and evoked synaptic activity (Leao 1944, 1947).

In the injured brain, SD clusters are associated with poor outcomes in both animal models (Back et al., 1996, Hartings et al., 2003) and clinical studies (Dreier, 2011; Hartings, et al. 2011**).** Additionally, SDs with prolonged DC shift durations increase the metabolic demand of recovery and contribute to the progression of acute brain injury (Dreier, 2009, Oliveira-Ferreira et al. 2010). However, while prospective studies are needed to determine if blockade of SD confers better outcomes in patients, there is the possibility that inhibiting SD prevent any theoretical benefits of SD in healthy brain regions (Hartings, 2017). Targeting SD consequences in vulnerable brain may be an alternative therapeutic approach for reducing SD-mediated damage, as opposed to outright block.

The late phase of the DC shift is accompanied by substantial glutamate release and excitotoxic *N*-Methyl-D- aspartate receptor (NMDAR) activation. In metabolically compromised tissue, NMDAR- mediated Ca^{2+} entry during late-SD contributes to irrecoverable neuronal injury (Aiba and Shuttleworth ,2012). In animal and clinical studies, the use-dependent NMDAR antagonist ketamine can reduce the frequency of SDs (Sanchez-Porras et al., 2014; Hertle et al., 2012, Carlson et al., 2018). There is also evidence that ketamine can reduce deleterious

consequences of SD in brain slices and thus may be a promising candidate for limiting SD-mediated injury in ICU patients (Reinhart and Shuttleworth, 2018). However, ketamine is often associated with unwanted side-effects and high abuse potential.

The goal of this study is to examine another use-dependent NMDAR antagonist memantine and test whether deleterious consequences of SD can be limited without employing high drug concentrations that block SD. We used electrophysiology and imaging techniques and found that memantine reduced the duration of DC shifts and accelerated recovery of synaptic activity after SD in brain slices. Additionally, we examined SD consequences in tissues with severe (OGD) and moderate metabolic compromise (described previously in Reinhart and Shuttleworth, 2018) and found that memantine attenuated SD-mediated intracellular Ca^{2+} loading in moderately impaired neurons that was otherwise irrecoverable in the absence of drug. The protective effect of memantine in reducing deleterious consequences of SD in brain slices support future studies to evaluate whether this protection can be observed after *in vivo* stroke and in clinical settings.

A.2 Materials and Methods

A.2.1 Animals and brain slice preparation

All animal procedures were performed in accordance with protocols approved by the UNM Health Sciences Center Institutional Animal Care and Use Committee. Brain slices were prepared from adult (6-8 week) C57Bl/6 mice purchased from The Jackson Laboratory. In experiments studying SD-mediated neuronal Ca^{2+} accumulation mice expressing the fluorescent Ca^{2+} indicator GCaMP5G were used. For all pharmacological intervention experiments, drug-treated SDs were compared to same-slice control SDs for each animal

unless stated otherwise. Brain slices were prepared as previously described (Shuttleworth et al., 2003). Briefly, animals were deeply anaesthetized with a ketamine-xylazine mixture and decapitated. Brains were quickly removed into ~150mL of oxygenated ice-cold cutting solution (in mM): Sucrose, 220; $NaHCO_3$, 26; KCl, 3; NaH_2PO_4, 1.5; $MgSO_4$, 6; glucose, 10; $CaCl_2$ 0.2; equilibrated with 95% O_2/5% CO_2 supplemented with 0.2mL ketamine (100mg mL^{-1}) to limit excitotoxicity during the cutting procedure. Coronal cortico-hippocampal slices (350µm) were prepared with a Pelco 102 Vibratome (Ted Pella, Inc., Redding, CA) and hemisected. Slices were transferred to artificial cerebrospinal fluid [aCSF; containing (in mM): NaCl, 126; $NaHCO_3$, 26; glucose, 10; KCl, 3; $CaCl_2$, 2, NaH_2PO_4, 1.5; $MgSO_4$, 1; equilibrated with 95% O_2/ 5% CO_2], at 35°C for 60 min. After this recovery period aCSF was replaced with chilled (20°C) aCSF and allowed to equilibrate to room temperature prior to recording sessions.

Generation of SD and metabolic compromise

Individual brain slices were transferred to a submersion recording chamber with nylon slice supports (RC-27, Warner Instruments, Hamden, CT). Moderate metabolic compromise was achieved by inverting the slice support and reducing super fusion of aCSF below the slice, as previously described (Reinhart and Shuttleworth, 2018). Severe compromise was achieved by substituting O_2 with N_2 bubbling of aCSF containing sucrose as a replacement for glucose, creating OGD conditions. For all recordings, slices were continuously super fused with aCSF at 2.4mL min^{-1} and bath temperature was maintained throughout experiments at 32°C by an inline heater assembly (TC-344B, Warner Instruments). After placement of the slice (and recording/stimulating electrodes), slices were allowed a 15-minute equilibration period prior to the start of recordings. In experiments testing the effect of drug application in moderately

compromised and during repetitive SDs, aCSF was replaced with modified aCSF containing 8mM KCl ([K^+]-aCSF) during warm up and continued throughout the recording. Following 15 minutes of equilibration SD was generated in the hippocampal stratum radiatum of CA1 by localized microinjection (10-40ms, 30psi) of KCl (1M) via a glass micropipette (1.8-6 MΩ) using a picospritzer (Parker Hannifin, OH, USA) or was spontaneously initiated after exposure to OGD. In experiments testing repetitive SDs (up to 7), each SD was generated (via K^+) at 15 minutes intervals to allow for full recovery between events. Two control SDs prior to drug application were generated to enable in-slice comparison of SD characteristics. After the second control SD, memantine was washed in for 10 minutes prior to the next SD stimulation.

Electrophysiology

Extracellular recordings were made using glass microelectrodes filled with aCSF (tip resistance 1.8-6MΩ) placed at a depth of 50µm in the CA1 stratum radiatum >200µm from the KCl micropipette. Extracellular DC potential was acquired at 1 kHz with an Axon MultiClamp 700A amplifier and Clampex 9.2 (Molecular Devices, Sunnyvale, CA), and digitized with a Digidata 1332 digitizer. For extracellular excitatory postsynaptic potential (EPSP) recordings, a concentric bipolar electrode (FHC) was positioned 50µm deep into the CA1 stratum radiatum between the KCl micropipette and recording electrode for stimulation of Schaffer collateral inputs. After electrode placements, slices were allowed to equilibrate for 15 min during which an input-output curve was generated (final 5 min of equilibration). Test pulses were delivered (50µs, 0.1Hz) at intensities that gave 50-60% of maximum EPSP responses (150 – 600µA). Responses were recorded at 10kHz and SD was generated after stabilization of baseline EPSPs. All analyses were performed using Clampfit 10.4 software and DC shift durations during SD

were measured as the width between 20% of the initial downward deflection of the peak amplitude to 80% of recovery to baseline levels.

Imaging

SD initiation and propagation were examined by monitoring brain slice intrinsic optical signals (IOS) trans-illuminated with visible light (≥600nm) using a 4x objective (Olympus 0.10 NA). IOS data were captured (0.5Hz) using a cooled CCD camera (Till Photonics) and analyzed with TillVision software (TillPhotonics, version 4.01). Data analysis involved normalizing to baseline transmitted light and expressing IOS as percent change in transmission ($\Delta T/T_0$ x 100). Fluorescence imaging of intracellular neuronal Ca^{2+} loading during SD was preformed using slices prepared from GCaMP5G animals. Slices were excited (480nm) at 4Hz using a 20X objective (Olympus) using a monochromator (TillPhotonics). Emitted light was passed through a dichroic mirror (515DCLP) prior CCD capture. Data analysis involved background subtraction and normalization of pixel intensities to pre-SD (baseline). Fluorescence values are thus expressed as the percent change in fluorescence from baseline ($\Delta F/F_0$ x 100).

Drugs

All chemicals including salts and sugars used in aCSF were obtained from Sigma-Aldrich (St. Louis, MO, USA) unless otherwise stated. Memantine-HCl was prepared as a 100mM stock in deionized water and stored in aliquots at -20°C until daily use.

Statistical Analysis

All data analyses and statistical tests were performed using GraphPad Prism 8.1.2. Unless otherwise stated, all data are represented as mean ± SEM.

A.3 Results

Repetitive SDs in hippocampal slices

We first evaluated the effect of low memantine concentrations (10μM) on single K^+ induced SDs in aCSF containing standard concentrations of K^+ (3mM). In this data set (n=9 slices for control and n=8 for memantine) there was no effect of memantine on SD propagation rate (3.4 ± 0.3 vs. 3.3 ± 0.4 mm min^{-1} for control and memantine, respectively; P>0.8), DC shift peak amplitudes (-6.3 ± 0.7 vs -5.9 ± 2.6 mV for control and memantine, respectively; P>0.7), or DC shift duration (34.6 ± 4.4 vs. 26.5 ± 2.5 s for control and memantine, respectively; P>0.1). We next verified recording conditions for repetitive SDs in slice according to our previous work (Reinhart and Shuttleworth, 2018). As shown in images of **Figure 1A**, SD was evoked via KCl microinjection into the hippocampal CA1 region, and intrinsic optical signals (IOS) used to track progression across the slice. The rate of SD spread was measured at the wave front which could be clearly distinguished based on IOS transmission changes. As noted in Methods, aCSF contained elevated basal K^+ (8mM; ($[K^+]$-aCSF), to facilitate repetitive SD initiation in both control and metabolically impaired slices. As previously reported (Reinhart and Shuttleworth, 2018) this modest elevation of K^+ did itself not generate SDs, but enhanced

SD propagation rate compared to 3mM KCl aCSF (Mean ±SEM) 3.2 ± 0.2 mm min $^{-1}$ (n=18) vs. 6.2 ± 0.3 mm min^{-1} (n=6); $P < 0.0001$), while other SD characteristics remained unchanged.

Figure 6.1

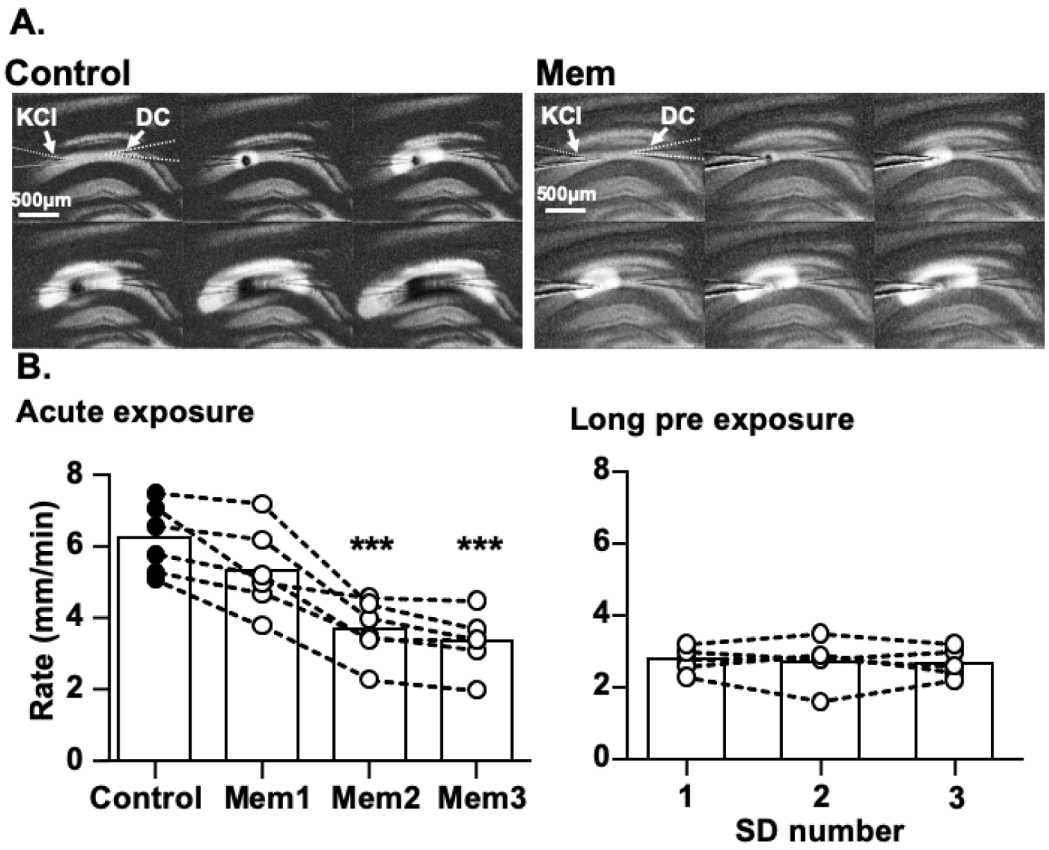

Figure 1. Effect of memantine on SD propagation rate. A. Representative transmission changes during SD in control (left; 2nd control SD), and in memantine (right; 3rd SD in Mem; same slice). SD was initiated in CA1 by KCl microinjection, and propagation rate was evaluated at the wave front. B. Right: summary data from 6 slices showing the effect of memantine on propagation rate during successive SDs,The first SD in memantine was not significantly slower compared to controls (P = 0.16). The maximum effect was achieved during the 2nd SD in memantine (Mem2), with no change in rate between Mem2 and Mem3 (P = 0.16). Right panel: maximum effect of memantine on SD propagation could be achieved with long (≥3 hours) incubations (n=5), ***P<0.001 compared to the second control SD.

Memantine slows SD and reduces DC shift duration

Memantine exposures (up to 300μM) did not prevent initiation of SD in any preparation, but 100-300 μM reliably slowed propagation rate across the CA1 subfield. Figure 1A shows an example of slowed progression in 100 μM memantine, compared to the control SD within the same slice. Figure 1B (left panel) shows mean data from 6 preparations and demonstrates that significant effects took time to develop during acute memantine exposures. Thus, the first SD after onset of memantine exposures (10 min) were not significantly different from control, but second and third SDs in memantine were reliably depressed. The lack of an effect of 100 μM memantine on the first SD was also observed in preliminary data sets conducted using 3mM KCl – supplemented aCSF (2.5 ± 0.3 vs. 2.6 ± 0.3 mm min^{-1} for control (n=8) and memantine

(n=7), respectively; P>0.9). When slices were incubated with memantine prior to recordings (3 or more hours), SD propagation rates were immediately slower, and did not require successive SDs to achieve the maximum effect (Figure 1B (right panel); n=5). Extended pre-exposures have also been utilized in earlier work which identified a slow time course of 100 μM memantine inhibition (as well as recovery) of NMDAR-mediated currents (EPSCs) (Frankiewicz, 1996). This indicates that memantine does not require the presence large depolarizations in order to reduce the spread of SD but does not rule out the possibility of use-

Figure 6.2

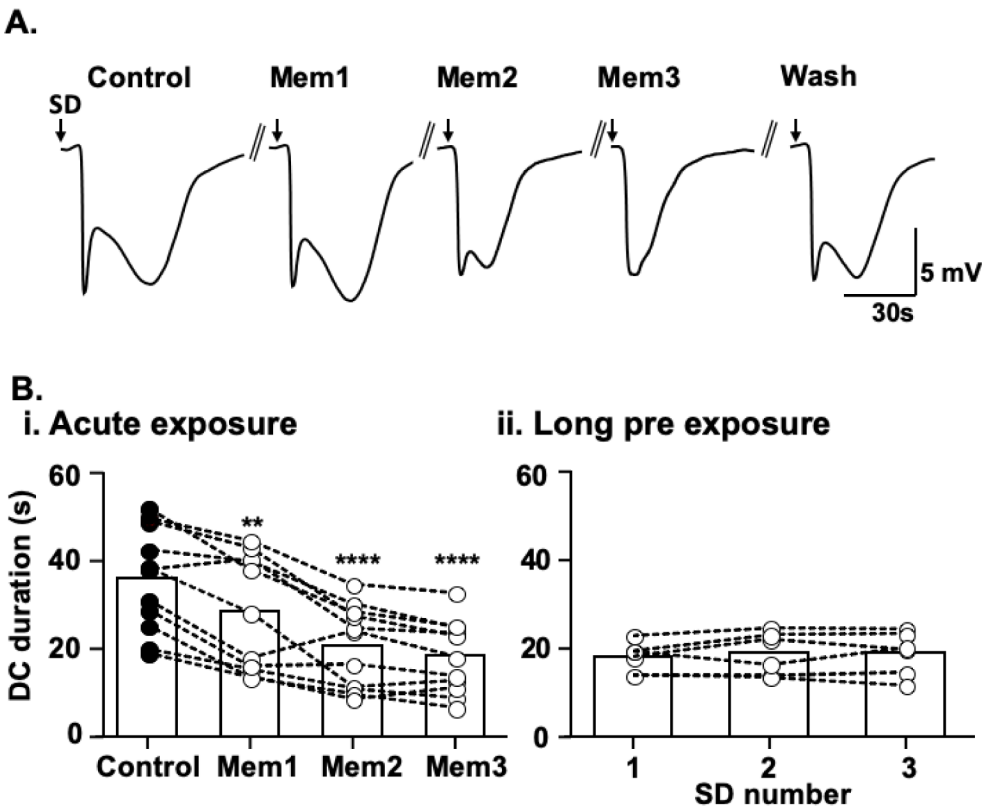

Figure 2. Memantine reduces SD duration.
A. Example trace demonstrating effect of memantine on DC shift duration during successive SDs in a single slice. Return to a biphasic waveform could be achieved after following memantine wash out. B (i). Summary data from 11 slices during memantine wash in. DC duration was measured from 20% depolarization to 80% recovery to baseline (ii). Maximum effect of memantine on neuronal depolarization duration could be achieved during long incubations(≥3hours)(n=6)**P<0.01,****P<0.0001

dependency of memantine block being contributed to by ongoing synaptic activity during long pre-exposures.

Consistent with previous studies (Reinhart and Shuttleworth, 2018) there was a gradual run-down on DC shift peak amplitude during successive SDs (data not shown) and thus was not attributed to NMDAR antagonist exposure. **Figure 2A** shows a representative trace demonstrating the effect of memantine wash in on the characteristics of DC potential shifts recorded during SD. Consistent with the related NMDAR antagonists including ketamine, the most drastic effect of memantine was on the duration of SD, and in particular the late phase of the DC shift present after passage of the wave front. The maximum effect on DC duration was also apparent during successive SDs at 15-minute intervals (Figure 2B (left panel)) or following extended incubation prior to recordings (Figure 2B, right panel). From the data set shown in Figure 2, EPSPs were recorded in 6/11 slices and results from these experiments are described below.

Memantine accelerates recovery of postsynaptic potentials after SD

To determine the physiological significance of shorter extracellular DC shifts, we monitored adenosine-A1 receptor (A_1R) -mediated suppression of evoked excitatory postsynaptic potentials (EPSPs) as a read-out of the metabolic demand of SD. In slices not exposed to memantine, there was a tendency for postsynaptic responses to recover more quickly after repetitive SDs (6.3 ± 0.6 vs. 5.5 ± 0.3 min, SD2 vs. SD5; P=0.06, n=5, paired t-test), perhaps a result of SD-induced plasticity mechanisms. Memantine further augmented this effect as revealed with successive SDs during acute drug exposures. **Figure 3A** shows a representative time course of EPSP recovery after the control SD (SD2) and the third SD following exposure to memantine (SD5) within the same slice. Mean data from such experiments are shown in the

right panel of Figure 3A demonstrating the further acceleration of EPSP recovery by the third SD in the presence of memantine (P= 0.0008, n=6). In the same preparations, shorter DC durations were correlated with shorter durations of EPSP suppression (Figure 3B). This suggests that memantine may reduce deleterious consequences of prolonged depolarizations allowing for quicker recovery of normal synaptic transmission in the wake of SD.

Figure 6.3

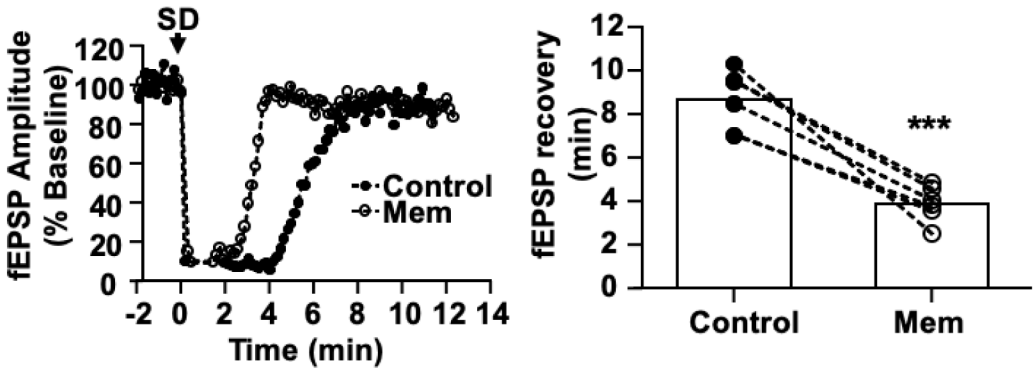

Figure 3. Memantine accelerates recovery of synaptic transmission after SD. Representative time course shows faster EPSP ampltidue recovery after SD in memantine (open circles) compared to control (filled circles) in an individual experiment. Right: mean from 6 such experiments shows acute memantine exposure reduces the duration of synaptic depression after SD (n=6; P=0.0008)

Memantine reduces neuronal Ca2+ loading during SD

Memantine prolongs duration of zinc transients during SD

Previous studies in our lab have demonstrated that increased glutamate release and subsequent NMDAR activation during late-SD contribute to long-lasting depolarization and prolonged Ca^{2+} elevations in neurons (Aiba & Shuttleworth, 2012). Additionally, recent work suggests that presynaptic NMDAR activation plays an important role in feedforward glutamate release during SD (Zhou et al., 2013). We utilized zinc fluorescence imaging to evaluate the effect of memantine on neurotransmitter release during SD. In this study, slices were pre exposed to memantine (100uM) for ≥3 hours in order to immediately achieve the maximum effect. **Figure 4A (i)** shows a representative change in zinc fluorescence during SD in memantine and interleaved control slices. In mice lacking synaptic zinc (ZnT3KO), there was no change in

fluorescence during SD (n=3). Summary data (Figure 4Aii), demonstrates that memantine (n=9) prolongs zinc transient durations compared to interleaved control (n=7) preparations (*P*=0.0101). To ensure that the effect of memantine was not an artifact of slow SD propagation, extracellular potassium was reduced to 3mM which significantly slowed SD propagation compared to [K^+]-aCSF (2.52± 0.30 vs. 4.68 ± 0.22 mm/min, 3mM (n=9) vs. 8mM KCl-aCSF (n=6), *P*=0.0002 unpaired two tailed t-test), but did not influence the duration of zinc transients (1921±209.9 vs. 2197 ±329.0 arbitrary units (a.u.s), 3mM (n=9) vs. 8mM KCl-aCSF (n=7), *P*= 0.5199 unpaired two-tailed T-test) . Figure 4B plots zinc transient duration as a function of SD propagation rate in memantine, [K^+]-aCSF, and 3mM KCl-aCSF demonstrating that slow SD spread has little effect on zinc fluorescence changes.

A.4 Discussion

General

We examined SD in brain slices exposed to varying degrees of metabolic impairment ranging from nominally healthy to severely compromised (OGD). In healthy slices, extended antagonist exposure to moderate concentrations (100 μM) or repeated SDs revealed that memantine could reduce SD propagation and DC shift durations. Shorter DC shift durations suggest that memantine reduces the energetic demand of SD which was also supported by accelerated synaptic recovery after SD observed in memantine. However, this same concentration of memantine (100 μM) did not influence SD or the resulting IOS decreases following OGD exposure, suggesting that memantine administration will likely not protect against SD-mediated injury in the core of ischemic infarcts. We next tested whether memantine could reduce deleterious consequences of SD in conditions of moderate compromise as memantine could still serve a protective role in tissues that are viable until the

additional hit of SD. We found that memantine in these conditions reduced intracellular neuronal Ca^{2+} consequences of SD that were irrecoverable in untreated preparations.

Deleterious consequences of SD mediated by NMDAR activation

SDs with long DC shift durations increase the metabolic demand of recovery and contribute to the progression of acute brain injury (Oliveira-Ferreira et al., 2010; Hartings et al., 2017). In addition to playing a role in SD initiation, NMDAR opening is prominent during the late-phase of SD when neurons are completely depolarized and presynaptic glutamate release is enhanced (Aiba and Shuttleworth, 2012). NMDAR antagonists are thus promising candidates for reducing deleterious NMDAR-mediated consequences of SD in hopes of improving outcomes after stroke and other acute brain injuries. Targeting consequences (rather than outright block) may be of further interest if future studies identify an important role of SD in recovery and repair mechanisms after injury.

In this study, memantine reduced the propagation (Figure 1) and duration of DC shifts (Figure 2) during successive SDs. DC shifts were most notably minimized (by memantine) during the late-phase of the DC shift (demonstrated in traces from one experiment in Figure 2) and this phase contributes to significant neuronal NMDAR-mediated Ca^{2+} (and likely Na^{+}) loading after passage of the SD wave front (Aiba and Shuttleworth, 2012). Subsequent experiments (Figures 3, 4) show improved recovery from adenosine-mediated synaptic suppression suggesting that SDs in memantine were less metabolically challenging (Lindquist and Shuttleworth, 2014).

Memantine

Memantine is an FDA approved use-dependent NMDAR antagonist that is used to improve cognition in symptomatic Alzheimer's disease patients. Memantine has also gained interest as a potential therapy for reducing migraine frequency based on previous findings that SD frequency (initiated by KCl) is reduced *in vivo* after memantine exposure in rats (Peeters et al., 2007). In addition to its clinical tolerability, the chemical structure and mode of action of memantine at NMDARs is almost indistinguishable from the related antagonist ketamine (Johnson, 2015). Preclinical and clinical studies have shown that high dose ketamine can reduce SD frequency after brain injury ((Hertle et al., 2012; Carlson et al., 2018) while lower non-blocking concentrations can limit deleterious consequences in brain slices (Reinhart and Shuttleworth, 2018). Problems with ketamine include psychotic behaviors, tolerance, potential for abuse and thus memantine may serve as an alternative option in some patients.

Previous work has demonstrated that memantine can be effective at reducing the size of infarction when administered acute prior to or after experimental stroke (Chen HS,et al. 1998, Gorgulu A, et al, 2000; Lapchak PA, 2006; Hao J, et al., 2008; Babu CS and Ramanathan M, 2009; Liu C, et al, 2009; Shih AY, et al, 2013). Beyond the acute stage of injury, chronic memantine treatment (30mg/kg per day) beginning >2 hours after photothrombotic stroke in mice can facilitate circuit recovery in peri-infarct brain regions via brain-derived neurotrophic factor (BDNF) signaling mechanisms (Lopez-Valdes, 2014). This study found no differences in infarct size but observed significant improvements in motor control 28 days after stroke. This is consistent with our findings that memantine does not prevent or delay SD (and associated structural demise based on IOS signals) following OGD exposure but can significantly limit deleterious consequences to neurons in metabolically vulnerable conditions.

Even though Lopez-Valdes and colleagues did not monitor SD after the thrombosis, we anticipate that oral delivery of 30mg/kg (per day) of memantine would not inhibit SD frequency, as memantine does not appear to have a potent effect on blocking SD. The ability of memantine to prevent SD after stroke would be further hindered by the ionic imbalances, including elevated extracellular K^+ (Petzold et al., 2005), observed in peri-infarct tissues. Even in studies conducted by Peeters and colleagues in the uninjured brain, i.p. injection of 10mg/kg memantine achieved prominent brain concentrations (~100μM) but could not prevent 100% of SDs initiated by KCl (Peeters et al., 2007). As such, inhibiting SD frequency after photo thrombosis may not be the mechanism behind memantine's promising outcomes, however it remains plausible that memantine exerts a protective effect by reducing neuronal consequences of SD.

It remains unresolved as to the potential benefits of SD, particularly in brain regions with preserved cerebral perfusion after focal ischemia. There is mounting preclinical evidence that SD stimulated days prior to a subsequent stroke induces preconditioning mechanisms resulting in a reduction in subsequent infarct size. This has largely been attributed to upregulation of BDNF (Yanamoto et al., 2004). If it is found that SD is a central upstream initiator of BDNF after focal ischemia, drugs that block these events may reduce the size of an infarct but at the expense of potential SD-mediated functional repair. Therefore, interventions like memantine or low concentration ketamine may provide approaches for reducing the damaging consequences of SD in vulnerable brain without preventing preconditioning and/or protective effects in metabolically intact tissues. Perhaps prior work (Lopez-Valdes, 2014) provides an initial test of this hypothesis, as BDNF was upregulated in memantine-treated animals.

Conclusions

In this study we tested whether the NMDAR antagonist memantine could reduce consequences of SD that are especially deleterious to metabolically vulnerable neurons. Collectively, this work provides initial evidence that memantine administration in the ICU may provide some protection against deleterious consequences of SD in salvageable brain tissues without preventing any benefits remotely.

Appendix B: Theoretical protective effects of SD

B.1 Abstract

Spreading depolarizations (SD) are slowly propagating waves of neuronal and glial depolarization that occur in stroke brain. SD causes irrecoverable injury to metabolically compromised tissues by over-excitation of NMDA receptors. On the other hand, SD may also promote NMDA receptor-dependent synaptic plasticity and protective preconditioning in healthy tissues surrounding infarcts. Previous work *in vivo* suggests that beneficial effects of SD (i.e. preconditioning) are mediated via upregulation of brain derived neurotrophic factor, BDNF (Yanamoto et al., 2000, 2004; Shen P et al., 2016). In these studies, SD was initiated days *prior* to subsequent middle cerebral artery occlusion, and therefore the acute protective role of SD remains unknown. Additionally, most studies have evaluated SD preconditioning effects *in vivo* and thus experiments in well-controlled brain slices would be useful for understanding the cellular mechanisms of SD-induced protection. Results of such studies are important for determining whether all SDs should be blocked in brain injured patients.

To determine if BDNF mRNA is upregulated *in vitro* after SD, acute cortico-hippocampal brain slices were prepared from C57Bl/6 mice. SD was initiated by KCl microinjection in CA1 and confirmed via extracellular DC potentials and loss of evoked excitatory postsynaptic potentials (EPSPs). The time course of BDNF mRNA changes after SD were assessed by rt-qPCR. We also tested the influence of ketamine (30μM – a concentration known to reduce deleterious consequences without blocking SD) on SD-induced BDNF changes. Total BDNF (BDNF-Pan) and activity-dependent BDNF (BDNF-L) mRNA from hippocampus was assessed before and 5,15,30,45, and 60min after SD. We found significant upregulation of both

total and activity-dependent BDNF mRNA beginning ~30 min. after SD (45 min. for total BDNF) that remained elevated at the 60 min time point (**Figure 1**, left panels). Based on these findings, we examined the 45 min. time point and found that ketamine did not reduce (and perhaps may increase) SD-induced BDNF upregulation (Figure 1, right panels). To determine if upregulation of BDNF could protect brain slices from SD in conditions of metabolic compromise, we initiated SD (via KCl microinjection) and allowed slices to recover for 45 min. prior to initiation of a second SD in metabolically vulnerable conditions (**Figure 2**). There was a modest improvement in the percent of slices that recovered from SD in damaging conditions, measured as the percent of slices capable of propagating successive SDs. However, this effect was greatly enhanced in the presence of ketamine. Similar effects were observed in

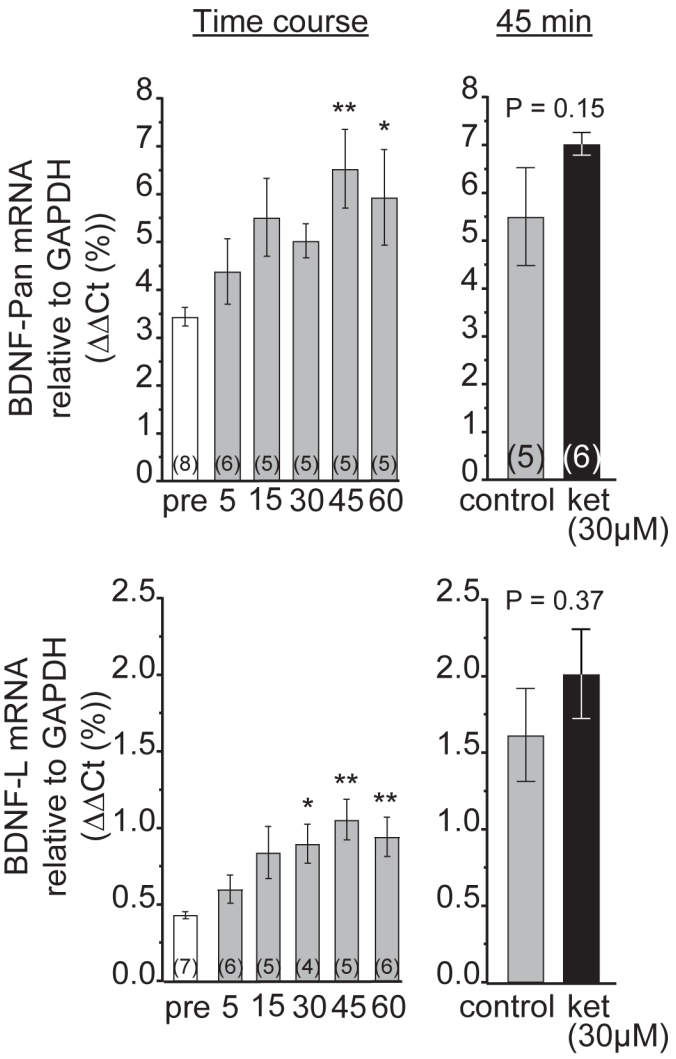

Figure 1. Acute increases in BDNF mRNA after SD in brain slices. BDNF-Pan (top) and activity-dependent (BDNF-L; below) mRNA changes relative to GAPDH before (pre) and at different time intervals after SD. Both total and activity-dependent forms of BDNF are upregulated by ~30 min after SD that last at least to 60 min (n=4-7 slices/group). Right panels show that ketamine did not prevent respesctive BDNF increases that were measured at the 45 min. time point after SD (n=5-6 slices/group).

EPSP recordings where ketamine conferred enhanced protection when combined with SD in healthy tissues (prior to subsequently deleterious SD).

These findings suggest that low ketamine concentrations can protect against damaging effects of SD while permitting propagation into peri-infarct regions. Such SDs could potentially contribute to protective preconditioning and support recovery and repair.

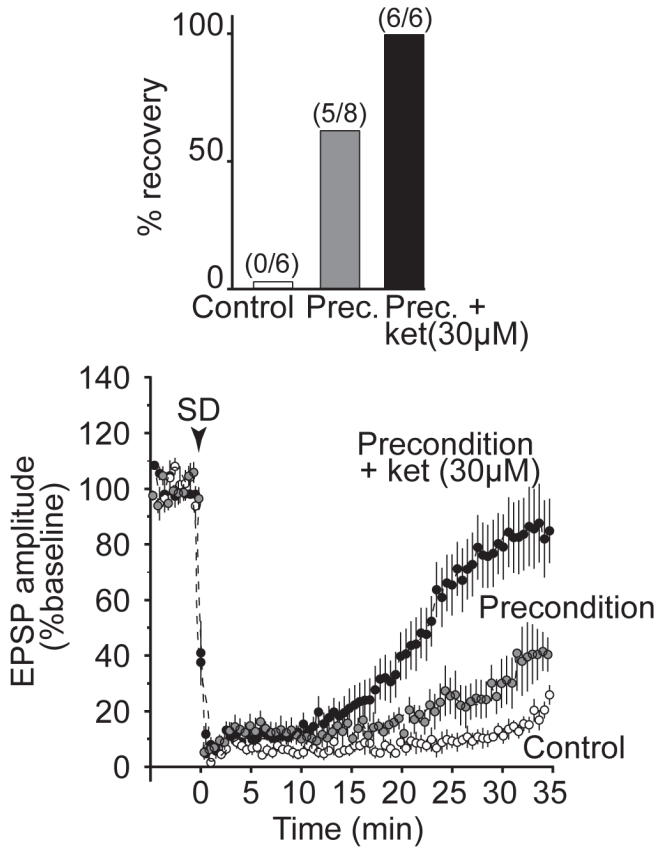

Figure 2. Preconditioning may improve recovery from subequent SD in metabolically compromised brain slices. Top: percent of preparations that recovered after SD was induced (via KCl) in metabolically vulnerable slices. Recovery was based on the ability of slices to propagate multiple SDs (evaluated via the presence of DC shifts). A single preconditioning SD alone prior to SD in vulnerable conditions confered some protection and mildly improved EPSP recovery (below), recorded during SD in vulnerabble recording conditions (i.e. not during preconditioning SDs). However, the mild effect of SD preconditioning was greatly enhanced in the presence of ketamine.

Appendix C: The degree of SD-induced excitotoxic glutamate increases is related to extent of brain slice metabolic impairment

Figure 6.4

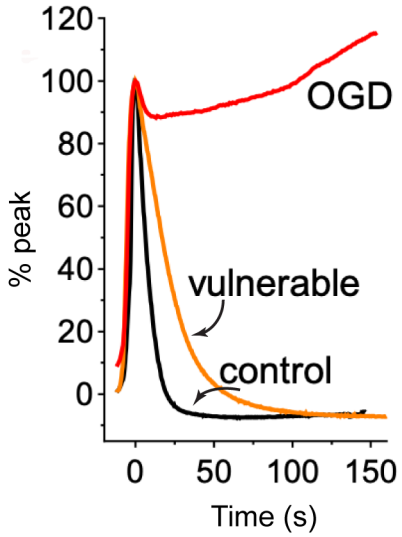

iGluSnFR transients representating the transformation into irrecoverabble glutamate increases during SD in 3 separate experiments in brain slices. SD was initiated by KCl microinjection in control and vulnerable experiments compared to SD induction via complete substrate removal (OGD). Glutamate increases coinciding with the DC shift (not shown) are relatively short-lasting in nominally healthy (control) slices and are progressiving longer in relation to the degree of metabolic impairment (i.e. most severe in OGD conditions). Traces are represented as the percent of the maximum iGluSnFR response amplitude during SD.

7. REFERENCES

Abe, H., Jitsuki, S., Nakajima, W., Murata, Y., Jitsuki-Takahashi, A., Katsuno, Y., Tada, H., Sano, A., Suyama, K., Mochizuki, N., Komori, T., Masuyama, H., Okuda, T., Goshima, Y., Higo, N., Takahashi, T., 2018. CRMP2-binding compound, edonerpic maleate, accelerates motor function recovery from brain damage. Science 360, 50–57.

Aiba, I., Carlson, A.P., Sheline, C.T., Shuttleworth, W.C., 2011. Synaptic release and extracellular actions of Zn2+ limit propagation of spreading depression and related events in vitro and in vivo. Journal of neurophysiology 107, 1032–41.

Aiba, I., Shuttleworth, W.C., 2012. Sustained NMDA receptor activation by spreading depolarizations can initiate excitotoxic injury in metabolically compromised neurons. The Journal of Physiology 590, 5877–5893.

Aiba, I., Noebels, J.L., 2015. Spreading depolarization in the brainstem mediates sudden cardiorespiratory arrest in mouse SUDEP models. Science Translational Medicine 7.

Albers, G.W., Olivot, J.-M., 2007. Intravenous alteplase for ischaemic stroke. Lancet 369, 249–250.

Astley Cooper, 1836. The Guy's Hospital Reports, No.III.

Amemori, T., Bures, J., 1990. Ketamine blockade of spreading depression: rapid development of tolerance. Brain research 519, 351–4.

Andrew, D.R., Hsieh, Y.-T., Brisson, D.C., 2016. Spreading depolarization triggered by elevated potassium is weak or absent in the rodent lower brain. Journal of Cerebral Blood Flow & Metabolism 0, 0271678X1665734. https://doi.org/10.1177/0271678x16657344

Andrew, D.R., Jarvis, C.R., Obeidat, A.S., 1999. Potential sources of intrinsic optical signals imaged in live brain slices. Methods 18, 185–196.

Astrup, J., Symon, L., Branston, N., Lassen, N., 2018. Cortical evoked potential and extracellular K+ and H+ at critical levels of brain ischemia. Stroke 8, 51–57. https://doi.org/10.1161/01.str.8.1.51

Ayata, C., Lauritzen, M., 2015. Spreading Depression, Spreading Depolarizations, and the Cerebral Vasculature. Physiological reviews 95, 953–93.

Avoli, M., Drapeau, C., Louvel, J., Pumain, R., Olivier, A., Villemure, J., 1991. Epileptiform activity induced by low extracellular magnesium in the human cortex maintained in vitro. Annals of neurology 30, 589–96.

Benjamin, E.J., Blaha, M.J., Chiuve, S.E., Cushman, M., Das, S.R., Deo, R., de Ferranti, S.D., Floyd, J., Fornage, M., Gillespie, C., Isasi, C.R., Jiménez, M.C., Jordan, L., Judd, S.E., Lackland, D., Lichtman, J.H., Lisabeth, L., Liu, S., Longenecker, C.T., Mackey, R.H., Matsushita, K., Mozaffarian, D., Mussolino, M.E., Nasir, K., Neumar, R.W., Palaniappan, L., Pandey, D.K., Thiagarajan, R.R., Reeves, M.J., Ritchey, M., Rodriguez, C.J., Roth, G.A.,

Rosamond, W.D., Sasson, C., Towfighi, A., Tsao, C.W., Turner, M.B., Virani, S.S., Voeks, J.H., Willey, J.Z., Wilkins, J.T., Wu, J., Alger, H.M., Wong, S.S., Muntner, P., and Subcommittee, A., 2017. Heart Disease and Stroke Statistics—2017 Update: A Report From the American Heart Association. Circulation 135, e146–e603.

Benveniste, H., Drejer, J., Schousboe, A., Diemer, N.H., 1984. Elevation of the Extracellular Concentrations of Glutamate and Aspartate in Rat Hippocampus During Transient Cerebral Ischemia Monitored by Intracerebral Microdialysis. Journal of Neurochemistry 43, 1369–1374.

Berdichevsky, E., Riveros, N., Sánchez-Armáss, S., Orrego, F., 1983. Kainate, N-methylaspartate and other excitatory amino acids increase calcium influx into rat brain cortex cells in vitro. Neuroscience Letters 36, 75–80

Bhaskar, S., Stanwell, P., Cordato, D., Attia, J., Levi, C., 2018. Reperfusion therapy in acute ischemic stroke: dawn of a new era? BMC Neurology 18, 8.

Boison, D., Sandau, U.S., Ruskin, D.N., Kawamura, M., Masino, S.A., 2013. Homeostatic control of brain function – new approaches to understand epileptogenesis. Front Cell Neurosci 7, 109.

Bouchard, M.B., Chen, B.R., Burgess, S.A., Hillman, E.M., 2009. Ultra-fast multispectral optical imaging of cortical oxygenation, blood flow, and intracellular calcium dynamics. Optics Express 17, 15670.

Bouvier, G., Bidoret, C., Casado, M., Paoletti, P., 2015. Presynaptic NMDA receptors: Roles and rules. Neuroscience 311, 322–40.

Bracard, S., Ducrocq, X., Mas, J., Soudant, M., Oppenheim, C., Moulin, T., Guillemin, F., investigators, T., 2016. Mechanical thrombectomy after intravenous alteplase versus alteplase alone after stroke (THRACE): a randomised controlled trial. The Lancet. Neurology 15, 1138–47.

Branston, N., Strong, A., Symon, L., 1982. Kinetics of resolution of transient increases in extracellular potassium activity: relationships to regional blood flow in primate cerebral cortex. Neurol Res 4, 1–19.

Branston, N.M., Strong, A.J., Symon, L., 1977. Extracellular potassium activity, evoked potential and tissue blood flow Relationships during progressive ischaemia in baboon cerebral cortex. J Neurol Sci 32, 305–321.

Burnashev, N., Schoepfer, R., Monyer, H., Ruppersberg, J., Gunther, W., Seeburg, Sakmann, B., 1992. Control by asparagine residues of calcium permeability and magnesium blockade in the NMDA receptor. Science 257, 1415–1419.

Burda, J., Danielisová, V., Némethová, M., Gottlieb, M., Kravčuková, P., Domoráková, I., Mechírová, E., Burda, R., 2009. Postconditioning and Anticonditioning: Possibilities to Interfere to Evoked Apoptosis. Cell Mol Neurobiol 29, 821–825.

Bureš, J., Hartman, G., 1967. Conduction block in capsula interna fibres caused by striatal spreading depression in rats. Experientia 23, 736–737

Busch, E., Gyngell, M.L., Eis, M., Hoehn-Berlage, M., Hossmann, K.-A., 1996. Potassium-Induced Cortical Spreading Depressions during Focal Cerebral Ischemia in Rats: Contribution to Lesion Growth Assessed by Diffusion-Weighted NMR and Biochemical Imaging. J Cereb Blood Flow Metabolism 16, 1090–1099

Canals, S., Larrosa, B., Pintor, J., Mena, M.A., Herreras, O., 2008a. Metabolic challenge to glia activates an adenosine-mediated safety mechanism that promotes neuronal survival by delaying the onset of spreading depression waves. Journal of Cerebral Blood Flow & Metabolism 28, 1835–1844.

Canals, S., Larrosa, B., Pintor, J., Mena, M.A., Herreras, O., 2008b. Metabolic Challenge to Glia Activates an Adenosine-Mediated Safety Mechanism that Promotes Neuronal Survival by Delaying the Onset of Spreading Depression Waves. Journal of Cerebral Blood Flow & Metabolism 28, 1835–

Carlson, A.P., Abbas, M., Alunday, R.L., Qeadan, F., Shuttleworth, W.C., 2018. Spreading depolarization in acute brain injury inhibited by ketamine: a prospective, randomized, multiple crossover trial. Journal of Neurosurgery 1–7.

Carter, R.E., Seidel, J.L., Lindquist, B.E., Sheline, C.T., Shuttleworth, C., 2013. Intracellular Zn2+ accumulation enhances suppression of synaptic activity following spreading depolarization. Journal of neurochemistry 125, 673–84.

Chambers, A.R., Rumpel, S., 2017. A stable brain from unstable components: Emerging concepts and implications for neural computation. Neuroscience 357, 172–184.

Choi, D., 1987. Ionic dependence of glutamate neurotoxicity. Journal of Neuroscience 7, 369–379.

Cole, T.B., Wenzel, J.H., Kafer, K.E., Schwartzkroin, P.A., Palmiter, R.D., 1999. Elimination of zinc from synaptic vesicles in the intact mouse brain by disruption of the ZnT3 gene. Proceedings of the National Academy of Sciences 96, 1716–1721.

Chung, D.Y., Sugimoto, K., Fischer, P., Böhm, M., Takizawa, T., Sadeghian, H., Morais, A., Harriott, A., Oka, F., Qin, T., Henninger, N., Yaseen, M.A., Sakadžić, S., Ayata, C., 2018. Real-time non-invasive in vivo visible light detection of cortical spreading depolarizations in mice. Journal of Neuroscience Methods.

Colleoni, S., Jensen, A.A., Landucci, E., Fumagalli, E., Conti, P., Pinto, A., Amici, M., Pellegrini-Giampietro, D.E., Micheli, C., Mennini, T., Gobbi, M., 2008. Neuroprotective Effects of the Novel Glutamate Transporter Inhibitor (–)-3-Hydroxy-4,5,6,6a-tetrahydro-3aH-pyrrolo[3,4-d]-isoxazole-4-carboxylic Acid, Which Preferentially Inhibits Reverse Transport (Glutamate Release) Compared with Glutamate Reuptake. J Pharmacol Exp Ther 326, 646–656.

CURTIS, D., ILLIS, J., WATKINS, J., 1959. Chemical Excitation of Spinal Neurones. Nature

183, 611.

Dahl, N., Balfour, W.M., 1964. Prolonged anoxic survival due to anoxia pre-exposure: brain ATP, lactate, and pyruvate. Am J Physiology-legacy Content 207, 452–456.
Dana, H., Mohar, B., Sun, Y., Narayan, S., Gordus, A., Hasseman, J.P., Tsegaye, G., Holt, G.T., Hu, A., Walpita, D., Patel, R., Macklin, J.J., Bargmann, C.I., rens, M., Schreiter, E.R., Jayaraman, V., Looger, L.L., Svoboda, K., Kim, D.S., 2016. Sensitive red protein calcium indicators for imaging neural activity. eLife 5, e12727.

Danbolt, N.C., 2001. Glutamate uptake. Prog Neurobiol 65, 1–105.

Dávalos, A., Castillo, J., Serena, J., Noya, M., 1997. Duration of glutamate release after acute ischemic stroke. Stroke; a journal of cerebral circulation 28, 708–10.
Dietz, R.M., Weiss, J.H., Shuttleworth, C.W., 2008. Zn2+ Influx Is Critical for Some Forms of Spreading Depression in Brain Slices. J Neurosci 28, 8014–8024.

Dawson, L.., Djali, S., Gonzales, C., Vinegra, M.., Zaleska, M.., 2000. Characterization of transient focal ischemia-induced increases in extracellular glutamate and aspartate in spontaneously hypertensive rats. Brain Res Bull 53, 767–776.

DeGraba, T.J., Hallenbeck, J.M., Pettigrew, K.D., Dutka, A.J., Kelly, B.J., 1999. Progression in Acute Stroke. Stroke 30, 1208–1212.

Dietz, R.M., Weiss, J.H., Shuttleworth, C.W., 2008. Zn2+ Influx Is Critical for Some Forms of Spreading Depression in Brain Slices. J Neurosci 28, 8014–8024.

Dirnagl, U., Simon, R.P., Hallenbeck, J.M., 2003. Ischemic tolerance and endogenous neuroprotection. Trends Neurosci 26, 248–254.

Dixon, A.K., Gubitz, A.K., Sirinathsinghji, D., Richardson, P.J., Freeman, T.C., 1996. Tissue distribution of adenosine receptor mRNAs in the rat. Brit J Pharmacol 118, 1461–1468.

Dohmen, C., Sakowitz, O.W., Fabricius, M., Bosche, B., Reithmeier, T., Ernestus, R.-I.I., Brinker, G., Dreier, J.P., Woitzik, J., Strong, A.J., Graf, R., of (COSBID), C.-O., 2008. Spreading depolarizations occur in human ischemic stroke with high incidence. Annals of neurology 63, 720–8.

Dreier, J.P., Körner, K., Ebert, N., Görner, A., Rubin, I., Back, T., Lindauer, U., Wolf, T., Villringer, A., Einhäupl, K., Lauritzen, M., Dirnagl, U., 1997. Nitric Oxide Scavenging by Hemoglobin or Nitric Oxide Synthase Inhibition by N-Nitro-L-Arginine Induces Cortical Spreading Ischemia When K+ Is Increased in the Subarachnoid Space. J Cereb Blood Flow Metabolism 18, 978–990.

Dreier, J., Woitzik, J., Fabricius, M., Bhatia, R., Major, S., Drenckhahn, C., Lehmann, -N T, Sarrafzadeh, A., Willumsen, L., Hartings, J., Sakowitz, O., Seemann, J., Thieme, A., Lauritzen, M., Strong, A., 2006. Delayed ischaemic neurological deficits after subarachnoid haemorrhage are associated with clusters of spreading depolarizations. Brain 129, 3224–3237.

Dreier, J.P., 2011. The role of spreading depression, spreading depolarization and spreading ischemia in neurological disease. Nature Medicine 17, 439–447.

Dreier, J.P., Reiffurth, C., 2015. The Stroke-Migraine Depolarization Continuum. Neuron 86, 902–922.

Dreier, J.P., Fabricius, M., Ayata, C., Sakowitz, O.W., Shuttleworth, W.C., Dohmen, C., Graf, R., Vajkoczy, P., Helbok, R., Suzuki, M., Schiefecker, A.J., Major, S., Winkler, M.K., Kang, E.-J.J., Milakara, D., Oliveira-Ferreira, A.I., Reiffurth, C., Revankar, G.S., Sugimoto, K., Dengler, N.F., Hecht, N., Foreman, B., Feyen, B., Kondziella, D., Friberg, C.K., Piilgaard, H., Rosenthal, E.S., Westover, M., Maslarova, A., Santos, E., Hertle, D., Sánchez-Porras, R., Jewell, S.L., Balança, B., Platz, J., Hinzman, J.M., Lückl, J., Schoknecht, K., Schöll, M., Drenckhahn, C., Feuerstein, D., Eriksen, N., Horst, V., Bretz, J.S., Jahnke, P., Scheel, M., Bohner, G., Rostrup, E., Pakkenberg, B., Heinemann, U., Claassen, J., Carlson, A.P., Kowoll, C.M., Lublinsky, S., Chassidim, Y., Shelef, I., Friedman, A., Brinker, G., Reiner, M., Kirov, S.A., Andrew, R., Farkas, E., Güresir, E., Vatter, H., Chung, L.S., Brennan, K., Lieutaud, T., Marinesco, S., Maas, A.I., Sahuquillo, J., Dahlem, M.A., Richter, F., Herreras, O., Boutelle, M.G., Okonkwo, D.O., Bullock, M., Witte, O.W., Martus, P., van den Maagdenberg, A.M., Ferrari, M.D., jkhuizen, R., Shutter, L.A., Andaluz, N., Schulte, A.P., MacVicar, B., Watanabe, T., Woitzik, J., Lauritzen, M., Strong, A.J., Hartings, J.A., 2017a. Recording, analysis, and interpretation of spreading depolarizations in neurointensive care: Review and recommendations of the COSBID research group. Journal of cerebral blood flow and metabolism : official journal of the International Society of Cerebral Blood Flow and Metabolism 37.

Dreier, J.P., Lemale, C.L., Kola, V., Friedman, A., Schoknecht, K., 2017b. Spreading depolarization is not an epiphenomenon but the principal mechanism of the cytotoxic edema in various gray matter structures of the brain during stroke. Neuropharmacology.

Dreier, J.P., Major, S., Foreman, B., Winkler, M.K., Kang, E., Milakara, D., Lemale, C.L., DiNapoli, V., Hinzman, J.M., Woitzik, J., Andaluz, N., Carlson, A., Hartings, J.A., 2018a. Terminal spreading depolarization and electrical silence in death of human cerebral cortex. Annals of Neurology 83, 295–310.

Dreier, J.P., Victorov, I.V., Petzold, G.C., Major, S., Windmüller, O., Fernández-Klett, F., Kandasamy, M., Dirnagl, U., Priller, J., 2018b. Electrochemical Failure of the Brain Cortex Is More Deleterious When it Is Accompanied by Low Perfusion. Stroke 44, 490–496.

Drejer, J., Benveniste, H., Diemer, N.H., Schousboe, A., 1985. Cellular Origin of Ischemia-Induced Glutamate Release from Brain Tissue In Vivo and In Vitro. J Neurochem 45, 145–151.

Edelstein, A., Amodaj, N., Hoover, K., Vale, R., Stuurman, N., 2010. Current Protocols in Molecular Biology 14.20.1-14.20.17.

Eising, E., Shyti, R., Hoen, P.A., Vijfhuizen, L.S., Huisman, S.M., Broos, L.A., Mahfouz, A., Reinders, M.J., Ferrari, M.D., Tolner, E.A., de Vries, B., van den Maagdenberg, A.M., 2017. Cortical Spreading Depression Causes Unique Dysregulation of Inflammatory Pathways in a Transgenic Mouse Model of Migraine. Mol Neurobiol 54, 2986–2996.

Emnett, C.M., Eisenman, L.N., Taylor, A.M., Izumi, Y., Zorumski, C.F., Mennerick, S., 2013. Indistinguishable Synaptic Pharmacodynamics of the N-Methyl-d-Aspartate Receptor Channel Blockers Memantine and Ketamine. Molecular Pharmacology 84, 935–947.

Enger, R., Tang, W., Vindedal, G., Jensen, V., Helm, J.P., Sprengel, R., Looger, L.L., Nagelhus, E.A., 2015. Dynamics of Ionic Shifts in Cortical Spreading Depression. Cerebral Cortex 25, 4469–4476.

Eriksen, N., Pakkenberg, B., Rostrup, E., Okonkwo, D.O., Mathern, B., Shutter, L.A., Strong, A.J., Woitzik, J., Pahl, C., Dreier, J.P., Martus, P., Lauritzen, M.J., Fabricius, M., Hartings, J.A., 2019. Neurostereologic Lesion Volumes and Spreading Depolarizations in Severe Traumatic Brain Injury Patients: A Pilot Study. Neurocritical Care 1–12.

Esposito, E., Desai, R., Ji, X., Lo, E.H., 2015. Pharmacologic pre- and postconditioning for stroke: Basic mechanisms and translational opportunity. Brain Circulation 1, 104–113. h

Fabricius, M., Fuhr, S., Bhatia, R., Boutelle, M., Hashemi, P., Strong, A.J., Lauritzen, M., 2006. Cortical spreading depression and peri-infarct depolarization in acutely injured human cerebral cortex. Brain : a journal of neurology 129, 778–90.

Fabricius, M., Jensen, L.H., Lauritzen, M., 1993. Microdialysis of interstitial amino acids during spreading depression and anoxic depolarization in rat neocortex. Brain Research 612, 61–69.

Feuerstein, D., Takagaki, M., Gramer, M., Manning, A., Endepols, H., Vollmar, S., Yoshimine, T., Strong, A.J., Graf, R., Backes, H., 2014. Detecting Tissue Deterioration after Brain Injury: Regional Blood Flow Level versus Capacity to Raise Blood Flow. J Cereb Blood Flow Metabolism 34, 1117–1127.

Frenguelli, B.G., 2017. The Purine Salvage Pathway and the Restoration of Cerebral ATP: Implications for Brain Slice Physiology and Brain Injury. Neurochemical Research 1–15.

Foster, K.A., Beaver, C.J., Turner, D.A., 2005. Interaction between tissue oxygen tension and NADH imaging during synaptic stimulation and hypoxia in rat hippocampal slices. Neuroscience 132, 645–657.

Frankiewicz, T., Potier, B., Bashir, Z., Collingridge, G., Parsons, C. (1996). Effects of memantine and MK-801 on NMDA-induced currents in cultured neurones and on synaptic transmission and LTP in area CA1 of rat hippocampal slices British Journal of Pharmacology 117(4), 689-697.

Gaspary, H.L., Simon, R.P., Graham, S.H., 1994. BW1003C87 and NBQX but not CGS19755 reduce glutamate release and cerebral ischemic necrosis. Eur J Pharmacol 262, 197–203.

Gee, M.J., Smith, N.A., Fernandez, F.R., Economo, M.N., Brunert, D., Rothermel, M., Morris, C.S., Talbot, A., Palumbos, S., Ichida, J.M., Shepherd, J.D., West, P.J., Wachowiak,

M., Capecchi, M.R., Wilcox, K.S., White, J.A., Tvrdik, P., 2014. Imaging Activity in Neurons and Glia with a Polr2a-Based and Cre-Dependent GCaMP5G-IRES-tdTomato Reporter Mouse. Neuron 83, 1058–1072.

Gladstone, D.J., Black, S.E., Hakim, A.M., 2002. Toward Wisdom From Failure. Stroke 33, 2123–2136.

Glasgow, N.G., Povysheva, N.V., Azofeifa, A.M., Johnson, J.W., 2017. Memantine and Ketamine Differentially Alter NMDA Receptor Desensitization. The Journal of neuroscience : the official journal of the Society for Neuroscience 37, 9686–9704.

Gorelova, N., Bures, J., 1983. Spiral waves of spreading depression in the isolated chicken retina. Journal of neurobiology 14, 353–63.

Gorelova, N.., Koroleva, V.., Amemori, T., Pavlík, V., Bureš, J., 1987. Ketamine blockade of cortical spreading depression in rats. Electroen Clin Neuro 66, 440–447.

Goyal, M., mchuk, A., Menon, B.K., Eesa, M., Rempel, J.L., Thornton, J., Roy, D., Jovin, T.G., Willinsky, R.A., Sapkota, B.L., Dowlatshahi, D., Frei, D.F., Kamal, N.R., Montanera, W.J., Poppe, A.Y., Ryckborst, K.J., Silver, F.L., Shuaib, A., Tampieri, D., Williams, D., Bang, O., Baxter, B.W., Burns, P.A., Choe, H., Heo, J.-H., Holmstedt, C.A., Jankowitz, B., Kelly, M., Linares, G., Mandzia, J.L., Shankar, J., Sohn, S.-I., Swartz, R.H., Barber, P.A., Coutts, S.B., Smith, E.E., Morrish, W.F., Weill, A., Subramaniam, S., Mitha, A.P., Wong, J.H., Lowerison, M.W., Sajobi, T.T., Hill, M.D., Investigators, E., 2015. Randomized Assessment of Rapid Endovascular Treatment of Ischemic Stroke. The New England Journal of Medicine 372, 1019–1030.

GRENELL, R., 1946. Central nervous system resistance; the effects of temporary arrest of cerebral circulation for periods of two to ten minutes. Journal of neuropathology and experimental neurology 5, 131–54.

Gustavsson, M., Mallard, C., Vannucci, S.J., Wilson, M., Johnston, M.V., Hagberg, H., 2006. Vascular Response to Hypoxic Preconditioning in the Immature Brain. J Cereb Blood Flow Metabolism 27, 928–938. h

Hadjikhani, N., del Rio, M., Wu, O., Schwartz, D., Bakker, D., Fischl, B., Kwong, K.K., Cutrer, M.F., Rosen, B.R., Tootell, R.B., Sorensen, G.A., Moskowitz, M.A., 2001. Mechanisms of migraine aura revealed by functional MRI in human visual cortex. Proc National Acad Sci 98, 4687–4692.

Hall, C.N., Klein-Flügge, M.C., Howarth, C., Attwell, D., 2012. Oxidative Phosphorylation, Not Glycolysis, Powers Presynaptic and Postsynaptic Mechanisms Underlying Brain Information Processing. The Journal of Neuroscience 32, 8940–8951.

Harreveld, V.A., 1959. COMPOUNDS IN BRAIN EXTRACTS CAUSING SPREADING DEPRESSION OF CEREBRAL CORTICAL ACTIVITY AND CONTRACTION OF CRUSTACEAN MUSCLE. Journal of Neurochemistry 3, 300–315.

Harreveld, V.A., 1958. Changes in the Diameter of Apical Dendrites During Spreading Depression. Am J Physiology-legacy Content 192, 457–463.

HARREVELD, V.A., HAWES, R., 1946. Asphyxial depolarisation in the spinal cord. Am J Physiology 147, 669–84.

Hartings, J.A., Rolli, M.L., Lu, X.-C., Tortella, F.C., 2003. Delayed secondary phase of peri-infarct depolarizations after focal cerebral ischemia: relation to infarct growth and neuroprotection. The Journal of neuroscience : the official journal of the Society for Neuroscience 23, 11602–10.

Hartings, J.A., Watanabe, T., Bullock, M., Okonkwo, D.O., Fabricius, M., Woitzik, J., Dreier, J.P., Puccio, A., Shutter, L.A., Pahl, C., Strong, A.J., on Depolarizations, C.-O., 2011. Spreading depolarizations have prolonged direct current shifts and are associated with poor outcome in brain trauma. Brain : a journal of neurology 134, 1529–40.

Hartings, J.A., Shuttleworth, C., Kirov, S.A., Ayata, C., Hinzman, J.M., Foreman, B., Andrew, R., Boutelle, M.G., Brennan, K., Carlson, A.P., Dahlem, M.A., Drenckhahn, C., Dohmen, C., Fabricius, M., Farkas, E., Feuerstein, D., Graf, R., Helbok, R., Lauritzen, M., Major, S., Oliveira-Ferreira, A.I., Richter, F., Rosenthal, E.S., Sakowitz, O.W., Sánchez-Porras, R., Santos, E., Schöll, M., Strong, A.J., Urbach, A., Westover, M., Winkler, M.K., Witte, O.W., Woitzik, J., Dreier, J.P., 2017. The continuum of spreading depolarizations in acute cortical lesion development: Examining Leão's legacy. Journal of cerebral blood flow and metabolism : official journal of the International Society of Cerebral Blood Flow and Metabolism 37.

Heinemann, U., Lux, H., 1977. Ceiling of stimulus induced rises in extracellular potassium concentration in the cerebral cortex of cat. Brain Research 120, 231–249.

Helassa, N., Dürst, C.D., Coates, C., Kerruth, S., Arif, U., Schulze, C., Wiegert, S.J., Geeves, M., Oertner, T.G., Török, K., 2018. Ultrafast glutamate sensors resolve high-frequency release at Schaffer collateral synapses. Proceedings of the National Academy of Sciences 115, 5594–5599.

Helleberg, B., Ellekjaer, H., Indredavik, B., 2016. Outcomes after Early Neurological Deterioration and Transitory Deterioration in Acute Ischemic Stroke Patients. Cerebrovascular Diseases 42, 378–386.

Hernández-Cáceres, J., Macias-González, R., Brozek, G., Bures, J., 1987. Systemic ketamine blocks cortical spreading depression but does not delay the onset of terminal anoxic depolarization in rats. Brain research 437, 360–4.

Hertle, D.N., Dreier, J.P., Woitzik, J., Hartings, J.A., Bullock, R., Okonkwo, D.O., Shutter, L.A., Vidgeon, S., Strong, A.J., Kowoll, C., Dohmen, C., Diedler, J., Veltkamp, R., Bruckner, T., Unterberg, A.W., Sakowitz, O.W., of (COSBID), C., 2012. Effect of analgesics and sedatives on the occurrence of spreading depolarizations accompanying acute brain injury. Brain : a journal of neurology 135, 2390–8.

Heurteaux, C., Lauritzen, I., Widmann, C., Lazdunski, M., 1995. Essential role of adenosine,

adenosine A1 receptors, and ATP-sensitive K+ channels in cerebral ischemic preconditioning. Proc National Acad Sci 92, 4666–4670.

Hinzman, J.M., DiNapoli, V.A., Mahoney, E.J., Gerhardt, G.A., Hartings, J.A., 2015. Spreading depolarizations mediate excitotoxicity in the development of acute cortical lesions. Experimental Neurology 267, 243–253.

HOFF, E., GRENELL, R., FULTON, J., 1945. HISTOPATHOLOGY OF THE CENTRAL NERVOUS SYSTEM AFTER EXPOSURE TO HIGH ALTITUDES, HYPOGLYCEMIA AND OTHER CONDITIONS ASSOCIATED WITH CENTRAL ANOXIA. Medicine 24, 161–217.

Hoskison, M., Shuttleworth, C., 2006. Microtubule disruption, not calpain-dependent loss of MAP2, contributes to enduring NMDA-induced dendritic dysfunction in acute hippocampal slices. Experimental neurology 202, 302–12.

Hoskison, M., Yanagawa, Y., Obata, K., Shuttleworth, C., 2007. Calcium-dependent NMDA-induced dendritic injury and MAP2 loss in acute hippocampal slices. Neuroscience 145, 66–79.

Iijima, T., Shimase, C., Iwao, Y., Sankawa, H., 1998. Relationships between glutamate release, blood flow and spreading depression: real-time monitoring using an electroenzymatic dialysis electrode. Neurosci Res 32, 201–207.

Iliodromitis, E.K., Lazou, A., Kremastinos, D., 2007. Ischemic preconditioning: protection against myocardial necrosis and apoptosis. Vasc Heal Risk Management 3, 629–37.

inohara, Dollinger, B., Brown, G., Rapoport, S., Sokoloff, L., 1979. Cerebral glucose utilization: local changes during and after recovery from spreading cortical depression. Science (New York, N.Y.) 203, 188–90.

Ivanov, A., Zilberter, Y. (2011). Critical State of Energy Metabolism in Brain Slices: The Principal Role of Oxygen Delivery and Energy Substrates in Shaping Neuronal Activity Frontiers in Neuroenergetics 3(), 9.

Jarvis, C.R., Anderson, T.R., Andrew, D.R., 2001. Anoxic Depolarization Mediates Acute Damage Independent of Glutamate in Neocortical Brain Slices. Cereb Cortex 11, 249–259.

Johnson, J.W., Glasgow, N.G., Povysheva, N.V., 2015. Recent insights into the mode of action of memantine and ketamine. Current opinion in pharmacology 20, 54–63.

Jovin, T.G., Chamorro, A., Cobo, E., de Miquel, M.A., Molina, C.A., Rovira, A., Román, L., Serena, J., Abilleira, S., Ribó, M., Millán, M., Urra, X., Cardona, P., López-Cancio, E., Tomasello, A., Castaño, C., Blasco, J., Aja, L., Dorado, L., Quesada, H., Rubiera, M., Hernandez-Pérez, M., Goyal, M., mchuk, A., von Kummer, R., Gallofré, M., Dávalos, A., Investigators, R., 2015. Thrombectomy within 8 Hours after Symptom Onset in Ischemic Stroke. The New England Journal of Medicine 372, 2296–2306.

Kabat, H., Dennis, C., Baker, A.B., 1941. Recovery of function following arrest of the brain circulation. American Journal of Physiology 737–747.

Kager, H., Wadman, W., Somjen, G., 2000. Simulated Seizures and Spreading Depression in a Neuron Model Incorporating Interstitial Space and Ion Concentrations. J Neurophysiol 84, 495–512.

Kaminogo, M., Suyama, K., Ichikura, A., Onizuka, M., Shibata, S., 1998. Anoxic depolarization determines ischemic brain injury. Neurol Res 20, 343–348.
Karakas, E., Furukawa, H., 2014. Crystal structure of a heterotetrameric NMDA receptor ion channel. Science 344, 992–997.

Karunasinghe, R.N., Lipski, J., 2013. Oxygen and glucose deprivation (OGD)-induced spreading depression in the Substantia Nigra. Brain Res 1527, 209–221.

Khlestova, E., Johnson, J.W., Krystal, J.H., Lisman, J., 2016. The Role of GluN2C-Containing NMDA Receptors in Ketamine's Psychotogenic Action and in Schizophrenia Models. The Journal of neuroscience : the official journal of the Society for Neuroscience 36, 11151–11157.

Kleinschnitz, C., Fluri, F., Schuhmann, M., 2015. Animal models of ischemic stroke and their application in clinical research. Drug Design, Development and Therapy Volume 9, 3445–3454.

Kobayashi, S., Harris, V.A., Welsh, F.A., 1995. Spreading Depression Induces Tolerance of Cortical Neurons to Ischemia in Rat Brain. Journal of Cerebral Blood Flow & Metabolism 15, 721–727.

Kocher, M., 1989. Metabolic and Hemodynamic Activation of Postischemic Rat Brain by Cortical Spreading Depression. Journal of Cerebral Blood Flow & Metabolism 10, 564–571.

Koroleva, V., Bures, J., 1996. The use of spreading depression waves for acute and long-term monitoring of the penumbra zone of focal ischemic damage in rats. Proceedings of the National Academy of Sciences of the United States of America 93, 3710–4.

Krüger, H., Heinemann, U., Luhmann, H.J., 1999. Effects of ionotropic glutamate receptor blockade and 5-HT1A receptor activation on spreading depression in rat neocortical slices. NeuroReport 10, 2651.

KURAOKA, M., FURUTA, T., MATSUWAKI, T., OMATSU, T., ISHII, Y., KYUWA, S., YOSHIKAWA, Y., 2009. Direct Experimental Occlusion of the Distal Middle Cerebral Artery Induces High Reproducibility of Brain Ischemia in Mice. Exp Anim Tokyo 58, 19–29.

Lai, T., Shyu, W.-C., Wang, Y., 2011. Stroke intervention pathways: NMDA receptors and beyond. Trends in Molecular Medicine 17, 266–275.

Lai, T., Zhang, S., Wang, Y., 2014. Excitotoxicity and stroke: Identifying novel targets for neuroprotection. Progress in Neurobiology 115, 157–188.

LASHLEY, K., 1941. PATTERNS OF CEREBRAL INTEGRATION INDICATED BY THE SCOTOMAS OF MIGRAINE. Archives Neurology Psychiatry 46, 331–339.

Lauritzen, M., Hansen, A., 1992. The Effect of Glutamate Receptor Blockade on Anoxic Depolarization and Cortical Spreading Depression. Journal of Cerebral Blood Flow &

Metabolism 12, 223–229.

LEAO, A., 1947. Further observations on the spreading depression of activity in the cerebral cortex. Journal of neurophysiology 10, 409–14.

Leao, A.A.P., 1944. Spreading Depression of Activity in the Cerebral Cortex. Journal of Neurophysiology 7, 359–390.

Leao, A.A.P., Morison, R.S., 1945. Propagation of spreading cortical depression. Journal of Neurophysiology 8, 33–45.

Lee, S.-H., Kim, Y.-J., Lee, K.-M., Ryu, S., Yoon, B.-W., 2007. Ischemic preconditioning enhances neurogenesis in the subventricular zone. Neuroscience 146, 1020–1031.

Lennox, W., Gibbs, F., Gibbs, E., 1938. THE RELATIONSHIP IN MAN OF CEREBRAL ACTIVITY TO BLOOD FLOW AND TO BLOOD CONSTITUENTS. J Neurol Psychiatry 1, 211.

Lindquist, B.E., Shuttleworth, C.W., 2012. Adenosine receptor activation is responsible for prolonged depression of synaptic transmission after spreading depolarization in brain slices. Neuroscience 223, 365–376.

Lindquist, B.E., Shuttleworth, W.C., 2014. Spreading Depolarization-Induced Adenosine Accumulation Reflects Metabolic Status In Vitro and In Vivo. Journal of Cerebral Blood Flow & Metabolism 34, 1779–1790.

Lindquist, B.E., Shuttleworth, W.C., 2016. Evidence that adenosine contributes to Leao's spreading depression in vivo. Journal of Cerebral Blood Flow & Metabolism 37, 1656–1669.

López-Valdés, H., Clarkson, A., Ao, Y., Charles, A., Carmichael, S., Sofroniew, M., Brennan, K. (2014). Memantine enhances recovery from stroke. Stroke 45(7), 2093-2100.

Ma, Y., Shaik, M.A., Kim, S.H., Kozberg, M.G., Thibodeaux, D.N., Zhao, H.T., Yu, H., Hillman, E.M., 2016. Wide-field optical mapping of neural activity and brain haemodynamics: considerations and novel approaches. Philosophical Transactions Royal Soc B Biological Sci 371.

Magistretti, P.J., Allaman, I., 2015. A Cellular Perspective on Brain Energy Metabolism and Functional Imaging. Neuron 86, 883–901.

Marrannes, R., Prins, D.E., Willems, R., Wauquier, A., 1988a. Mechanisms of Cerebral Hypoxia and Stroke 303–304.

Marrannes, R., Willems, R., Prins, D.E., Wauquier, A., 1988b. Evidence for a role of the N-methyl-D-aspartate (NMDA) receptor in cortical spreading depression in the rat. Brain research 457, 226–40.

Marvin, J.S., Borghuis, B.G., Tian, L., Cichon, J., Harnett, M.T., Akerboom, J., Gordus, A., Renninger, S.L., Chen, T.-W., Bargmann, C.I., Orger, M.B., Schreiter, E.R., Demb, J.B., Gan, W.-B., Hires, A.S., Looger, L.L., 2013. An optimized fluorescent probe for visualizing glutamate neurotransmission. Nature Methods 10.

Marvin, J.S., Scholl, B., Wilson, D.E., Podgorski, K., Kazemipour, A., Müller, J., Schoch, S., Quiroz, F., Rebola, N., Bao, H., Little, J.P., Tkachuk, A.N., Cai, E., Hantman, A.W., Wang, S., DePiero, V.J., Borghuis, B.G., Chapman, E.R., Dietrich, D., DiGregorio, D.A., Fitzpatrick, D., Looger, L.L., 2018. Stability, affinity, and chromatic variants of the glutamate sensor iGluSnFR. Nat Methods 15, 936–939.

Matsushima, K., Schmidt-Kastner, R., Hogan, M.J., Hakim, A.M., 1998. Cortical spreading depression activates trophic factor expression in neurons.

Meldrum, D.R., 1997. Mechanisms of Cardiac Preconditioning: Ten Years after the Discovery of Ischemic Preconditioning. J Surg Res 73, 1–13.

Mergenthaler, P., Lindauer, U., Dienel, G.A., Meisel, A., 2013. Sugar for the brain: the role of glucose in physiological and pathological brain function. Trends Neurosci 36, 587–597.

Meurer, W.J., Barth, B.E., Gaddis, G., Vilke, G.M., Lam, S.H., 2017. Rapid systematic review: intra-arterial thrombectomy (“clot retrieval”) for selected patients with acute ischemic stroke. The Journal of emergency medicine 52, 255–261.

Mies, G., Paschen, W., 1984. Regional changes of blood flow, glucose, and ATP content determined on brain sections during a single passage of spreading depression in rat brain cortex. Exp Neurol 84, 249–258.

Mies, G., Iijima, T., Hossmann, K.-A., 1993. Correlation between periinfarct DC shifts and ischaemic neuronal damage in rat. NeuroReport 4, 709–711.

Mitani, A., Kubo, H., Iga, K., Imon, H., Kadoya, F., Kataoka, K., 1990. A New Enzymatic Cycling Technique for Glutamate Determination in Brain Microdialysates. J Neurochem 54, 709–711.

Moldestad, O., Karlsen, P., Molden, S., Storm, J.F., 2009. Tracheotomy improves experiment success rate in mice during urethane anesthesia and stereotaxic surgery. J Neurosci Meth 176, 57–62.

Müller, M., Somjen, G.G., 2000. Na+ dependence and the role of glutamate receptors and Na+ channels in ion fluxes during hypoxia of rat hippocampal slices. Journal of Neurophysiology 84, 1869–1880.

Murphy, T.H., Li, P., Betts, K., Liu, R., 2008. Two-photon imaging of stroke onset in vivo reveals that NMDA-receptor independent ischemic depolarization is the major cause of rapid reversible damage to dendrites and spines. The Journal of neuroscience : the official journal of the Society for Neuroscience 28, 1756–72.

Murry, C., Jennings, R., Reimer, K., 2018. Preconditioning with ischemia: a delay of lethal cell injury in ischemic myocardium. Circulation 74, 1124–1136.
Murphy, T.H., Corbett, D., 2009. Plasticity during stroke recovery: from synapse to

behaviour. Nat Rev Neurosci 10.

Nakamura, H., Strong, A.J., Dohmen, C., Sakowitz, O.W., Vollmar, S., Sué, M., Kracht, L., Hashemi, P., Bhatia, R., Yoshimine, T., Dreier, J.P., Dunn, A.K., Graf, R., 2010. Spreading depolarizations cycle around and enlarge focal ischaemic brain lesions. Brain : a journal of neurology 133, 1994–2006.

Nakanishi, N., Axel, R., Shneider, N., 1992. Alternative splicing generates functionally distinct N-methyl-D-aspartate receptors. Proc National Acad Sci 89, 8552–8556.

Nedergaard, M., Hansen, A., 1988. Spreading depression is not associated with neuronal injury in the normal brain. Brain research 449, 395–8.

Nedergaard, M., Hansen, A., 1993. Characterization of Cortical Depolarizations Evoked in Focal Cerebral Ischemia. Journal of Cerebral Blood Flow & Metabolism 13, 568–574.

Norton, L., Gibson, R.M., Gofton, T., Benson, C., Dhanani, S., Shemie, S.D., Hornby, L., Ward, R., Young, B.G., 2017. Electroencephalographic Recordings During Withdrawal of Life-Sustaining Therapy Until 30 Minutes After Declaration of Death. Can J Neurological Sci J Can Des Sci Neurologiques 44, 139–145.

Nogueira, R.G., Jadhav, A.P., Haussen, D.C., Bonafe, A., Budzik, R.F., Bhuva, P., Yavagal, D.R., Ribo, M., Cognard, C., Hanel, R.A., Sila, C.A., Hassan, A.E., Millan, M., Levy, E.I., Mitchell, P., Chen, M., English, J.D., Shah, Q.A., Silver, F.L., Pereira, V.M., Mehta, B.P., Baxter, B.W., Abraham, M.G., Cardona, P., Veznedaroglu, E., Hellinger, F.R., Feng, L., Kirmani, J.F., Lopes, D.K., Jankowitz, B.T., Frankel, M.R., Costalat, V., Vora, N.A., Yoo, A.J., Malik, A.M., Furlan, A.J., Rubiera, M., Aghaebrahim, A., Olivot, J.-M., Tekle, W.G., Shields, R., Graves, T., Lewis, R.J., Smith, W.S., Liebeskind, D.S., Saver, J.L., Jovin, T.G., Investigators, D., 2018. Thrombectomy 6 to 24 Hours after Stroke with a Mismatch between Deficit and Infarct. The New England Journal of Medicine 378, 11–21.

Obeidat, A., Andrew, R., 1998. Spreading depression determines acute cellular damage in the hippocampal slice during oxygen/glucose deprivation. The European journal of neuroscience 10, 3451–61.

Obeidat, A.S., Jarvis, C.R., Andrew, D.R., 1999. Glutamate Does Not Mediate Acute Neuronal Damage after Spreading Depression Induced by O2/Glucose Deprivation in the Hippocampal Slice. J Cereb Blood Flow Metabolism 20, 412–422.

Okiyama, K., Smith, D.H., Gennarelli, T.A., Simon, R.P., Leach, M., McIntosh, T.K., 1995. The Sodium Channel Blocker and Glutamate Release Inhibitor BW1003C87 and Magnesium Attenuate Regional Cerebral Edema Following Experimental Brain Injury in the Rat. J Neurochem 64, 802–809.

Peltoniemi, M.A., Hagelberg, N.M., Olkkola, K.T., Saari, T.I., 2016. Ketamine: A Review of Clinical Pharmacokinetics and Pharmacodynamics in Anesthesia and Pain Therapy. Clin Pharmacokinet 55, 1059–1077.

Pietrobon, D., Moskowitz, M.A., 2014. Chaos and commotion in the wake of cortical spreading depression and spreading depolarizations. Nature reviews. Neuroscience 15, 379–93.

Pincherle, A., Pace, M., Sarasso, S., Facchin, L., Dreier, J.P., Bassetti, C.L., 2018. Sleep, Preconditioning and Stroke. Stroke 48, 3400–3407.

Petzold, G.C., Windmüller, O., Haack, S., Major, S., Buchheim, K., Megow, D., Gabriel, S., Lehmann, T.-N., Drenckhahn, C., Peters, O., Meierkord, H., Heinemann, U., Dirnagl, U., Dreier, J.P., 2005. Increased Extracellular K+ Concentration Reduces the Efficacy of N-methyl-d-aspartate Receptor Antagonists to Block Spreading Depression-Like Depolarizations and Spreading Ischemia. Stroke 36, 1270–1277.

Pietrobon, D., Moskowitz, M.A., 2014. Chaos and commotion in the wake of cortical spreading depression and spreading depolarizations. Nature reviews. Neuroscience 15, 379–93.

Pignataro, G., Scorziello, A., Renzo, G., Annunziato, L., 2009. Post-ischemic brain damage: effect of ischemic preconditioning and postconditioning and identification of potential candidates for stroke therapy. Febs J 276, 46–57.

Pincherle, A., Pace, M., Sarasso, S., Facchin, L., Dreier, J.P., Bassetti, C.L., 2018. Sleep, Preconditioning and Stroke. Stroke 48, 3400–3407.

Powers, W.J., Rabinstein, A.A., Ackerson, T., Adeoye, O.M., Bambakidis, N.C., Becker, K., Biller, J., Brown, M., maerschalk, B., Hoh, B., Jauch, E.C., Kidwell, C.S., Leslie-Mazwi, T.M., Ovbiagele, B., Scott, P.A., Sheth, K.N., utherland, A., Summers, D.V., Tirschwell, D.L., Council, A., 2018. 2018 Guidelines for the Early Management of Patients With Acute Ischemic Stroke: A Guideline for Healthcare Professionals From the American Heart Association/American Stroke Association. Stroke 49, e46–e99.

Qian, J., Noebels, J.L., 2005. Visualization of transmitter release with zinc fluorescence detection at the mouse hippocampal mossy fibre synapse. The Journal of Physiology 566, 747–758.

Reinhart, K.M., Shuttleworth, W.C., 2018. Ketamine reduces deleterious consequences of spreading depolarizations. Exp Neurol 305, 121–128.

Retchless, B., Gao, W., Johnson, J.W., 2012. A single GluN2 subunit residue controls NMDA receptor channel properties via intersubunit interaction. Nat Neurosci 15, 406.

Revah, O., Lasser-Katz, E., Fleidervish, I.A., Gutnick, M.J., 2016. The earliest neuronal responses to hypoxia in the neocortical circuit are glutamate-dependent. Neurobiol Dis 95, 158–167.

Risher, W., Ard, D., Yuan, J., Kirov, S.A., 2010. Recurrent spontaneous spreading depolarizations facilitate acute dendritic injury in the ischemic penumbra. The Journal of neuroscience : the official journal of the Society for Neuroscience 30, 9859–68.

Rogers, M.L., Leong, C., Gowers, S.A., Samper, I.C., Jewell, S.L., Khan, A., McCarthy, L., Pahl, C., Tolias, C.M., Walsh, D.C., Strong, A.J., Boutelle, M.G., 2016. Simultaneous monitoring of potassium, glucose and lactate during spreading depolarization in the injured human brain – Proof of principle of a novel real-time neurochemical analysis system, continuous online microdialysis. Journal of Cerebral Blood Flow & Metabolism 37.

Rodgers, C.I., Amstrong, G., Shoemaker, K.L., LaBrie, J.D., Moyes, C.D., Robertson, M.R., 2007. Stress Preconditioning of Spreading Depression in the Locust CNS. PLoS ONE 2.

Rodgers, C.I., Armstrong, G., Robertson, M.R., 2010. Coma in response to environmental stress in the locust: A model for cortical spreading depression. Journal of Insect Physiology 56, 980–990.

Rossen, L.R., Kabat, H., Anderson, J.P., 1943. Acute Arrest of Cerebral Circulation in Man. Archives of Neurology and Psychiatry 50, 510–528.

Rossi, D.J., Oshima, T., Attwell, D., 2000. Glutamate release in severe brain ischaemia is mainly by reversed uptake. Nature 403, 316–321.

Rumpel, S., 2018. Supporting recovery from brain injury. Science 360, 30–31.

Sakowitz, O.W., Kiening, K.L., Krajewski, K.L., Sarrafzadeh, A.S., Fabricius, M., Strong, A.J., Unterberg, A.W., Dreier, J.P., 2009. Preliminary evidence that ketamine inhibits spreading depolarizations in acute human brain injury. Stroke 40, e519-22.

Sánchez-Porras, R., Santos, E., Schöll, M., Stock, C., Zheng, Z., Schiebel, P., Orakcioglu, B., Unterberg, A.W., Sakowitz, O.W., 2014. The effect of ketamine on optical and electrical characteristics of spreading depolarizations in gyrencephalic swine cortex. Neuropharmacology 84, 52–61.

Santos, E., Schöll, M., Sánchez-Porras, R., Dahlem, M.A., Silos, H., Unterberg, A., Dickhaus, H., Sakowitz, O.W., 2014. Radial, spiral and reverberating waves of spreading depolarization occur in the gyrencephalic brain. NeuroImage 99, 244–255.

Saver, J.L., Goyal, M., Bonafe, A., Diener, H.-C., Levy, E.I., Pereira, V.M., Albers, G.W., Cognard, C., Cohen, D.J., Hacke, W., Jansen, O., Jovin, T.G., Mattle, H.P., Nogueira, R.G., Siddiqui, A.H., Yavagal, D.R., Baxter, B.W., Devlin, T.G., Lopes, D.K., Reddy, V.K., du de Rochemont, R., Singer, O.C., Jahan, R., Investigators, S., 2015. Stent-Retriever Thrombectomy after Intravenous t-PA vs. t-PA Alone in Stroke. The New England Journal of Medicine 372, 2285–2295.

Sawant-Pokam, P., Suryavanshi, P., Mendez, J., Dudek, F., Brennan, K., 2017. Mechanisms of Neuronal Silencing After Cortical Spreading Depression. Cereb Cortex 27, 1311–1325.

Schiefecker, A., Beer, R., Pfausler, B., Lackner, P., Broessner, G., Unterberger, I., Sohm, F., Mulino, M., Thome, C., Humpel, C., Schmutzhard, E., Helbok, R., 2015. Clusters of Cortical Spreading Depolarizations in a Patient with Intracerebral Hemorrhage: A Multimodal

Neuromonitoring Study. Neurocritical Care 22, 293–298.

Schindelin, J., Arganda-Carreras, I., Frise, E., Kaynig, V., Longair, M., Pietzsch, T., Preibisch, S., Rueden, C., Saalfeld, S., Schmid, B., Tinevez, J.-Y., White, D., Hartenstein, V., Eliceiri, K., Tomancak, P., Cardona, A., 2012. Fiji: an open-source platform for biological-image analysis. Nature Methods 9, 676.

Schöll, M., Santos, E., Sanchez-Porras, R., Kentar, M., Gramer, M., Silos, H., Zheng, Z., Gang, Y., Strong, A., Graf, R., Unterberg, A., Sakowitz, O.W., Dickhaus, H., 2016. Large field-of-view movement-compensated intrinsic optical signal imaging for the characterization of the haemodynamic response to spreading depolarizations in large gyrencephalic brains. Journal of Cerebral Blood Flow & Metabolism.

Schurr, A., Reid, K.H., Tseng, M.T., West, C., Rigor, B.M., 1986. Adaptation of adult brain tissue to anoxia and hypoxia in vitro. Brain Res 374, 244–248.

Seidel, J.L., Shuttleworth, C.W., 2011. Contribution of astrocyte glycogen stores to progression of spreading depression and related events in hippocampal slices. Neuroscience 192, 295–303.

SEWELL, W., KOTH, D., HUGGINS, C., 1955. Ventricular fibrillation in dogs after sudden return of flow to the coronary artery. Surgery 38, 1050–3.

Shen, P., Hou, S., Ma, D., Zhao, M., Zhu, M., Zhang, J., Feng, L., Cui, L., Feng, J., 2016. Cortical spreading depression-induced preconditioning in the brain. Neural Regeneration Research 11, 1857–1864.

Shen, P., Hou, S., Zhu, M., Zhao, M., Ouyang, Y., Feng, J., 2017. Cortical spreading depression preconditioning mediates neuroprotection against ischemic stroke by inducing AMP-activated protein kinase-dependent autophagy in a rat cerebral ischemic/reperfusion injury model. J Neurochem 140, 799–813.

Shin, H., Dunn, A.K., Jones, P.B., Boas, D.A., Moskowitz, M.A., Ayata, C., 2005. Vasoconstrictive Neurovascular Coupling during Focal Ischemic Depolarizations. J Cereb Blood Flow Metabolism 26, 1018–1030.

Shuttleworth, W.C., 2010. Use of NAD(P)H and flavoprotein autofluorescence transients to probe neuron and astrocyte responses to synaptic activation. Neurochemistry International 56, 379–386.

Shuttleworth, W.C., Brennan, A.M., Connor, J.A., 2003. NAD(P)H Fluorescence Imaging of Postsynaptic Neuronal Activation in Murine Hippocampal Slices. J Neurosci 23, 3196–3208.

Simon, R.P., Niiro, M., Gwinn, R., 1993. Prior ischemic stress protects against experimental stroke. Neurosci Lett 163, 135–137.

Smith, S.E., Lekieffre, D., Sowinski, P., Meldrum, B.S., 1993. Cerebroprotective effect of BW619C89 after focal or global cerebral ischaemia in the rat. Neuroreport 4, 1339–1342.

Somjen, G., 2001. Mechanisms of spreading depression and hypoxic spreading depression-like depolarization. Physiological reviews 81, 1065–96.

Somjen, G.G., 2002. Ion regulation in the brain: implications for pathophysiology. The Neuroscientist : a review journal bringing neurobiology, neurology and psychiatry 8, 254–67.

Stenzel-Poore, M.P., Stevens, S.L., Xiong, Z., Lessov, N.S., Harrington, C.A., Mori, M., Meller, R., Rosenzweig, H.L., Tobar, E., Shaw, T.E., Chu, X., Simon, R.P., 2003. Effect of ischaemic preconditioning on genomic response to cerebral ischaemia: similarity to neuroprotective strategies in hibernation and hypoxia-tolerant states. Lancet 362, 1028–1037.

Strong, A., Anderson, P., Watts, H., Virley, D., Lloyd, A., Irving, E., Nagafuji, T., Ninomiya, M., Nakamura, H., Dunn, A., Graf, R., 2006. Peri-infarct depolarizations lead to loss of perfusion in ischaemic gyrencephalic cerebral cortex. Brain 130, 995–1008.

Strong, A.J., Fabricius, M., Boutelle, M.G., Hibbins, S.J., Hopwood, S.E., Jones, R., Parkin, M.C., Lauritzen, M., 2002. Spreading and Synchronous Depressions of Cortical Activity in Acutely Injured Human Brain. Stroke 33, 2738–2743.

Sugar, O., Gerard, R.W., 1938. Anoxia and Brain Potentials. Journal of Neurophysiology 1, 558–572.

Sukhotinsky, I., Dilekoz, E., Moskowitz, M.A., Ayata, C., 2008. Hypoxia and Hypotension Transform the Blood Flow Response to Cortical Spreading Depression from Hyperemia into Hypoperfusion in the Rat. J Cereb Blood Flow Metabolism 28, 1369–1376.

Takano, T., Tian, G.-F., Peng, W., Lou, N., Lovatt, D., Hansen, A.J., Kasischke, K.A., Nedergaard, M., 2007. Cortical spreading depression causes and coincides with tissue hypoxia. Nature Neuroscience 10, 754–762.

Tang, Y.T., Mendez, J.M., Theriot, J.J., want, P., López-Valdés, H.E., Ju, Y., Brennan, K., 2014. Minimum conditions for the induction of cortical spreading depression in brain slices. Journal of neurophysiology 112, 2572–9.

Thijssen, D.H., Maxwell, J., Green, D.J., Cable, T.N., Jones, H., 2016. Repeated ischaemic preconditioning: a novel therapeutic intervention and potential underlying mechanisms. Exp Physiol 101, 677–692.

Tissue Plasminogen Activator for Acute Ischemic Stroke, 1995. . New Engl J Medicine 333, 1581–1588.

Toki, H., Ichikawa, T., Mizuno-Yasuhira, A., Yamaguchi, J., 2018. A rapid and sensitive chiral LC–MS/MS method for the determination of ketamine and norketamine in mouse plasma, brain and cerebrospinal fluid applicable to the stereoselective pharmacokinetic study of ketamine. Journal of Pharmaceutical and Biomedical Analysis 148, 288–297.

Tu, W., Xu, X., Peng, L., Zhong, X., Zhang, Wenfeng, Soundarapandian, M.M., Belal, C., Wang, M., Jia, N., Zhang, Wen, Lew, F., Chan, S., Chen, Y., Lu, Y., 2010. DAPK1 Interaction with NMDA Receptor NR2B Subunits Mediates Brain Damage in Stroke. Cell 140, 222–234.

Urbach, A., Baum, E., Braun, F., Witte, O.W., 2016. Cortical spreading depolarization increases adult neurogenesis, and alters behavior and hippocampus-dependent memory in mice. Journal of Cerebral Blood Flow & Metabolism 0, 0271678X1664373.

van Harreveld, A., 1978. Two mechanisms for spreading depression in the chicken retina. J Neurobiol 9, 419–431.

van HARREVELD, A., 1946. Depolarisation in the spinal cord caused by asphyxiation. Fed Proc 5, 41.

van Rensburg, R., Errington, D.R., Ennaceur, A., Lees, G., Obrenovitch, T.P., Chazot, P.L., 2009. A new model for the study of high-K+-induced preconditioning in cultured neurones: Role of N-methyl-d-aspartate and α7-nicotinic acetylcholine receptors. J Neurosci Meth 177, 311–316.

Vetrovoy, O., Rybnikova, E., Samoilov, M., 2017. Cerebral mechanisms of hypoxic/ischemic postconditioning. Biochem Mosc 82, 392–400.

von Bornstädt, D., Houben, T., Seidel, J.L., Zheng, Y., Dilekoz, E., Qin, T., Sandow, N., ekanth Kura, Eikermann-Haerter, K., Endres, M., Boas, D.A., Moskowitz, M.A., Lo, E.H., Dreier, J.P., Woitzik, J., Sakadžić, S., Ayata, C., 2015. Supply-Demand Mismatch Transients in Susceptible Peri-infarct Hot Zones Explain the Origins of Spreading Injury Depolarizations. Neuron 85, 1117–1131.

Wang, X., Zhang, C., Szábo, G., Sun, Q.-Q., 2013. Distribution of CaMKIIα expression in the brain in vivo, studied by CaMKIIα-GFP mice. Brain Research 1518, 9–25.

Weih, M., Kallenberg, K., Bergk, A., Dirnagl, U., Harms, L., Wernecke, K., Einhäupl, K., 1999. Attenuated Stroke Severity After Prodromal TIA. Stroke 30, 1851–1854.

Weilinger, N.L., Lohman, A.W., Rakai, B.D., Ma, E.M., Bialecki, J., Maslieieva, V., Rilea, T., Bandet, M.V., Ikuta, N.T., Scott, L., Colicos, M.A., Teskey, C.G., Winship, I.R., Thompson, R.J., 2016. Metabotropic NMDA receptor signaling couples Src family kinases to pannexin-1 during excitotoxicity. Nat Neurosci 19.

Woitzik, J., Hecht, N., Pinczolits, A., Sandow, N., Major, S., Winkler, M., Weber-Carstens, S., Dohmen, C., Graf, R., Strong, A.J., Dreier, J.P., Vajkoczy, P., 2013. Propagation of cortical spreading depolarization in the human cortex after malignant stroke. Neurology 80, 1095–1102.

Wu, Q., Tymianski, M., 2018. Targeting NMDA receptors in stroke: new hope in neuroprotection. Molecular Brain 11, 15.

Yanamoto, H., Xue, J.-H., Miyamoto, S., Nagata, I., Nakano, Y., Murao, K., Kikuchi, H., 2004. Spreading depression induces long-lasting brain protection against infarcted lesion development via BDNF gene-dependent mechanism. Brain Research 1019, 178–188.

Yang, O., Cuccia, D., Choi, B., 2011. Real-time blood flow visualization using the graphics processing unit. J Biomed Opt 16.

Yellon, D.M., Dana, A., 2000. The Preconditioning Phenomenon. Circ Res 87, 543–550.

Yu, Y., ntos, L., Mattiace, L.A., Costa, M.L., Ferreira, L.C., Benabou, K., Kim, A.H., Abrahams, J., Bennett, M.V., Rozental, R., 2012. Reentrant spiral waves of spreading depression cause macular degeneration in hypoglycemic chicken retina. Proceedings of the National Academy of Sciences of the United States of America 109, 2585–9.

Yuzawa, I., Sakadžić, S., nivasan, V.J., Shin, H., Eikermann-Haerter, K., Boas, D.A., Ayata, C., 2011. Cortical Spreading Depression Impairs Oxygen Delivery and Metabolism in Mice. J Cereb Blood Flow Metabolism 32, 376–386.

Zanos, P., Gould, T., 2018. Mechanisms of ketamine action as an antidepressant. Mol Psychiatr 23, 801.

Zanos, P., Moaddel, R., Morris, P.J., Georgiou, P., Fischell, J., Elmer, G.I., Alkondon, M., Yuan, P., Pribut, H.J., Singh, N.S., Dossou, K.S., Fang, Y., Huang, X.-P., Mayo, C.L., Wainer, I.W., Albuquerque, E.X., Thompson, S.M., Thomas, C.J., Jr, C.A., Gould, T.D., 2016. NMDAR inhibition-independent antidepressant actions of ketamine metabolites. Nature 533, 481.

Zhao, H., 2009. Ischemic Postconditioning as a Novel Avenue to Protect against Brain Injury after Stroke. J Cereb Blood Flow Metabolism 29, 873–885.

Zhou, N., Rungta, R.L., Malik, A., Han, H., Wu, D., MacVicar, B.A., 2013. Regenerative Glutamate Release by Presynaptic NMDA Receptors Contributes to Spreading Depression. Journal of Cerebral Blood Flow & Metabolism 33, 1582–1594.